Characterization of starch-based system for parenteral controlled drug release applications

Kumulative Dissertation

zur Erlangung des

Doktorgrades der Naturwissenschaften (Dr. rer. nat.)

der

Naturwissenschaftlichen Fakultät I

– Biowissenschaften –

der Martin-Luther-Universität Halle-Wittenberg,

vorgelegt von

Frau Golbarg Esfahani

Gutachter/innen:

1. Prof. Dr. Karsten Mäder

2. Prof. Dr. Detlef Reichert

3. Prof. Dr. Miriam Breunig

Tag der öffentlichen Verteidigung: 30.01.2024

علم بالست مرغ جانت را بر سپهر او بر د روانت را

Saadi Shirazi, 1200

Science is the wings for the bird of your life, elevating your soul to the skies.

Die Wissenschaft ist wie die Flügel des Vogels des Lebens, die die Seele in den Himmel hebt.

Table of Contents

Table of content

List of Figures

List of Figures

List of Tables

Abbreviations

AM	Artemether
AM/AP	Amylose/Amylopectin
API	Active Pharmaceutical Ingredient
AS	Artesunate
DDS	Drug Delivery System
DiR	1,1′-Dioctadecyl-3,3,3′,3′- Tetramethylindotricarbocyanine-Iodide
DSC	Differential Scanning Calorimetry
EPR	Electron Paramagnetic Resonance
et al.	and others
FDA	Food and Drug Administration
FI	Fluorescence Imaging
GMS	Glycerol Monostearate
H&E	Hematoxylin-eosin
HME	Hot Melt Extrusion
ICG	Indocyanine Green
ICH	International Council for Harmonization of Technical Requirements for Pharmaceuticals for Human Use
IVIS	In Vivo Imaging System
LHRH	Luteinizing Hormone-Releasing Hormone
MCT	Medium-chain triglycerides
NIR	Near-Infrared
NMD	Nimodipine
NMD-20	Implant containing 20% nimodipine

Abbreviations

NMD-40	Implant containing 40% nimodipine
NMR	Nuclear Magnetic Resonance
OI	Optical Imaging
PBS	Phosphate Buffered Saline
PEA	Polyesteramide
PLA	Poly(lactic acid)
PLGA	Poly(lactide-co-glycolide)
SAH	Subarachnoid haemorrhage
SDS	Sodium dodecyl sulfate
SEM	Scanning Electron Microscopy
SC	Subcutaneously
T_2	Spin-spin relaxation time
TB	Tempol benzoate
TL	Tempol
WHO	World Health Organization
XRD	X-ray diffraction
3D	3-dimensional
2D	2-dimensional

1. Introduction

1.1 Parenteral depot systems

Parenteral depot systems, also known as long-acting injectables or implantable drug delivery systems (DDS) have a huge potential to improve pharmacotherapy for the benefit of patients. They can provide a constant concentration of a drug in the target tissue for a specified duration. These systems enhance patient compliance by reducing the need for frequent applications. Additionally, these depot formulations can minimize undesirable side effects associated with the fluctuating drug levels commonly observed with immediate-release products [1,2]. An ideal parenteral depot system is expected to possess the following features:

- High degree of biocompatibility and no toxic effects
- Easy application
- Reproducible and predictable drug release kinetics
- Full disappearance during or shortly after completion of drug release (by degradation and/or erosion)
- Sterility

Preformed implants and microparticles are the most widely used forms of parenteral depot systems [3,4]. Nonetheless, microparticle systems have certain limitations. These include complex and expensive production processes, sintering of particles by inappropriate shipping and storage temperatures, and a more time-consuming and difficult administration procedure that poses the risk of incomplete dispersion of the microparticles, syringe clogging, and the likelihood of administering an incomplete dose [5]. In comparison to microparticles, preformed implants can be manufactured using cost-effective and simple methods such as Hot Melt Extrusion (HME), enabling large-scale production of the system [6]. They can be implanted in various parts of the body such as the ear (intracochlear implant [7]) or eye (intravitreal implant [8]) or be placed directly at the site during surgery depending on the target organ [9].

The first one to describe a subcutaneously (SC) implanted dosage form was Lafargue [10], who used a simple form of the trocar to apply implants consisting of gum arabic and atropine as early as 1861. Almost one century later Folkman and Long [11] added to this concept the aspect of controlled release by using silastic implants to prolong the pharmacological effect of different drugs. The first commercially available parenteral

controlled DDS was the intrauterine device Progestasert® emerged in the early 1970s [12]. Later on, a SC implanted contraceptive device releasing levonorgestrel over a 5-year period (NORPLANT®) was developed [13]. Although these products provided prolonged drug delivery with relatively constant release rates, the need for surgical removal of the spent devices was a significant drawback.

Investigations of biodegradable polymers of poly(hydroxy acids) for drug delivery applications began in the 1960s and 1970s, and these polymers continue to be utilized today. In 1967, Schmitt and Polestina at Davis & Geck (Cyanamid Co.) synthesized poly(glycolic acid) (PGA) for use as a degradable suture [14]. Ethicon added lactic acid to the composition, licensed PGA technology from Davis and Geck, and introduced the degradable poly(lactide-co-glycolide) (PLGA) suture known as Vicryl® in 1974 [15]. Furthermore, implants composed of PLGA have undergone extensive research for various applications, including the delivery of luteinizing hormone-releasing hormone (LHRH) analogues. In 1989, the Zoladex® implant was introduced as a PLGA matrix system designed to deliver the LHRH analogue goserelin for the treatment of prostate cancer, breast cancer, and endometriosis [16,17]. Typically, preformed implants are manufactured using melt extrusion and are administered SC using a special application device or through a large needle. These SC implants generally adopt a cylindrical shape, measuring 10 mm in length with a diameter of 1 mm, as seen in Zoladex®. These implants are administered via a 16-gauge needle with an outer diameter of 1.65 mm. Smaller implants are used for eye diseases, such as Ozurdex® (dexamethasone implant), featuring dimensions of 6 mm in length and 0.46 mm in diameter [8,18]. Commercially, SC implants are also available in larger dimensions, such as the non-biodegradable one-year implant Vantas® (histrelin acetate implant used for prostate cancer treatment), with a length of 35 mm and diameter of 3 mm [19]. As of today, poly(lactic acid) (PLA) and PLGA stand as the prevailing polymers employed in the pharmaceutical industry for the manufacture of parenteral depot systems [20–22].

1.2 Challenges of the available products

As mentioned earlier, currently, PLA and PLGA are the most commonly used polymers in the pharmaceutical industry to produce parenteral depot systems [20–22]. The initial clinical application of PLGA implants focused on hormonal peptide therapeutics (e.g. GnrH

superagonists such as leuprolide, octreotide, buserelin, and others), diabetes GLP-1 peptide, and growth hormone [23]. PLGA's biodegradability makes it an interesting candidate for a parenteral depot system, as there is no need to take out the injected implant or formulation after the release period. This leads to high patient compliance for receiving the drug. Nonetheless, the degradation of PLGA produces the highly acidic monomers glycolic and lactic acid, which gives rise to certain distinct drawbacks. As a result, the internal pH in PLGA implants in vivo might drop to very low pH values. The very first report (using pH-sensitive nitroxides) on pH values inside preformed PLGA implants showed a time-dependent drop of pH values with final values of pH 2 [24]. Years later, using Optical Imaging (OI), pH drops from 7 to 3 were observed for in situ forming implants [25]. Highly acidic microenvironments (pH 3) were also measured in vitro for microparticles by Schwendeman et al. [26]. The low pH values can cause autocatalytic polymer degradation and degradation of various peptides and proteins [27–31].

Drug release profile from PLGA polymer can have multiple phases including (a) an initial burst phase (b) a lag (or induction), during which there is minimal polymer erosion, and drug release may be negligible and (c) an active erosion phase, characterized by continuous polymer mass loss and a sustained drug release pattern [23]. In a study performed by Mäder et al, the release pattern from PLGA implant was examined both in vitro and in vivo. Their research revealed the formation of an acidic liquid compartment at the core of the implant due to the accumulation of carboxylic groups. This acidic compartment (pH 4 to pH 2) with low viscosity can exert substantial influences on drug stability, solubility, bioavailability, pharmacokinetics, and, consequently, therapeutic efficacy. Bulk hydrolysis has been proposed as the dominating mechanism of release from PLGA implants, leading to a non-linear and complex release profile [24]. Marketed products frequently exhibit similar non-linear release profiles [24].

Risperdal Consta® is a PLGA-based controlled-release DDS of Risperidone for the treatment of schizophrenia. The formulation exhibits an undesirable two-week lag time, as demonstrated both in vitro and in vivo [32–35] (Figure 1). Consequently, patients are initially required to take tablets even though the formulation has already been injected [36]. As patients with schizophrenia often struggle with adherence to the therapy, the need for dual medication should be minimized to enhance treatment efficacy.

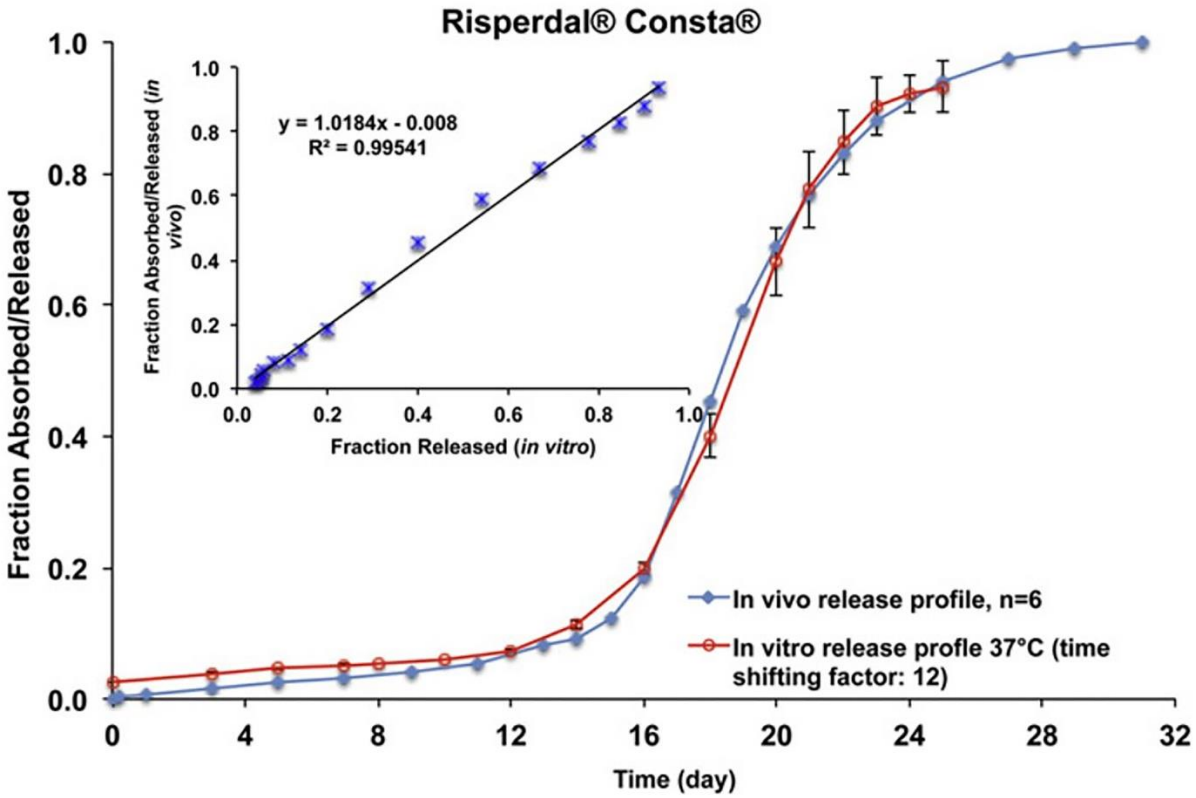

Figure 1. In vivo absorption/release and in vitro release profile of Risperdal Consta® in 10 mM PBS (Phosphate Buffered Saline). The inserted figure shows a linear correlation between fractions released in vitro (37 °C) and fraction absorbed/released in vivo [33].

In addition to the mentioned points, the encapsulation of the PLGA implant as a result of the host inflammatory response is reported by several studies which can compromise the function of the implant system and hinder the efficacy of the drug [37–39].

Considering the mentioned challenges associated with the PLA and PLGA, exploring alternative biodegradable materials becomes imperative for the advancement of future parenteral depot systems. Unfortunately, the selection possibility for biodegradable materials for the production of parenteral depot systems is rather limited. In the following section, current efforts to find alternative materials are explained briefly.

1.3 Current efforts for finding alternative materials

The synthesis of new polymers with less acidic monomers is one of the most extensively explored approaches to find alternative materials [40]. In a study conducted by Creemer et al., polyesteramide (PEA) microspheres loaded with triamcinolone acetate were produced and compared with PLGA microspheres. They noted a more favorable outcome with PEA microspheres when compared to PLGA [41]. Despite promising results emerging in this area, it's important to note that the development of new polymers that progress to clinical phases is highly resource-intensive and time-consuming due to the strong and demanding regulatory requirements which include acute and chronic toxicity studies in several animal species.

Lipids are the second major class of chemical compounds utilized in manufacturing DDSs [42]. They serve diverse roles. For example, they can be used as a carrier or they might have complementary roles such as an antifriction agent in tablet production [43]. Furthermore, lipids have been widely investigated for their potential in combination with polymers to form a controlled release system. In a study conducted by Steiner et al., fatty acid-modified poly(glycerol adipate) was utilized to produce microparticles loaded with dibenzoyl thiamine using a solvent evaporation process. Their study demonstrated the ability of poly(glycerol adipate)-behenic acid microparticles to provide a sustained release of dibenzoyl thiamine over a two-week period [44]. Lipids have not only been investigated in combination with polymers but also as standalone components in forming controlled release systems. Manufacturing lipid implants by compression was the production method of choice in the early stages of this technology because it was considered fast and uncomplicated [45,46]. Nowadays, production primarily relies on HME, utilizing either single- or twin-screw devices. This process facilitates achieving a more uniform distribution of the drug within the implant in comparison to other methods [47]. However, employing solid lipids presents certain common challenges, including issues related to polymorphic transitions and limited enzymatic degradability due to the crystalline structure of lipids [48]. Additionally, the production of lipid blends with drugs by melting and casting involves higher temperatures than those used in extrusion processes, which can lead to instabilities in the active pharmaceutical ingredients (APIs) [49]. As a result, the ongoing research for alternative materials remains imperative in addressing these challenges. It was therefore the main aim of the thesis to explore the potential of starch as an alternative to PLGA for the formation of biodegradable implants.

1.4 Starch and starch-lipid complexes

Starch is the second most abundant biopolymer on earth and a major energy storage reserve carbohydrate synthesized in many parts of plants [50]. Starch (nonmodified form) is in general fully biodegradable. Its degradation in the body produces non-toxic and non-acidic monomers [51]. Starch-based materials are already clinically used as bioresorbable medical products for providing hemostasis and preventing postoperative tissue adhesion [52,53]. It is also a major excipient in the pharmaceutical industry but is mainly used for oral formulations due to its certain drawbacks such as weak mechanical properties and rapid degradation in the body over a few days. Therefore, if it can be modified it could be a valuable alternative to PLA/PLGA, aligning with the principles of green and sustainable industry.

Starch granules are mainly composed of amylose and amylopectin. Proteins, lipids and minerals are the minor components of starch [54,55]. The amylose/amylopectin (AM/AP) ratio in starch granules, alongside their molecular structure, influences starch processability parameters including the gelatinization temperature, viscosity, gelation and final product's characteristics [56]. In general, the ratio of AM/AP and their structural variability strongly depend on the botanical origin. Conventional starches typically contain around 70–80% amylopectin and 20–30% amylose, while waxy starches exhibit less than 10% amylose, and high-amylose starches contain more than 40% amylose [55]. Amylose has a linear structure with α-1,4 glycosidic bonds, whereas amylopectin has a highly branched structure with α-1,4 and α-1,6 glycosidic bonds. These components produce a semi-crystalline structure in starch granules, and the crystalline regions are attributed to the formation and packing of double helices of the branches in amylopectin (Figure 2) [57].

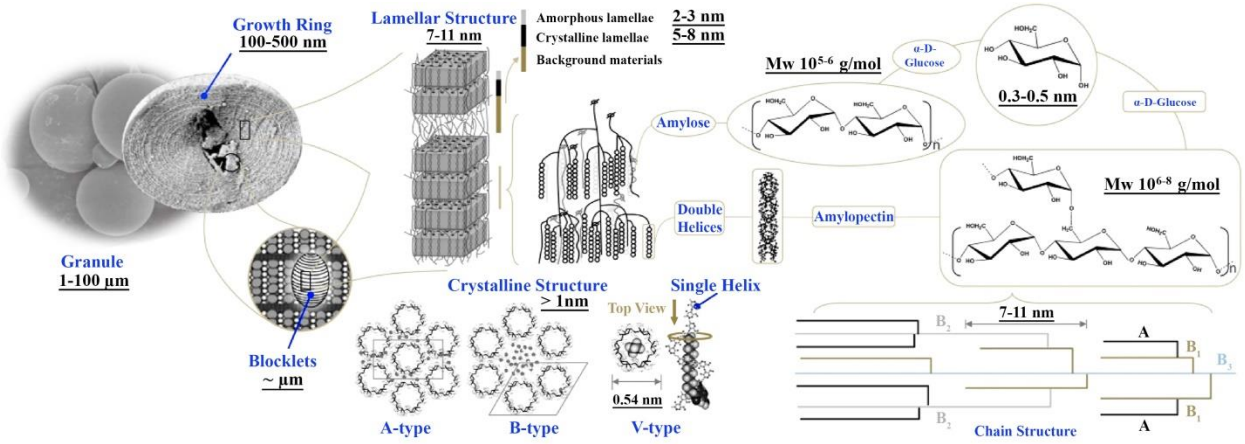

Figure 2. The schematic representation of starch hierarchical structures. Amylose binds with hydrophobic guest molecules and forms V-type crystals. Amylopectin associates to form double helices and then arranges into A- or B-type crystals. The orderly-packed A- or B-type crystals and double helices contribute to the formation of lamellar structures that are stacked with amorphous lamellae and crystalline lamellae. Growth rings and blocklets are semi-crystalline structures with alternating stacks of amorphous and crystalline lamellae [58].

Starch properties can be modified using chemical or physical modifications [59]. Extensive research has been conducted on the chemical modifications of starch, encompassing techniques such as esterification, etherification, crosslinking, grafting, and condensing reactions. These methods aim to substitute the hydrophilic OH groups of the starch with hydrophobic groups. Modified starches exhibiting excellent hydrophobicity play an increasingly vital role in the advancement and utilization of novel biomaterials, particularly in the fields of packaging and pharmaceutical applications. However, the substantial use of organic solvents in the chemical modifications of starch is not in line with green and sustainable chemistry. Consequently, alternative environmentally friendly methods, such as reactive extrusion, high hydrostatic pressure treatment, and enzyme modification, have been explored. Nevertheless, these approaches have limitations due to their rigorous conditions or equipment requirements [60]. Compared to chemical modifications, physical modifications of starch are simple, cost-effective and eco-friendly [61]. Hence, this study focuses on the physical modification of starch, aligning with the goals of a greener and more sustainable production procedure.

Physical modifications of starch have been implemented by changing the temperature, pressure, humidity and shear stress. When starch granules are heated in the presence of water and other molecules such as plasticizers, several changes at the molecular and

structural levels occur. These alterations of the starch structure are related to the granule-specific gelatinization behavior, which is strongly affected by several inherent characteristics including granule composition (in particular the AM/AP ratio), granule size, granule molecular architecture (especially the amylopectin branch chain lengths and distribution) and molecular weight of amylose and amylopectin molecules [62,63]. The progress and extent of the thermal gelatinization of starch are also affected by a wide range of external factors, including temperature, moisture content, heating time, heating rate, shear stress, presence of further ingredients such as plasticizer, the amount and type of plasticizer, starch preparation and storage conditions [64,65]. Amylopectin is suggested to be responsible for granule swelling while the fraction of amylose–lipid complexes may retard the swelling and induce an increase in gelatinization temperature [62].

The addition of components such as proteins, lipids, and nonstarch polysaccharides represents another important aspect of physical modifications. Studies have shown that starch can form complexes with certain lipids such as fatty acids or mono-glycerides, and this lipid complexation can be facilitated at elevated temperatures through an extrusion [66,67]. The formation and stabilization of these complexes involve a series of noncovalent interactions including hydrogen bonds, hydrophobic attractions, and van der Waals forces [68–70]. The hydrophilic hydroxyl groups of α[1→4] glucan helices are arranged on the outer surface, whereas methylene groups and the oxygens of the glucosidic bonds line the inner core forming a hydrophobic cavity that can accommodate suitable ligands. Comprehensive studies of starch-lipid complexes using techniques such as X-ray diffraction (XRD), Raman spectroscopy, nuclear magnetic resonance (NMR) spectroscopy, and molecular modelling reveal that the aliphatic chain of the lipid inserts itself into the internal cavity of the amylose helix. In contrast, the carboxyl group of the fatty acid or the glyceride moiety of a monoacylglycerol remains exposed on the exterior of the helix due to steric hindrance and electrostatic repulsions (Figure 3) [71–73].

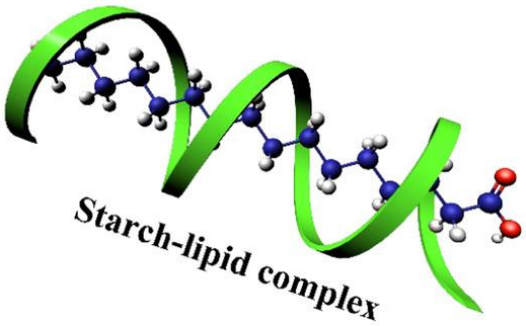

Figure 3. Schematic structure of starch–lipid complex at the molecular level (after [74]).

It has been reported that the formation of starch-lipid complexes makes starch more resistant to enzymatic digestion [75,76]. Introducing lipids into starch is therefore a rational approach to decrease enzymatic degradation and to slow down the drug release. It was therefore one goal of the thesis to study the impact of lipid addition on starch-based implant characteristics.

1.5 Parenteral depot systems characterization methods

For the development of an optimized DDS, it is essential to characterize it with suitable characterization techniques. The characterization methods can be divided into three main categories: 1. Methods for the general physicochemical characterization, 2. Methods for the characterization of the microenvironment (microviscosity, micropolarity, and microacidity) and 3. Methods for in vivo characterization [3].

1.5.1 Characterization methods for the general physicochemical properties

Differential scanning calorimetry (DSC) is an analytical technique employed to monitor thermal events, including melting, crystallization processes and the glass transition temperature. As mentioned earlier, HME is the most used method to prepare the preformed implants. The formed implant is a solid dispersion in which a drug is dispersed in the polymeric matrix. The system can have multiple structures depending on the components' characteristics and the production parameters (Figure 4). It is important to know if the drug is incorporated as a crystalline solid or in the amorphous form. Many drug molecules

exhibit various polymorphs, each with distinct dissolution kinetics. In most cases, the polymorphs can be traced by DSC due to their different melting points. The presence or absence of amorphous drug molecules or distinct polymorphs depends on the production and storage conditions.

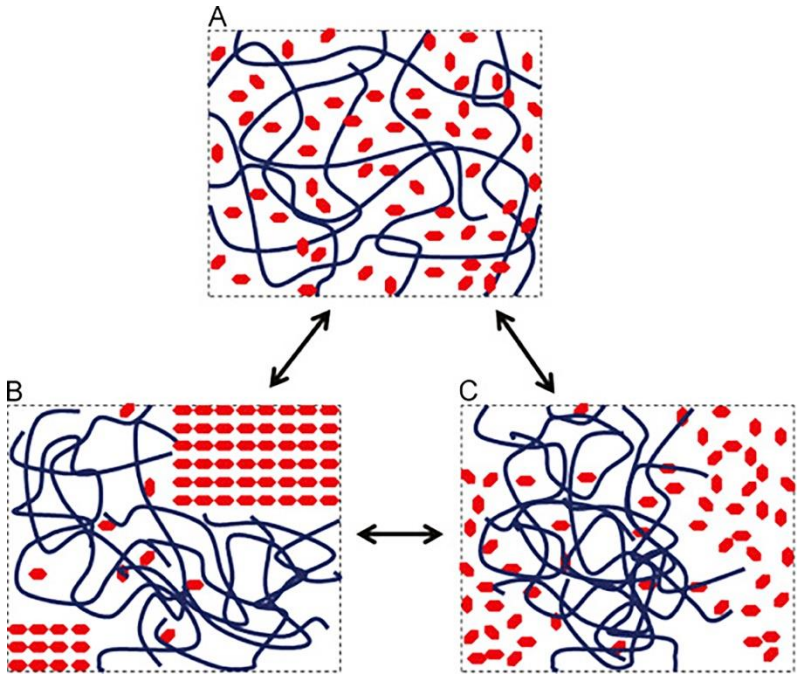

Figure 4. The three possible structures of a drug/polymer solid dispersion where hexagonal symbols represent drug molecules and curvy lines represent polymer chains. A) The drug is molecularly dispersed in the polymer matrix. B) crystalline and amorphous drug inside the polymer matrix. C) a drug-polymer system containing amorphous drug-rich domains dispersed in the polymer matrix [77].

X-ray diffraction is another widely utilized method in the characterization of solid dispersions. Using this method, it is possible to confirm the presence of crystalline materials and identify various polymorphs. Other spectroscopic techniques including **infrared (IR)**, **near-IR (NIR)**, **Raman spectroscopy**, **Terahertz spectroscopy,** or **solid-state Nuclear Magnetic Resonance (NMR)** are employed less frequently, but they can provide valuable insights into the physical state of materials within the DDS [3].

1.5.2 Characterization of the microenvironment (microviscosity, micropolarity, and microacidity)

The monitoring of the microenvironment is a determining aspect of the optimization of parenteral depot systems. Frequently, diverse microenvironments coexist within microparticles or implants. Key components of the microenvironment include microviscosity, micropolarity, and microacidity. Several potent techniques to obtain information about microviscosity are based on NMR and Electron Paramagnetic Resonance (EPR). NMR requires a nuclear spin, while EPR requires the presence of an electron spin. The majority of the DDSs are EPR-silent. The electron spins can be introduced either noncovalently as spin probes or covalently attached (e.g., to polymers) as spin labels. Nitroxides are commonly employed spin probes, offering a wide range of options with varying hydrophilicities. The spectrum of nitroxide probes results from the anisotropic interaction of the electron spin with the nuclear spin of the nitrogen molecule. The EPR spectrum is sensitive to mobility as illustrated in Figure 5.

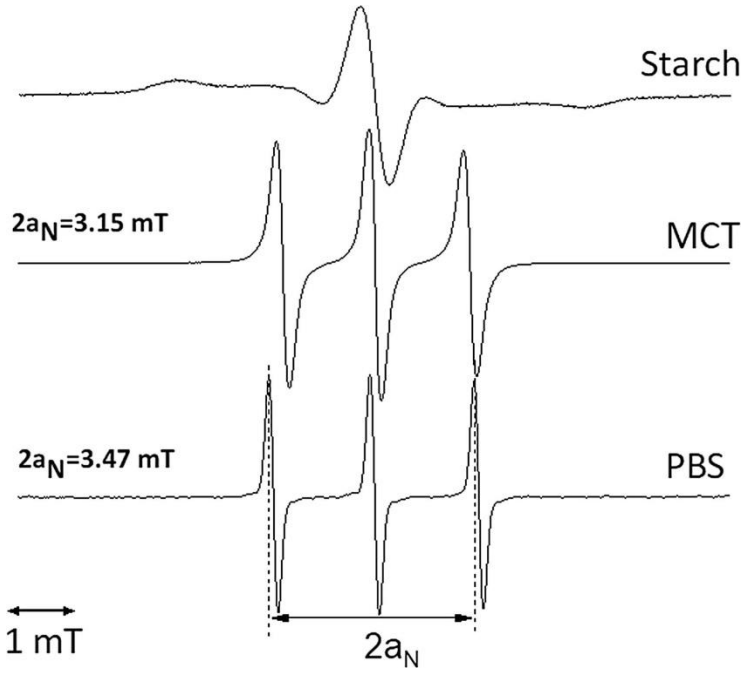

Figure 5. EPR spectrum of TB in starch (powder-like spectrum), Medium-chain triglycerides (MCT) (less polar environment, shorter distance between the outer lines, $2a_N$ = 3.15 mT) and PBS (polar environment with longer distance between the outer lines, $2a_N$ = 3.47 mT) [78].

In solid materials, the anisotropic spectrum with broad lines and the dominating centerline is observed (top spectrum). In liquids, three lines emerge as a result of a partial (viscous media) or almost complete (low viscous media) averaging of the anisotropy of the hyperfine splitting. The spacing between these three lines in liquid samples depends on the polarity of the environment (see dotted line). Larger values are observed in polar media. The different polarity of the environments is reflected in the different hyperfine coupling constants a_N. EPR spectroscopy can also be used to monitor drug release mechanisms. This application is explained in detail in Chapter 3.1.

In contrast to EPR, NMR spectroscopy and imaging find much broader applications in both preclinical and clinical research. This preference is attributed to several factors, which include 1. the higher penetration depth of the frequency, 2. the development of pulsed methods (challenging to implement in EPR due to the short half relaxation times), and 3. the use of inherent signals (e.g., protons). The NMR properties are closely linked to the mobility of molecules. When it comes to solid materials, standard NMR cannot be employed; instead, solid-state NMR is utilized for characterization [79]

By variation of the NMR sequence, different properties (relaxation times and diffusion coefficients) can be obtained, including their spatial distribution. In many instances, it's possible to attribute these signals to distinct molecule groups or segments, such as aromatic protons from the drug, PEG chains, polymer degradation products, and other excipients. The low-cost and low-frequency benchtop NMR systems are valuable tools to measure relaxation times and diffusion coefficients, which change during hydration and release processes. The information obtained by benchtop NMR is often less specific compared with high-field NMR but easy to measure and useful. However, it is characterized by its ease of measurement and practical usefulness. Some instruments also permit imaging [3,80,81]. In this project, a low-frequency benchtop NMR system has been used to evaluate water penetration into the system. A detailed explanation is provided in chapter 3.2.

1.5.3 Methods for in vivo characterization

Despite all the efforts to simulate in vivo conditions using in vitro tests, numerous reports highlight poor correlations between in vitro and in vivo results. These discrepancies arise from distinct environmental factors, such as varying volumes, the presence or absence of surface-active components, and differing pH values, as well as the influence of cells and enzymes on degradation and release processes. For example, implants could be encapsulated by fibrous tissue and smaller microparticles could be phagocytosed by macrophages. Therefore, it is important to monitor release processes in vivo. Preferred

methods are noninvasive and provide specific information about important parameters of drug release. Some methods include EPR, NMR, ultrasound imaging, OI, computed tomography (CT), and radioactive methods [3]. In this thesis, OI is utilized to evaluate the fate of the optimized system in vivo. A detailed explanation is provided in chapter 3.3.

1.6 Aim of work

The main objective of the thesis was the development of a starch-based DDS for parenteral controlled drug release applications as alternative for PLA/PLGA DDS. This objective setting was focused on the following three pillars:

1. **Identification of suitable starch/lipid mixtures and optimization of processing parameters of HME.**

   As mentioned earlier, starch characteristics need to be modified using physical modifications during the extrusion process. These modifications are strongly affected by several inherent starch characteristics [62,63]. Therefore, **finding an appropriate type of starch and lipid and optimization of HME parameters to achieve a controlled release system was a primary step of the thesis.** As mentioned earlier, the addition of the lipid to the system can strongly influence the structure and the characteristics of extruded products [82]. Therefore, to assess the effect of the addition of the lipid to the system, the **characterization of the system with and without lipid** was the second step of the project. As the rate of water penetration into the system is a crucial step in the prediction of the release profile from the system, **evaluation of water penetration and swelling of the two systems using EPR and NMR relaxometry** were the further steps of the project.

2. **Characterization of controlled-release starch-nimodipine implant**

   Subarachnoid haemorrhage (SAH) is a serious, life-threatening type of stroke where cerebral vasospasm remains a serious complication and a major cause of death and disability in these patients. Nimotop® (Nimodipine 30 mg capsule, Bayer) is an FDA-(Food and Drug Administration) approved drug for the treatment of SAH-induced vasospasm [83]. Nimodipine (NMD) is a hydrophobic API with very low oral bioavailability, reported to range from 3 to 30%, exhibiting extensive variability among patients [84–86]. Therefore, a parenteral depot of NMD with the ability to release the drug over the desired period is needed. With the aim of achieving a parenteral depot with the desired characteristics, NMD was loaded in the optimized

formulation and subsequently characterized. Most of the analytical techniques applied for the characterization of solid dispersions only focus on the API. However, the polymeric carrier contributes to the performance of the formulation to a great extent. Therefore, the **effect of the production process both on NMD and starch** characteristics was studied. The system was characterized with and without the API using different analytical techniques. Moreover, **interactions between starch and NMD were evaluated using NMR and IR spectroscopy**. **The possible effects of NMD on the polymer** were also investigated using DSC and SEM. In addition, the release kinetics from the systems with different NMD content was studied to evaluate the impact of drug properties and drug load on the release rate. As the prepared system is going to be administered parenterally, finding an appropriate sterilization method was of great importance. Based on ICH guidelines "For those products intended to be sterile, an appropriate method of sterilization for the drug product and primary packaging material should be chosen and the choice justified" [87]. **The effect of the chosen sterilization method on the NMD and the polymer was also investigated using NMR spectroscopy**.

3. **In vivo evaluation of the starch-based implant (Release profile/fate of the system)**

   Despite all the efforts to simulate in vivo conditions using in vitro tests, numerous reports highlight poor correlations between in vitro and in vivo results. Therefore, it is important to monitor release processes in vivo. Before in vivo studies, the system's ability to create a controlled release system was proved using various in vitro tests, and a suitable sterilization method was identified. Surpisingly, there were no previous reports on the in vivo release profile of parenterally administered starch-based implants. **Optical imaging** as a non-invasive and commonly used technique in the visualization of in vivo processes, was used. OI necessitates **selecting suitable dyes and their appropriate concentrations to visualize the implant** formulation. Therefore, in this part of the project appropriate fluorescent dyes were selected, the appropriate concentration for each dye was determined and the SC-injected implant was visualized. The release kinetics of dyes, namely Indocyanine Green (ICG) and 1,1′-Dioctadecyl-3,3,3′,3′-Tetramethylindotricarbocyanine-Iodide(DiR) loaded into the implant as models of a hydrophilic and hydrophobic drug, were evaluated. Moreover, the possibility of quantification and evaluation of the release kinetics by

3-dimensional **(3D) reconstructions of the implants** was assessed and compared to 2-dimensional (2D) quantifications in vivo.

2. Cumulative part

2.1 Overview of journals

Table 1. Overview of journals where peer-reviewed articles were published

Journal	Impact factor (2023)	5-year impact factor	Publisher
International Journal of Pharmaceutics	**6.51**	**6.05**	**Elsevier**
Molecular Pharmaceutics	**5.36**	**4.82**	**American Chemical Society**
Journal of Controlled Release	**11.467**	**10.38**	**Elsevier**

2.2 Peer-reviewed publications

The three publications described in this section were subject to a peer-review publication process as full research articles. They have been published in the journals listed above (Table 1). These publications reflect the major part of the experiments that were conducted in the course of this doctoral thesis. As such, all methods used are described in detail in the articles and the results acquired were carefully discussed.

In **publication I**, two aims were achieved: 1. Identification of the appropriate type of starch and lipid to be implemented in further steps, 2. Optimization of HME parameters to acquire a homogenous, physically stable implant. The experimental work of this publication can be divided into two main parts. In the first part, the EPR method is implemented to evaluate the potential of the system in the formation of a controlled release system. One key benefit of EPR lies in its remarkable sensitivity to spin probes, even at extremely low concentrations, typically within the range of 5-10 mM. Given that the introduction of an active substance can potentially change the system's properties, the method's high sensitivity and the use of very low concentrations of the spin probe serve to assess the intrinsic attributes of the carrier with minimal influence from the active substance. Two spin probes, namely Tempol (TL) and Tempol Benzoate (TB), were loaded into the implants as a model of hydrophilic and hydrophobic drugs respectively. The release profile of the

spin probes provides us with valuable information regarding several critical aspects, including the rate of water penetration into the implant, as well as the micropolarity and microviscosity within the system. These parameters help us better understand the involved release mechanisms and predict the release profile of a real drug from the implant. In the second part of the publication, two antimalarial agents namely artesunate (AS) and artemether (AM) were loaded into the implants and the implants were characterized with different methods. The selection of formulation compositions aimed to assess how varying the lipid amount influences the release profile of the active substance. The results of this publication provided us with two crucial pieces of information: 1) Starch implant has the potential to provide a sustained release of a hydrophobic substance if the starch is gelatinized during the extrusion process. 2) The presence of lipid in the formulation prevents starch gelatinization at the used temperatures (Due to the thermal sensitivity of many drugs, it is not desirable to use temperatures higher than 90 °C, the maximum used temperature in the study for starch implants without API). As the experiments confirmed the potential of starch implant in the formation of a controlled release system, this system was chosen for further studies.

Publication II focuses on the comprehensive characterization of starch implants and nimodipine-loaded implants. The primary objective was to develop a parenteral depot of NMD for the treatment of SAH-induced vasospasm. For this purpose, NMD was incorporated into the optimized formulation. To assess the impact of drug load on the system, two formulations with 20% and 40% NMD were prepared and characterized. NMR relaxometry was employed to evaluate the water penetration into the systems providing a better understanding of possible release mechanisms. As NMD has different modifications, various techniques including DSC, IR and Raman Spectroscopy were applied to investigate possible changes in these modifications during the extrusion process. Additionally, different techniques were utilized to assess the potential effects of the API (NMD) on the polymeric system and vice versa. As the system was designed for parenteral administration, finding an appropriate sterilization method was of utmost importance. Challenges in finding a suitable method for the sterilization of the NMD-loaded system have been reported previously due to the instability of the NMD during the sterilization process [88]. This publication confirms the ability of the developed system to protect NMD during the production and sterilization process.

Publication III is a detailed explanation of the in vivo studies with starch implant. To the best of our knowledge, there were no previous reports and information regarding the in

vivo release profile of parenterally administered starch implants. In vivo studies were required to ensure the potential of the system in providing a biocompatible, biodegradable sustained release system in vivo. In this part of the project, OI as a non-invasive technique was used. Two fluorescent dyes, namely ICG and DiR, were incorporated into the implants as a model of a hydrophilic and hydrophobic drug, respectively. The release profiles of the two substances from the implants were assessed in vitro and in vivo. The in vivo imaging was performed both in 2D and 3D mode. The 3D mode permitted the 3D reconstruction of the SC-injected implant. Here, the 3D reconstruction was used for a very small implant with a regular shape. This can be expanded to the use of 3D reconstruction for the visualization of in vivo forming implants and to assess the release kinetics in 3D mode from these systems in the future. The results of this study confirmed the biodegradability and biocompatibility of the starch implant and its potential to form a controlled release system for a hydrophobic drug.

Declaration of own contribution to the original articles presented in this thesis:

A: Planning, execution, analysis and evaluation of the corresponding experiments, B: Contribution to the manuscript

I. **Esfahani, G.**, Häusler, O. and Mäder, K., 2022. Controlled release starch-lipid implant for the therapy of severe malaria. International Journal of Pharmaceutics, 622, p.121879.

A: 90%, B: 85%

II. **Esfahani, G.**, Trutschel, M.L., Reichert, D. and Mäder, K., 2023. Characterization of Controlled Release Starch-Nimodipine Implant for Antispasmodic and Neuroprotective Therapies in the Brain. Molecular Pharmaceutics.

A: 80%, B: 85%

III. **Esfahani, G.**, Lucas, H., Syrowatka, F. and Mäder, K., 2023. A starch-based implant as a controlled drug release system: Non-invasive in vivo characterization using multispectral fluorescence imaging. Journal of Controlled Release, 358, pp.358-367.

A: 80%, B: 85%

2.2.1 Identification of suitable starch/lipid mixtures and optimization of processing parameters of HME.

Title: Controlled release starch-lipid implant for the therapy of severe malaria

International Journal of Pharmaceutics

DOI: https://doi.org/10.1016/j.ijpharm.2022.121879

Link: https://www.sciencedirect.com/science/article/pii/S0378517322004343

Abstract

Parenteral depot systems can provide a constant release of drugs over a few days to months. Poly(lactic acid) (PLA) and Poly(lactide-co-glycolide) (PLGA) are the most commonly used polymers in the production of these systems. Finding alternatives to these polymers is of great importance to avoid certain drawbacks of these polymers (e.g. microacidity) and to increase the selection possibilities. In this study, different types of starch in combination with glycerol monostearate (GMS) were developed and investigated for their physicochemical properties and release characteristics. The noninvasive method of electron paramagnetic resonance (EPR) was used to study the release kinetics and mechanisms of nitroxide model drugs. The studies demonstrated the general suitability of the system composed of high AM starch and GMS to form a controlled release system. For further characterization of the prepared system, formulations with different proportions of starch and GMS, loaded with the antimalarial agents artesunate or artemether were prepared. The implants were characterized with X-ray powder diffraction (XRPD) and texture analysis. The in vitro release studies demonstrated the sustained release of artemether over 6 days from a starch-based implant which matches desired kinetic for the treatment of severe malaria. In summary, a starch-based implant with appropriate mechanical properties was produced that can be a potential candidate for the treatment of severe malaria.

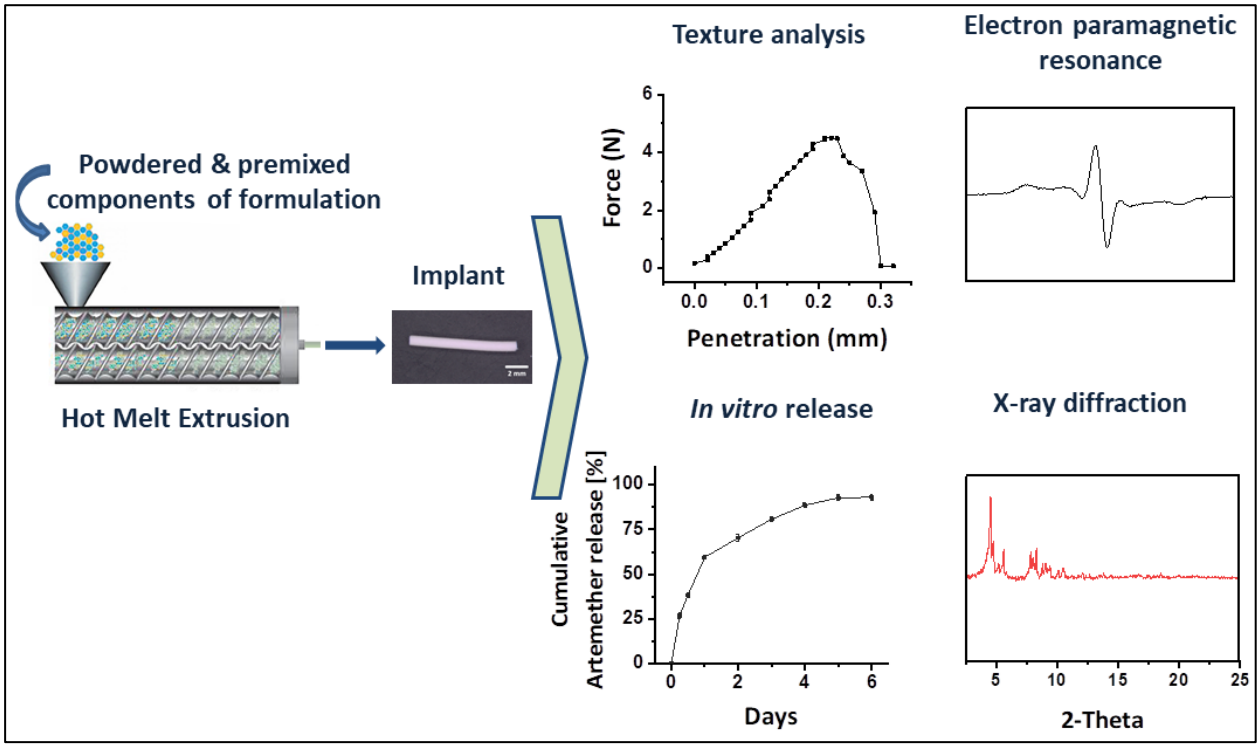

Figure 6. Graphical abstract to Esfahani et al. [78].

2.2.2 Characterization of controlled release starch-nimodipine implant.

Title: Characterization of Controlled Release Starch-Nimodipine Implant for Antispasmodic and Neuroprotective Therapies in the Brain

Molecular Pharmaceutics

DOI: https://doi.org/10.1021/acs.molpharmaceut.3c00618

Link: https://pubs.acs.org/doi/full/10.1021/acs.molpharmaceut.3c00618

Abstract

Parenteral depot systems can provide a constant release of drugs over a few days to months. Most of the parenteral depot products on the market are based on poly(lactic acid) and poly(lactide-co-glycolide) (PLGA). Studies have shown that acidic monomers of these polymers can lead to nonlinear release profiles or even drug inactivation before release. Therefore, finding alternatives for these polymers is of great importance. Our previous study showed the potential of starch as a natural and biodegradable polymer to form a controlled release system. Subarachnoid hemorrhage (SAH) is a life-threatening type of stroke and a major cause of death and disability in patients. Nimotop® (nimodipine (NMD)) is an FDA-approved drug for treating SAH-induced vasospasms. In addition, NMD has, in contrast to other Ca antagonists, unique neuroprotective effects. The oral administration of NMD is linked to variable absorption and systemic side effects. Therefore, the development of a local parenteral depot formulation is desirable. To avoid the formation of an acidic microenvironment and autocatalytic polymer degradation, we avoided PLGA as a matrix and investigated starch as an alternative. Implants with drug loads of 20 and 40% NMD were prepared by hot melt extrusion (HME) and sterilized with an electron beam. The effects of HME and electron beam on NMD and starch were evaluated with NMR, IR, and Raman spectroscopy. The release profile of NMD from the systems was assessed by high-performance liquid chromatography. Different spectroscopy methods confirmed the stability of NMD during the sterilization process. The homogeneity of the produced system was proven by Raman spectroscopy and scanning electron microscopy images. In vitro release studies demonstrated the sustained release of NMD over more than 3 months from both NMD systems. In summary, homogeneous nimodipine-starch implants were produced and characterized, which can be used for therapeutic purposes in the brain.

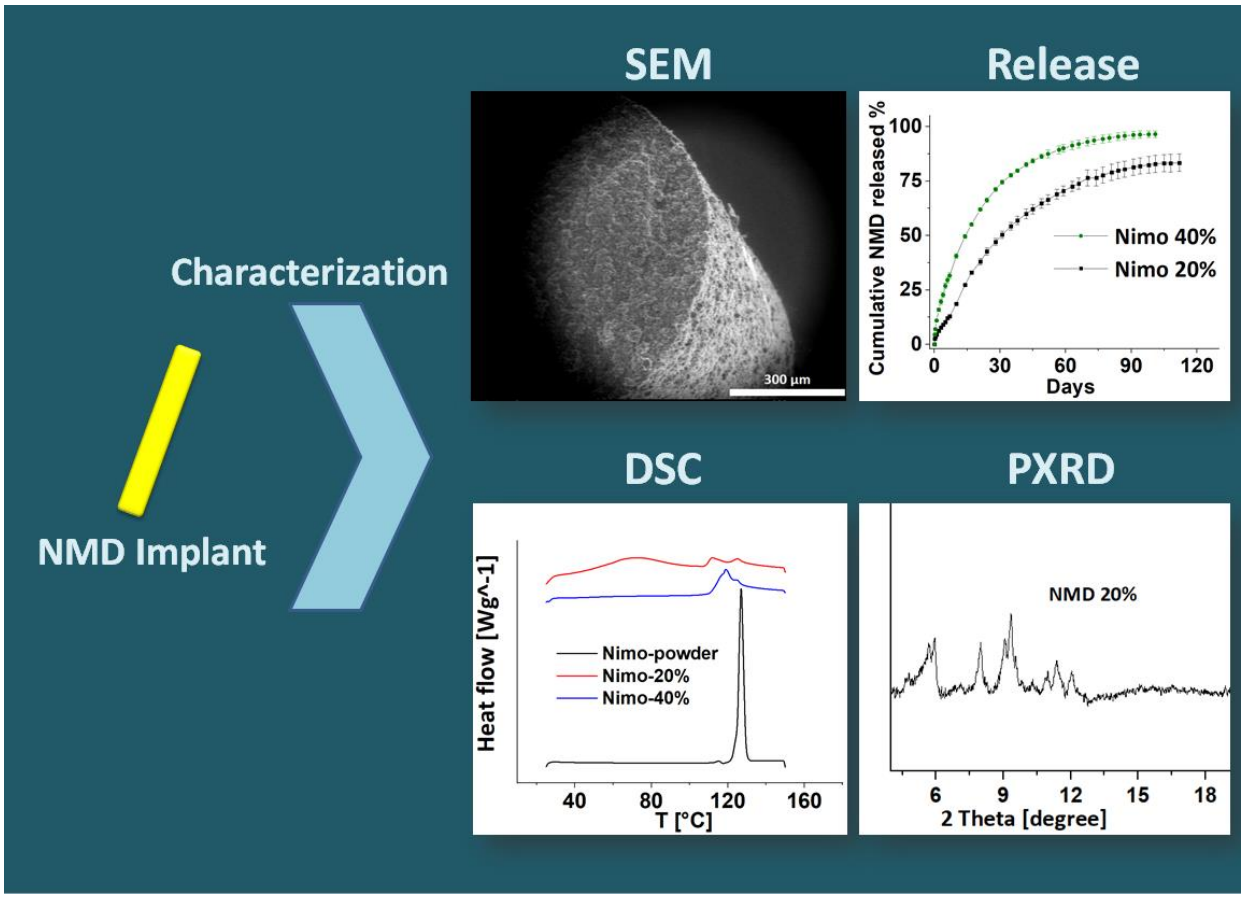

Figure 7. Graphical abstract to Esfahani et al. [89].

2.2.3 In vivo evaluation of the starch-based implant (Release profile/fate of the system)

Title: A starch-based implant as a controlled drug release system: non-invasive in vivo characterization using multispectral fluorescence imaging.

Journal of Controlled Release

DOI: https://doi.org/10.1016/j.jconrel.2023.05.006

Link: https://www.sciencedirect.com/science/article/pii/S016836592300319X

Abstract

Solid implants are parenteral depot systems that can provide a controlled release of drugs in the desired body area over a few days to months. Finding an alternative for the two most commonly used polymers in the production of parenteral depot systems, namely Poly(lactic acid) (PLA) and Poly(lactide-co-glycolide) (PLGA), is of great importance due to their certain drawbacks. Our previous study showed the general suitability of starch-based implants for controlled drug release. system. In this study, the system is further characterized and the release kinetics are investigated in vitro and in vivo by fluorescence imaging (FI). ICG and DiR, two fluorescent dyes with different hydrophobicity serving as a model for hydrophilic and hydrophobic drugs, have been used. In addition to 2D FI, 3D reconstructions of the starch implant were also used to assess the release kinetics in 3D mode. The in vitro and in vivo studies showed a fast release of ICG and a sustained release of DiR over 30 days from the starch-based implant. No treatment-related adverse effects were observed in mice. Our results indicate the promising potential of the biodegradable biocompatible starch-based implant for the controlled release of hydrophobic drugs.

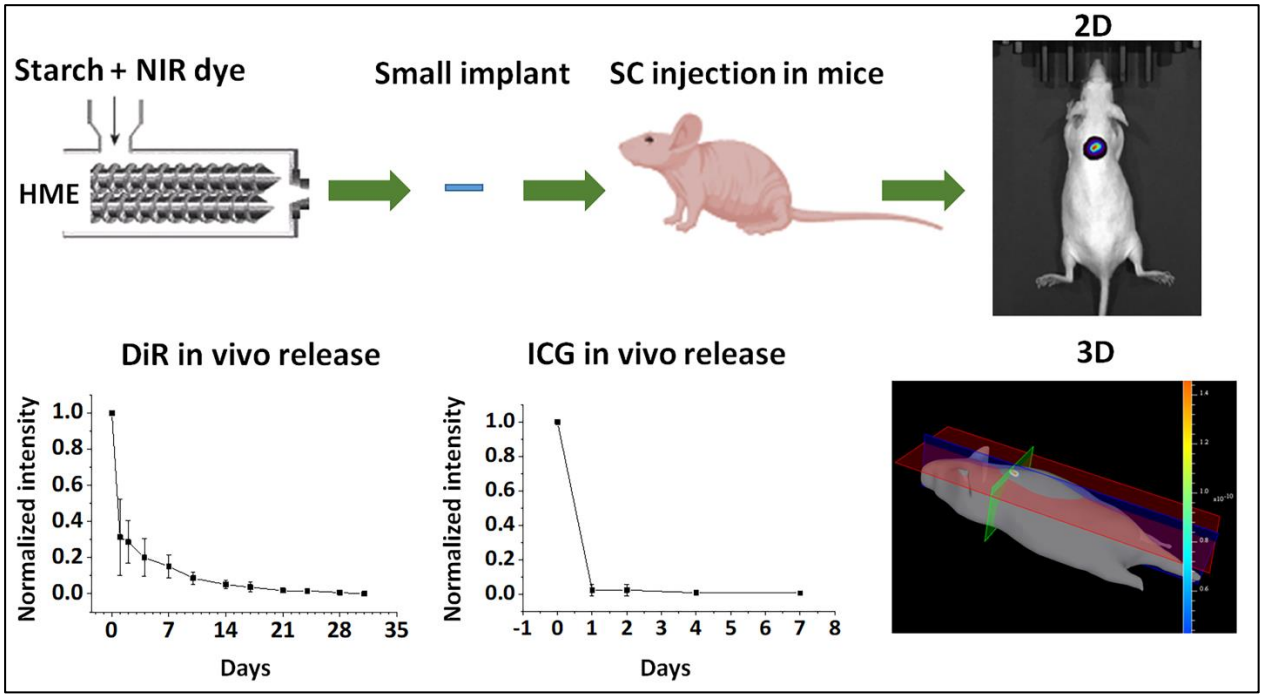

Figure 8. Graphical abstract to Esfahani et al. [90].

3. Results and Discussion

3.1 Identification of suitable starch/lipid mixtures and optimization of processing parameters of HME

This thesis aimed to develop and characterize a controlled drug release system based on starch as an alternative for PLA/PLGA polymers. Native starches come from different botanic origins and therefore, own various physical properties, such as different gelatinization temperatures. Hence, choosing an appropriate type of starch for the formation of a controlled release system was an important step in prescreening studies. It should also be considered that both pressure and temperature of the HME process and the water content can alter the thermal properties of starch significantly [91–93]. These parameters affect the mechanical properties of the final product. Therefore, finding an optimized temperature and extrusion speed, as well as the right water content was another critical step in prescreening studies. At this stage two criteria were considered for choosing the appropriate materials: a) Homogeneity of the prepared implant, and b) Physical stability of the prepared implant at 37 °C in a shaking water bath (50 rpm). Based on these results high-amylose starch (Amylo-N400®) and glycerol monostearate (IMWITOR 491®) were chosen. To investigate the effect of the addition of the lipid to the system, two different implants one containing only starch and the other containing starch and lipid (GMS) (4:3) were produced by HME with heating zone temperatures of 70, 80 and 90 °C. In the next step, the capability of the produced systems in the formation of a controlled release system was evaluated by EPR.

Two spin probes with different hydrophilicities, namely tempol (TL) and tempol benzoate (TB), were loaded separately into both systems and the release profile of each spin probe was evaluated. TL and TB were used as models for hydrophilic and hydrophobic drugs (Figure 9).

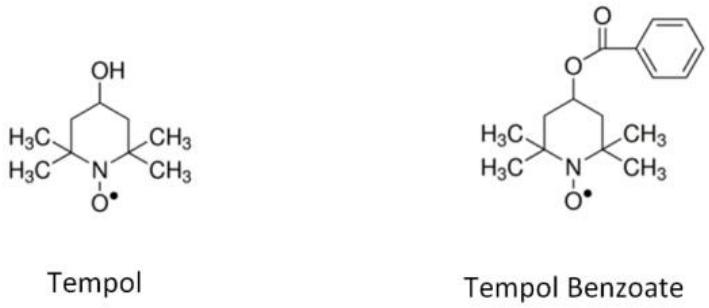

Figure 9. Chemical structure of tempol, and tempol benzoate.

EPR spectra are sensitive to the rotational motion of the spin probes. Polarity and microviscosity are the parameters that affect the spin probe's rotational motion and therefore the shape of the EPR spectra. Higher polarities cause larger distances between the lines of the spectra. In low viscous media, the spin probes tumble freely resulting in spectra with three narrow lines of approximately equal height that can be seen in spectra of TB in PBS. As the viscosity increases, due to slower motions, the lines broaden and the signal amplitude decreases [94]. In a solution, anisotropic interactions are averaged out and the line's widths are narrower compared to less mobile and more viscous systems. In solid materials, the anisotropy is not averaged and typical ''powder spectra" can be recorded [95,96]. The EPR spectrum of TB loaded implant made of starch shows a ''powder like spectra" due to immobilization of TB inside the solid system. Figure 10 shows the EPR spectra of TB-loaded implants in the dry state and after different times of exposure to PBS. The EPR spectra are magnified by the mentioned number next to each signal to make the comparison easier. A decrease in the signal amplitude of both implants was observed over two weeks which shows the extended release of the TB from both implants. Comparing the two implants, it can be seen that the starch-lipid implant shows a slower release rate. This is probably due to slower water penetration into this system. The release of TB from the starch implant was almost completed after 14 days. After this time, only a very noisy signal was observed, due to the very low remaining amount of TB inside the implant. In contrast, no decrease in the signal amplitude of the starch-lipid implant was observed after the 15th day. This is probably due to the part of the TB that is trapped in the lipid part of the implant, which is not released from the system during this in vitro time period.

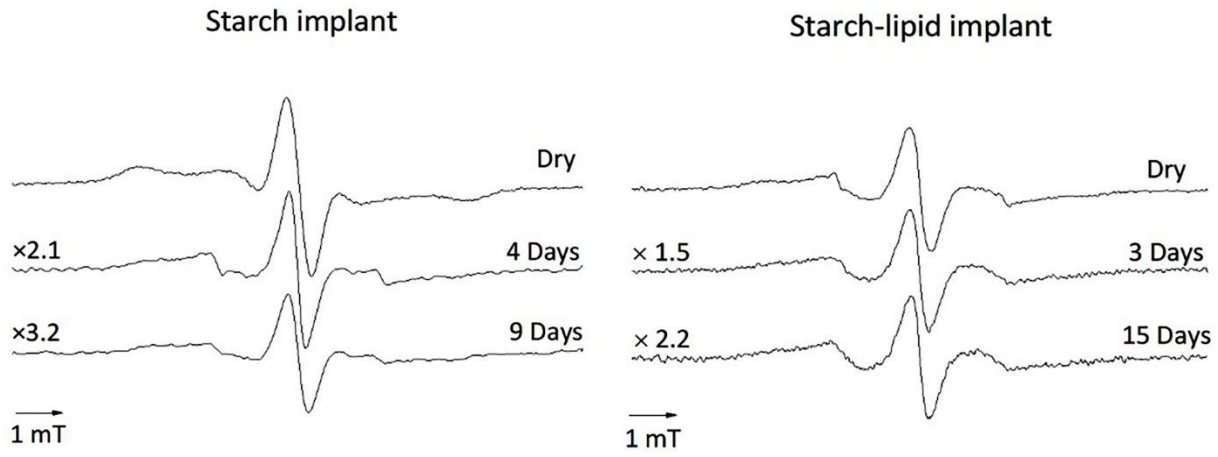

Figure 10. EPR-Spectra of TB-loaded implants after different times of exposure to PBS.

In the next step, TL as a hydrophilic spin probe was used to assess the water penetration into the implants in more detail. Figure 11 shows the EPR spectra of the TL-loaded implants in the dry state and after different exposure times to PBS. The EPR spectrum of the TL in PBS is shown to make the comparison easier.

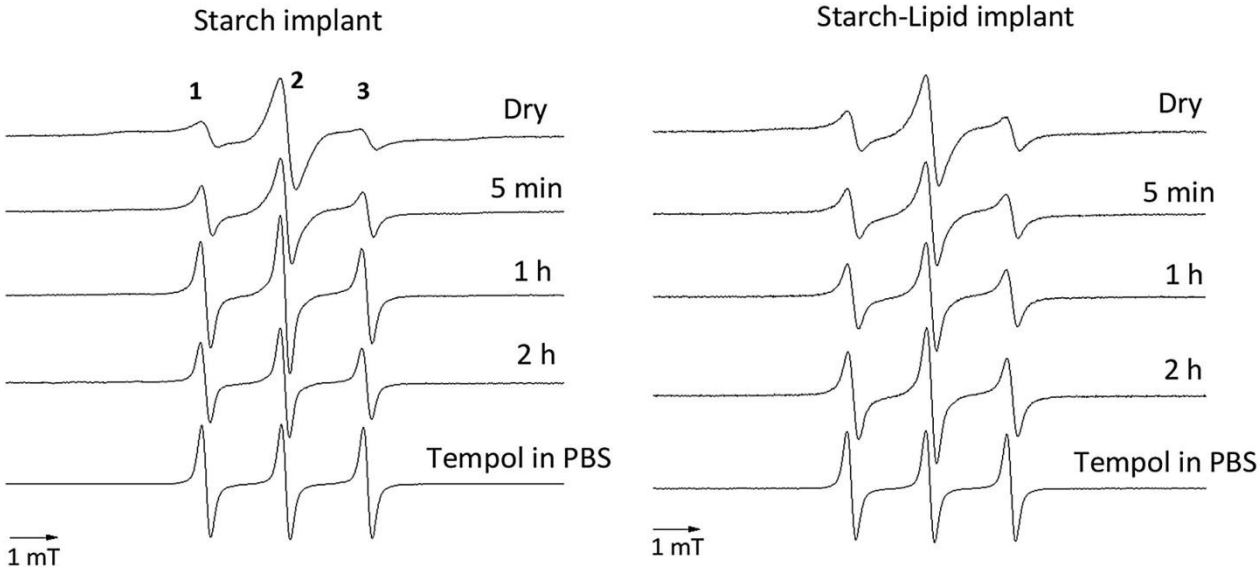

Figure 11. EPR-Spectra of TL-loaded implants after different times of exposure to PBS.

As can be seen in Figure 11 the EPR spectra of the TL-loaded implants in the dry state do not show a real powder-like spectrum like what was observed in the dry state of TB-loaded implants. The three broad lines of these spectra show that most part of TL have moderate mobility (indicating mobility in a viscous environment) even before exposure to buffer. Due to their different hydrophilicities, TL and TB will localize in different environments in heterogeneous media. TL is much more hydrophilic. It was therefore assumed that the three-line spectrum of TL arises from the localization in viscous microregions of high polarity (e.g. adsorbed water). After exposure of both TL-loaded implants to PBS, a continuous decrease in the width of all three lines was observed over the whole time period. These results prove a very fast water penetration into both systems.

These results align with the findings obtained by NMR relaxometry. T_2 represents the spin-spin relaxation time, where a smaller T_2 value indicates a more rigid system. The penetration of water into the implant affects the mobility of polymer chains, leading to an increase in the T_2 value. Figure 12 shows the T_2 values for each system before and after exposure to PBS. As can be seen in the figure, both systems exhibited two distinct T_2 even in the dry state, indicating the presence of water in both systems. After exposing the systems to PBS for 1 h, a noticeable increase in the T_2 values was observed in the part of the system with a longer T_2, demonstrating water penetration into both systems.

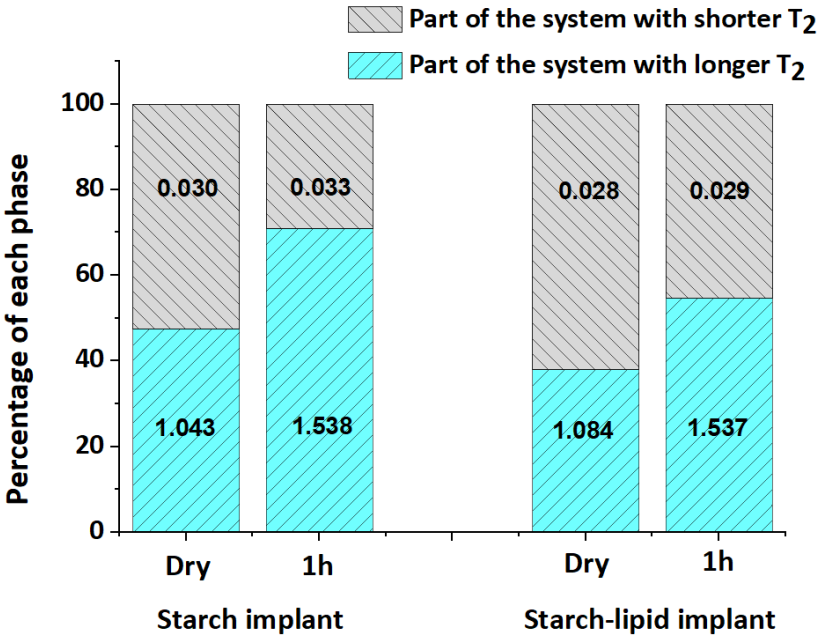

Figure 12. The T_2 values (ms) of each system calculated by fitting mono and double exponential decay curves.

Based on these results, both the starch implant and starch-lipid implant demonstrated the potential to be used as a controlled release system for more lipophilic drugs. Hydrophilic small molecules are expected to be released similar to TL.

In the next step, two antimalarial agents artemether (AM) and artesunate (AS), were loaded into the systems. To assess the effect of the amount of lipid (GMS) on the system's characteristics, three formulations including starch implant, starch-low lipid implant, and, starch-high lipid implant were produced and characterized. The heating zone temperatures were set at 60, 65, and 70 °C, as higher temperatures led to drug degradation. The exact components of each formulation are shown in Table 2.

Table 2. Composition of investigated formulations in gram.

Formulation No	Formulation name	Components [g]			
		High amylose maize Starch	GMS	Artemether	water
1	Starch-AM implant	5	-	5	2.5
2	Starch-AM-Low lipid implant	4	1	5	2
3	Starch-AM-High lipid implant	4	3	7	1

The prepared implants were characterized using different methods. The complete characterization of the systems is explained in detail in the first publication. Here, only the results of the release studies for AM are discussed, as it was the turning point of this project. As can be seen in Figure 13, the release kinetics were not as anticipated. AM was released over a longer period of time (6 days) from the starch implant, while the release was shortened to 3 days in the starch-low lipid implant.

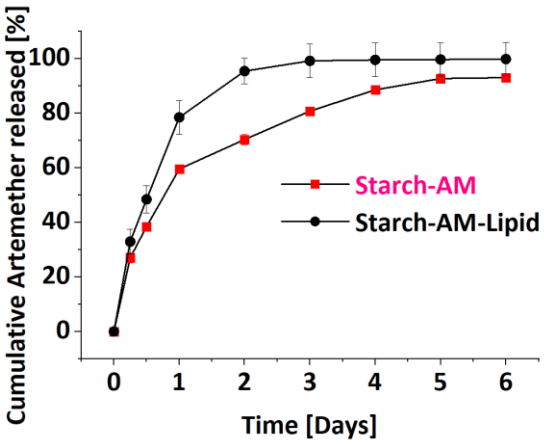

Figure 13. Cumulative release of artemether from different implants in PBS plus 1% SDS (Sodium dodecyl sulfate) pH 7.4; n = 3; the error bars indicate the standard deviation.

The release kinetics of starch-AM implant match the desired release profile for the treatment of severe malaria. Per WHO guidelines, artemether is the drug of choice in case parenteral artesunate is not available [97]. Therefore, this formulation can be a potential candidate to be used in the treatment of severe malaria. Further studies are needed to evaluate the system in vivo using appropriate animal models.

Interestingly, the results demonstrated that starch alone has the potential to provide sustained release of artemether for an even longer duration than formulations containing lipids. These results clarified that achieving a controlled release system requires specific alterations to the native structure of starch [78]. These changes primarily occur through starch gelatinization during the extrusion process. The addition of the lipid to the formulation can prevent the leaching of granule content during gelatinization, inhibit the swelling of starch granules during heating and reduce the water-binding capacity of starch [98–100]. Consequently, achieving gelatinized starch would require significantly higher temperatures. However, increasing the extrusion process temperature is constrained by several factors: 1. The length of the mini extruder, which has a significantly shorter chamber length compared to industrial versions (Using temperatures higher than the lipid's

melting point can result in lipid separation from the system before complex formation, causing the lipid to exit the chamber faster than other components), 2. Thermal instability of many drugs including artemether. As a result, instead of using higher temperatures, it was decided to continue the investigations with starch-based implants. Figure 14 shows the SEM image of the starch implant. The SEM image shows the freshly broken surface of the implant. Looking closer at the breakage surface, it becomes apparent that the starch granules have undergone gelatinization, causing the granule contents to leak out.

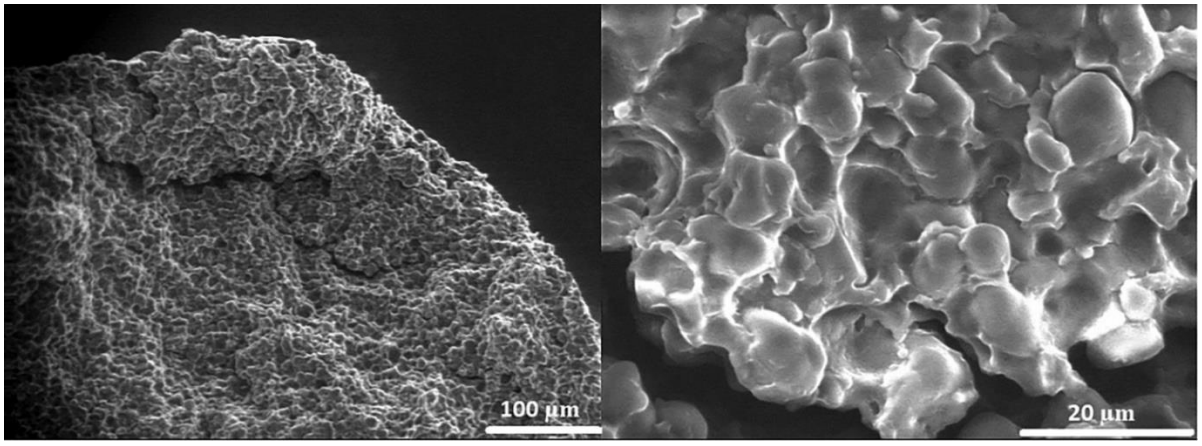

Figure 14. SEM image of the broken surface of the implant.

3.2 Characterization of controlled release starch-nimodipine implant

Subarachnoid haemorrhage (SAH) is a serious, life-threatening type of stroke where cerebral vasospasm remains a serious complication and a major cause of death and disability in affected patients. Nimotop® (Nimodipine 30 mg capsule, Bayer) is an FDA-approved drug for the treatment of SAH-induced vasospasm [83]. NMD inhibits the influx of calcium ions through voltage-gated L-type calcium channels in vascular smooth muscles, leading to vasorelaxation [101,102]. It has been demonstrated to dilate blood vessels and prevent vasoconstriction, particularly in small arterioles with diameters ranging from 70 to 100 µm [103,104]. Additionally, NMD elevates adenosine levels in the central nervous system, leading to the subsequent suppression of the excitatory neurotransmitter glutamate—a potential neuroprotective mechanism of NMD [105,106]. According to FDA guidelines, NMD should be administered at a dose of 60 mg (two capsules) every 4 hours for a continuous 21-day period [36]. As the administration dosing regimen shows, it has very

low oral bioavailability, primarily due to slow dissolution and decomposition in stomach acid [84]. NMD oral bioavailability is reported to range from 3 to 30% exhibiting considerable variability among patients [85,86]. Therefore, there is a need for a parenteral depot formulation of NMD capable of releasing the drug over the desired duration (Figure 15).

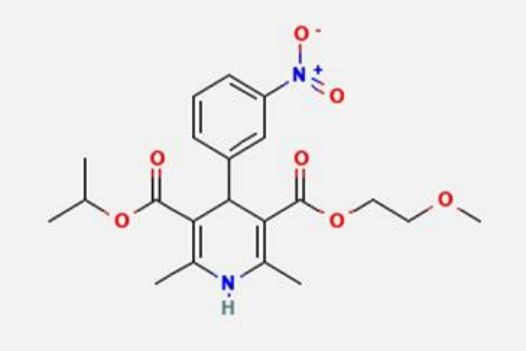

Figure 15. Chemical structure of Nimodipine.

As explained in the previous chapter, the release of artemether, with a log P-value of 3.1, which is similar to the log P of NMD, was observed over 6 days from the starch-based system. The investigations clarified that some critical changes in the native structure of starch are needed to achieve a controlled release system [78]. These changes are mainly formed by the gelatinization of the starch during the extrusion process. The plasticizer effect of NMD during the HME process has been previously reported [18]. The possible plasticizer effect of NMD may enhance the system's cohesiveness through physical interactions with starch, resulting in a more extended release profile.

The goal of this part of the thesis was to achieve a deeper insight into the system. The aim was to investigate possible interactions between the drug and the polymer, assess the impact of the extrusion process on both the polymer and the API and evaluate the potential effects of the API on the polymer and vice versa. To achieve this, the implants without NMD, implants containing 20% NMD (NMD-20) and implants containing 40% NMD (NMD-40) were produced and characterized.

Figure 16 shows the release profile of NMD from both implants. The release from the NMD-40 implant during the first week of release (32%) was nearly three times higher than that of the NMD-20 implant (13%). After 101 days, 96.3% of the NMD was released from an NMD-

40 implant and the release was almost completed, while this value was 83% for the NMD-20 implant. About 17% of NMD remained inside the NMD-20 system and it did not release from the implant within this time period. Both systems were further characterized to identify the factors contributing to the differences in release behavior.

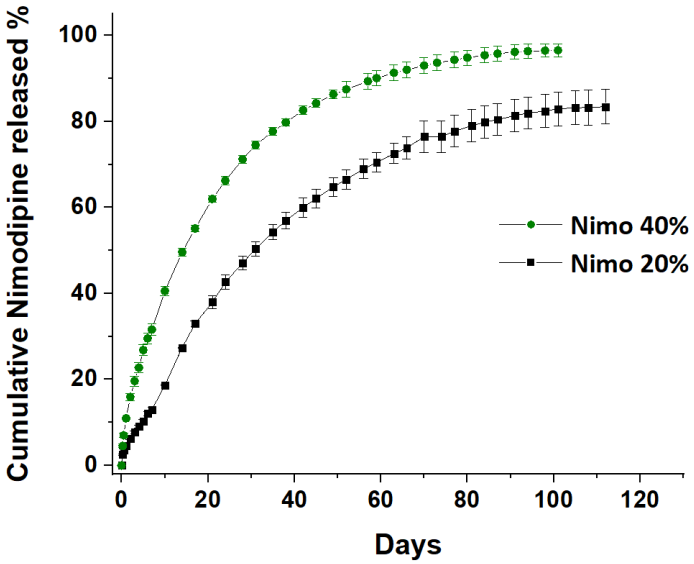

Figure 16. Cumulative release of NMD from NMD-40 (green) and NMD-20 (black) in PBS plus 1% SDS pH 7.4; n=3; the error bars indicate the standard deviation.

As previously mentioned, the gelatinization of starch is a crucial requirement for forming a controlled release system. Looking closer at the SEM images of the samples (Figure 17), it becomes evident that gelatinization occurred in all three samples but to varying degrees. In starch implant, leakage of the granule's content is clear but the granules have retained their native form. This observation aligns with previous findings by Zhou et al., who reported the preservation of granule structure in high-amylose-containing starch, even after cooking processes [107]. However, in the samples containing NMD, most of the granules have undergone complete gelatinization and a granule with its native form can hardly be seen. Comparing the structure of the NMD-20 and NMD-40 under low vacuum (to prevent possible changes in the internal structure), it can be seen that in NMD-40 the granules are completely destroyed and the formed structure seems similar to the honeycomb structure of the gelatinized starch gel [108]. The internal structure provides an explanation for the difference in the release behavior of the two systems. The more porous structure of NMD-

40 leads to a faster release rate and complete release of NMD from the system, as compared to NMD-20. We assume that part of the NMD in the NMD-20 system remained inaccessible to the media, preventing complete drug release from the system.

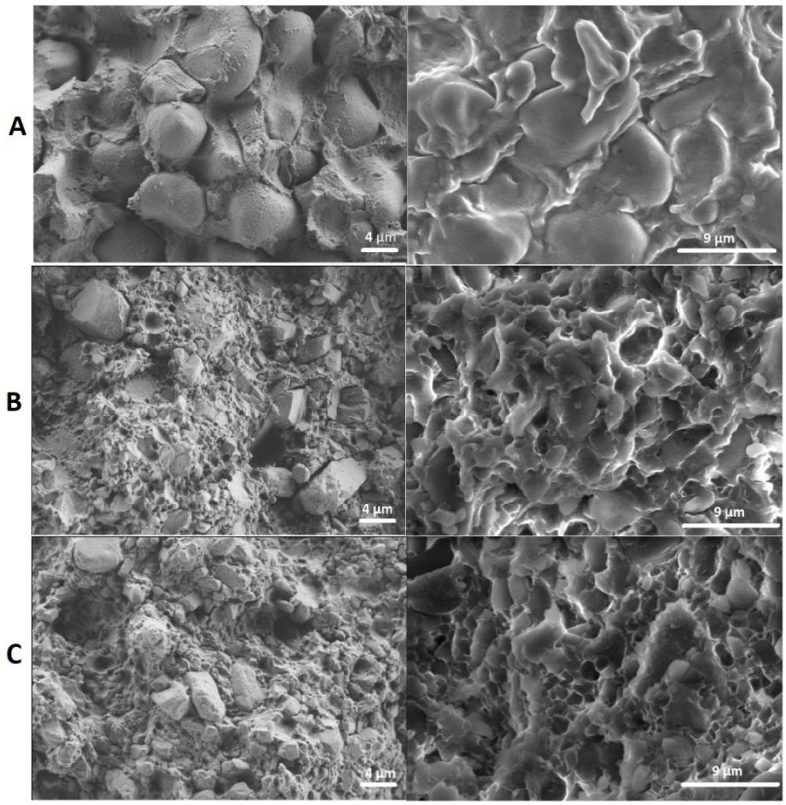

Figure 17. SEM images of the implants taken under high vacuum (left) and low vacuum (right) (A) starch implant, (B) NMD-20, and (C) NMD-40.

Considering the observed structure in the samples using SEM, to evaluate the possible effect of NMD on starch, DSC measurements were performed. Figure 18 shows the DSC curve of the physical mixture of samples. As can be seen in the DSC curves, there is a broad peak starting from 40 °C in all three samples. These peaks correspond to water evaporation and partial gelatinization of starch during the heating cycle. The maximum peaks of gelatinization are at 76.7, 85.17 and 104.5 °C for NMD-40, NMD-20 and starch-water samples, respectively. Since water content in all samples was constant and half of the weight of the starch (starch:water, 2:1), it can be concluded that the presence of nimodipine lowered the gelatinization temperature of the starch. A similar plasticizing effect of NMD on polyvinylpyrrolidone/vinyl acetate copolymer has been reported by Zheng et al. [109]. This result is in line with the observed structure of the samples in SEM images (Figure 17). As

can be seen in the SEM image, in the starch implant sample many of the granules are still in their native form after the extrusion process, while the complete gelatinization of starch is observed in NMD-40 leading to a porous structure.

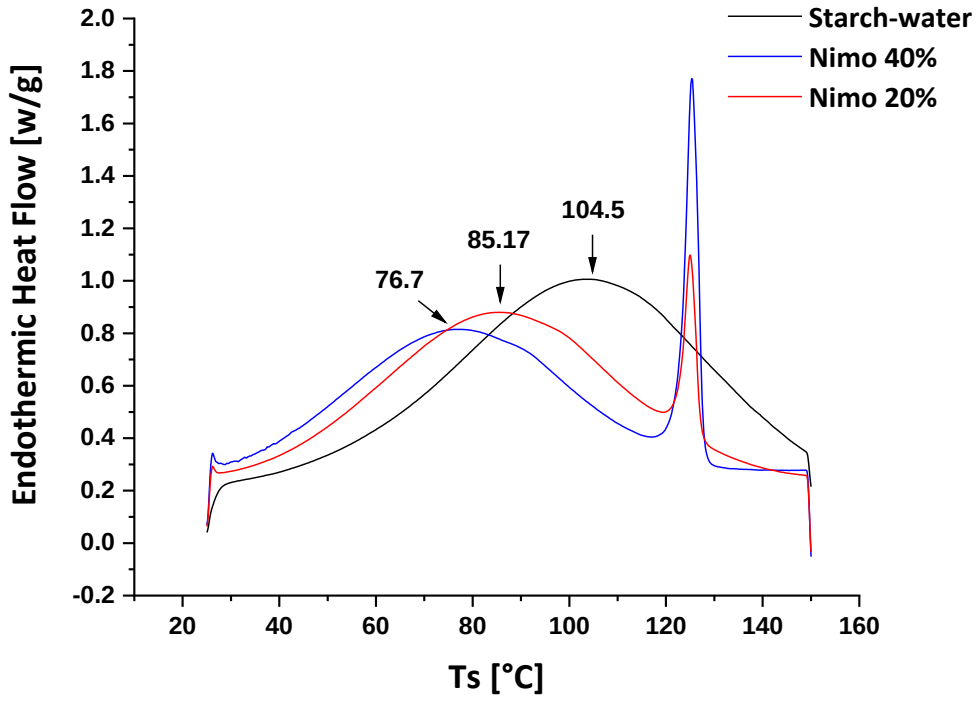

Figure 18. Thermograms of samples with different NMD content. Measurements were carried out with a heating rate of 10 K/min between 25 and 150 °C.

To evaluate possible changes in NMD modifications during the extrusion process, Raman Spectroscopy and DSC were employed. NMD has two different modifications: Modification I, the metastable form with a melting point of approximately 124 °C and Modification II, the stable form with a melting point of around 116 °C [40]. As illustrated in Figure 19, NMD powder (as received from the company) is predominantly composed of modification I. Following the extrusion process, a significant change in NMD peaks becomes apparent. It has been previously reported by George et al. that NMD crystallizes slowly, resulting in the absence of a crystallization peak during the cooling cycle. However, the crystallization of glassy NMD during storage at room temperature is not preventable and can lead to the formation of Modification II crystals which are less soluble [41]. We think that part of the NMD powder could become amorphous due to the presence of water and high pressure

during the extrusion process, subsequently forming Modification II crystals during cooling at room temperature and storage in the fridge. The possible changes in the NMD modification were also evident through other techniques, including IR and Raman Spectroscopy.

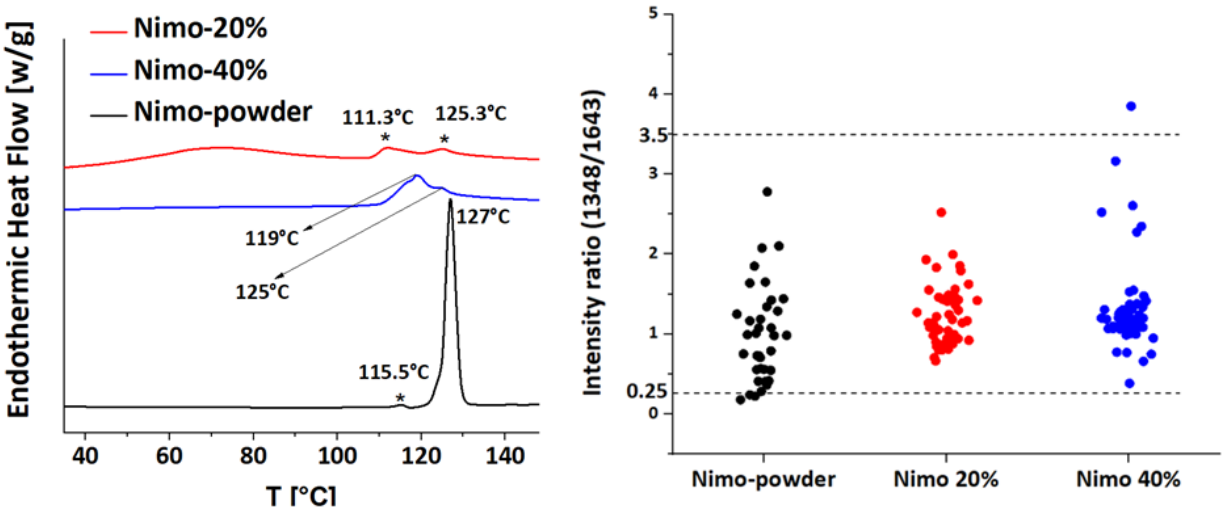

Figure 19. Thermograms of different samples (Left). Measurements were carried out with a heating rate of 10 K/min between 25 and 150 °C. Calculated values of the peak intensity ratio of each sample at 1347/1642 cm^{-1} with Raman Spectroscopy. 30 measurements were performed for each sample (Right).

The differentiation between different polymorphs of the NMD using Raman spectroscopy has been reported previously [110–114]. Based on previous studies, the intensity ratio of the NO_2 group stretch at 1347 cm^{-1} to the C double bond C stretch of the dihydropyridine ring at 1642 cm^{-1} was used to distinguish between the three solid states of NMD. These studies concluded that the values below 0.25 and above 3.5 definitely correspond to modification II and modification I, respectively. However, determining the modification for values between 0.25 and 3.5 is more complex, as these values correspond to regions with submicron crystal sizes and/or amorphous regions [114]. As shown in Figure 19, the intensity ratio values for all three samples mostly fall between 0.25 and 3.5. Therefore, NMD in all samples exists in the form of submicron size crystals and/or in its amorphous state. A slight variation in the dispersion of the calculated values can be observed among the different samples, consistent with the results of DSC thermograms for the samples after the

extrusion process. Although it was not possible to quantitatively show the changes in NMD modifications, the results confirmed the appeared changes in NMD modifications observed with other methods.

Raman Spectroscopy was also used to confirm the homogeneous dispersion of the API within the implant. Figure 20 provides an example of Raman measurements. For each group measurement, a line within the sample was selected and then different points of the line were measured automatically by the device. A total of 30 measurements were conducted for each sample. In all measurements obtained from both samples, the characteristic peaks corresponding to NMD were consistently observed. This confirms the uniform dispersion of NMD throughout the entire implant. The content uniformity of the implants was also proved using HPLC analysis based on European Pharmacopeia guidelines (paragraph 2.9.6).

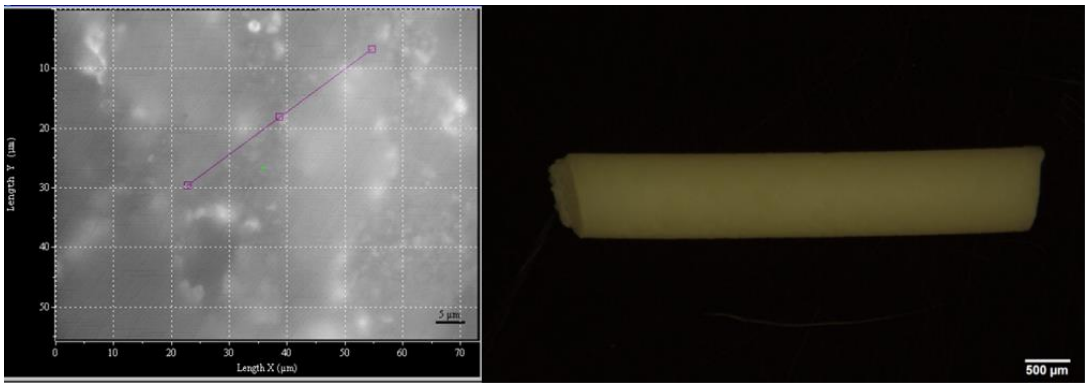

Figure 20. Example of Raman measurements (Left), NMD-40 implant (Right).

As the implant is intended for parenteral administration, finding the appropriate sterilization method was of utmost importance. Sterilization of NMD-loaded formulations has been reported by several studies previously, but the stability of the NMD is rarely investigated after the sterilization process [115,116]. In a study conducted by Zech et al., partial degradation of NMD was reported following the electron irradiation sterilization [88]. In this study, the effect of the electron beam on NMD and the polymer was assessed using HPLC, IR and NMR spectroscopy.

As demonstrated in Figure 21, in both formulations, NMD-40 and NMD-20, no significant decrease in the drug content was observed. The slight increase in the NMD content in the NMD-20 formulation is probably due to water evaporation during the sterilization process. The stability of the NMD during the sterilization process is further confirmed by NMR and

IR spectroscopy. The investigation of NMD chemical structure and its polymorphism using ^{1}H-NMR and ^{13}C-NMR has been previously reported by several studies [110,117]. Comparing the NMR spectra of NMD powder and NMD-40 before and after the electron beam sterilization, it can be seen that the crucial peaks arising from NMD [118] are detectable affirming the nimodipine stability, during the production and the sterilization process. As expected for the starch, the peaks corresponding to starch were observable in both samples [117].

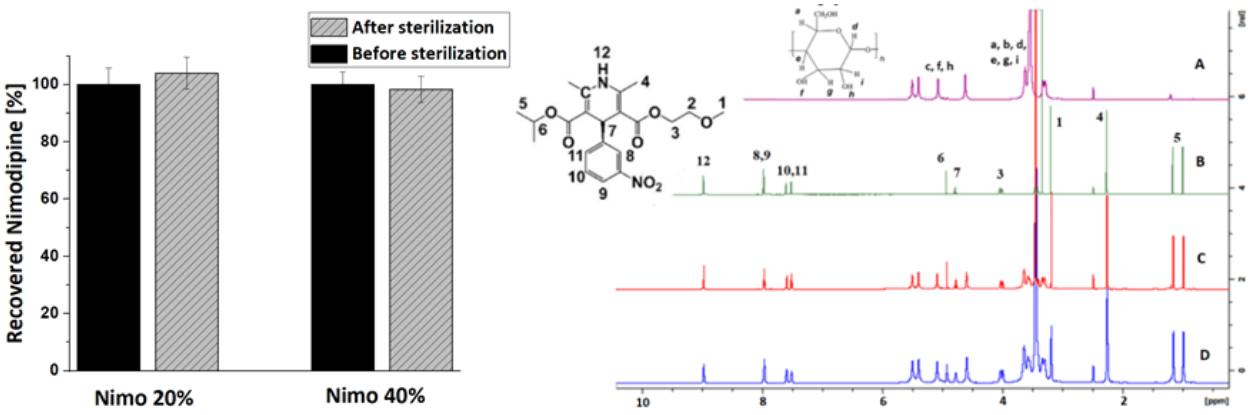

Figure 21. Effect of the electron beam on drug content in NMD-20 and NMD-40 implants before (black) and after (dashed) the sterilization, assessed with HPLC; n=3; the error bars indicate the standard deviation (Left). ^{1}H-NMR spectra of (A) Starch, (B) Nimodipine, (C) Nimo-40, (D) Nimo-40 after electron beam sterilization (Right).

These results were confirmed by IR spectroscopy. As shown in Figure 22, the characteristics peaks of NMD, C-CH_3 at 1381 cm^{-1}, NO_2 group at 1523cm^{-1}, carbonyl group at 1695 cm^{-1}, C=C stretching of dihydropyridine at 1640 cm^{-1}, C=C stretches of the aromatic ring at 1620 cm^{-1} [119,120] were detectable in samples before and after the sterilization process, confirming the stability of NMD during the sterilization process.

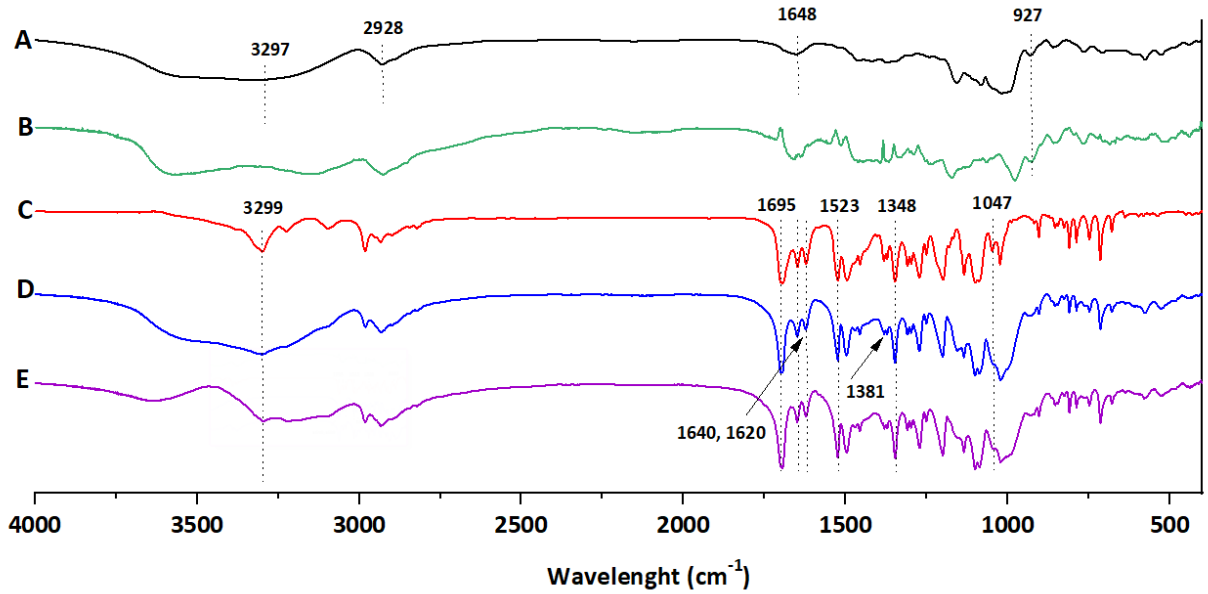

Figure 22. FTIR spectrum of the samples: A) Starch powder, B) Sterilized starch implant, C) NMD powder, D) NMD-40 implant, E) Sterilized NMD-40 implant.

In a previous study conducted by Zech et al., a partial degradation of NMD (about 20%) was reported after the electron beam sterilization of NMD-loaded PLGA nanofibers. As they used the same sterilization technique and the same HPLC method for the quantification of NMD, it can be concluded that starch serves as a better polymeric matrix compared to PLGA for preserving NMD during sterilization. This protective effect of the polymer was also observed in our prior study, where we employed electron beam sterilization for implants loaded with fluorescent dyes [90].

3.3 In vivo evaluation of the starch-based implant (Release profile/fate of the system)

Despite all the efforts to simulate in vivo conditions using in vitro tests, numerous reports highlight poor correlations between in vitro and in vivo results. Therefore, it is important to monitor release processes in vivo. As previously explained, the system's ability to create a

controlled release system was proved using various in vitro tests, and a suitable sterilization method was identified. Given the proven biosafety of starch by several studies [121,122], we possessed all the necessary data to commence our in vivo investigation.

OI is one of the most commonly used non-invasive techniques in the visualization of in vivo processes. It necessitates selecting suitable dyes and their appropriate concentrations to visualize the implanted formulation. Therefore, in this part of the project appropriate fluorescent dyes were selected, the appropriate concentration for each dye was determined and the SC injected implants were visualized using an In Vivo Imaging System (IVIS). The fluorescent dyes ICG and DiR were loaded into the implants as examples of hydrophilic and hydrophobic molecules. The SC-injected implants were evaluated over time with OI.

Figure 23 shows the release of ICG both in vitro and in vivo. The signal intensity is significantly decreased after the first day, confirming the rapid release of ICG from the system both in vitro and in vivo. These findings align with the results of the EPR experiment. Tempol, used as a model of a hydrophilic drug, exhibited rapid solubilization after exposure to the buffer and displayed a similar release behavior to ICG in vitro [78]. OI as a more sensitive method than the EPR, enabled us to non-invasively assess the implant's biodegradability and the release of a hydrophilic drug model from the implant in vivo.

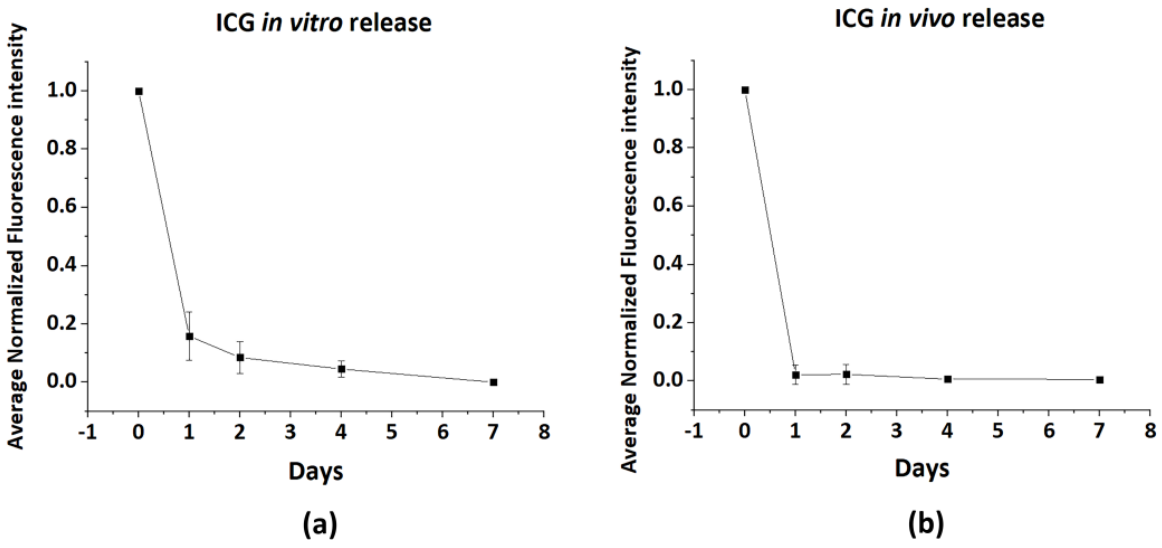

Figure 23. Kinetics of ICG signals from starch extrudates after: (a) incubation in buffer (in vitro); (b) injection into mice (in vivo); (Mean±SD, n=7).

Figure 24 presents the release profiles of the lipophilic dye DiR, both in vitro and in vivo. As depicted in the figure, DiR signals were detectable for a duration of 30 days. In comparison to ICG, DiR exhibits a significantly longer release period. The majority of the DiR dye is released from the system over two weeks, both in vitro and in vivo. These results align with the findings from the EPR experiment. Tempol benzoate, used as a model of a hydrophobic drug, demonstrated sustained release over two weeks from the starch implant in vitro [78]. Surprisingly, the in vitro and in vivo release profiles of DiR were very similar, contrary to our initial expectations. After 4 weeks, the experiment was finished and the implantation site was examined ex vivo. The implant was completely degraded after 4 weeks, as no residue of the implant could be observed in any of the mice's tissue at the injection site macroscopically. In vitro, the starch extrudate remained as a monolithic extrudate after 4 weeks. These findings suggest complete degradation of the starch in vivo by enzymes, most likely amylases. Amylases are produced not only by salivary glands, pancreas and liver but also by other tissues and exist in serum at a normal level. These enzymes break down the amylose and amylopectin molecules of starch into dextrins, which are further degraded into fermentable sugars, mainly maltose but also some glucose [123]. The difference in behavior between in vitro and in vivo environments suggests that nonenzymatic hydrolysis is not the primary mechanism of starch degradation in vivo, in contrast to PLA and PLGA implants, where autocatalytic hydrolysis is the primary mechanism for polymer degradation.

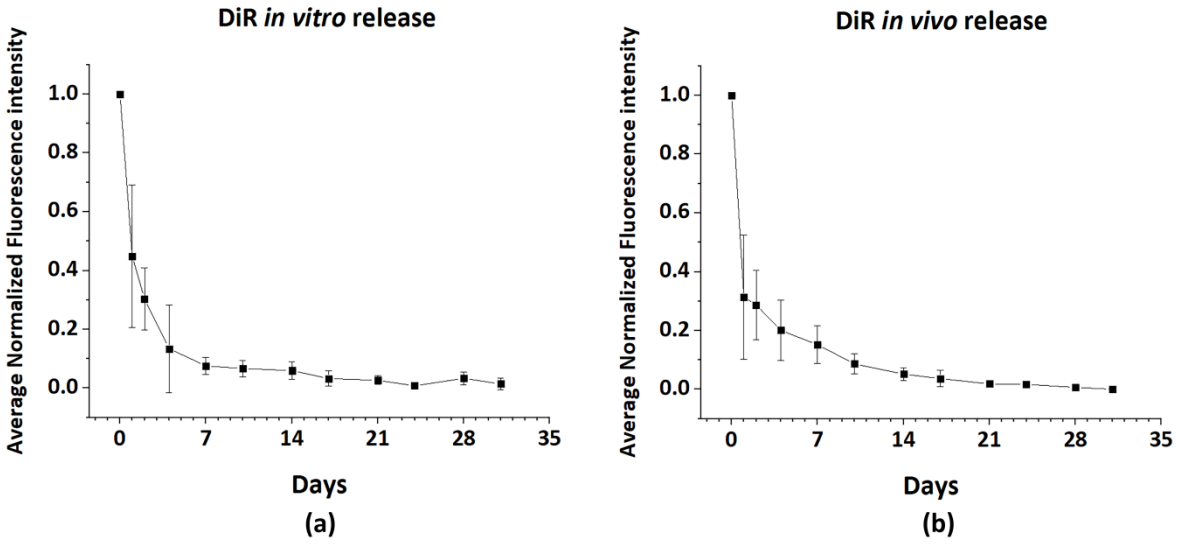

Figure 24. Kinetics of DiR signals from starch extrudates after: (a) incubation in buffer (in vitro); (b) injection into mice (in vivo); (Mean±SD, n=7).

The tissue at the injection site was stained with hematoxylin-eosin (H&E). As can be seen in the picture (Figure 25), no significant changes were observed in the tissue.

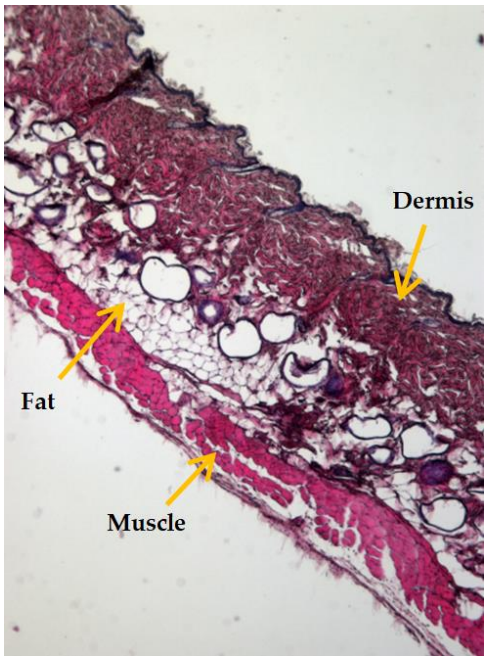

Figure 25. The surrounding tissue of the injection site stained with hematoxylin–eosin (H&E).

These results proved the promising potential of the starch-based implant as a biodegradable and biocompatible system in forming a controlled release system for a hydrophobic drug.

4. Summary

PLA and PLGA stand as the predominant polymers in the pharmaceutical industry for the development of parenteral controlled drug release systems. However, their use is associated with certain drawbacks including their degradation into highly acidic monomers and autocatalysis which can lead to degradation of the active substance before release or non-linear/complex release profiles [24,33]. This thesis aimed to explore an alternative material for these polymers, to expand the spectrum of options available to the manufacturers. Starch (nonmodified form) is in general fully biodegradable. Its degradation in the body produces non-toxic and non-acidic monomers [51]. Starch-based materials are already clinically used as bioresorbable medical products for providing hemostasis and preventing postoperative tissue adhesion [52,53]. It is also a major excipient in the pharmaceutical industry but is mainly used for oral formulations due to its certain drawbacks including its weak mechanical properties and its fast degradation in the body over a few days. Therefore, starch as a natural, abundant and cheap polymer could be a valuable alternative for these materials if it can be modified. Starch properties can be modified using chemical or physical modifications. Chemical modifications of starch usually involve using organic solvents which does not align with the principles of green and sustainable chemistry. Consequently, alternative environmentally friendly methods, such as reactive extrusion, high hydrostatic pressure treatment, and enzyme modification, have been explored. Nevertheless, these approaches have limitations due to their rigorous conditions or equipment requirements [60]. In contrast, physical modifications of starch are simple, cost-effective and eco-friendly [61]. This study aimed to modify the starch using physical modifications. In the first part of the thesis, using massive prescreening studies, the appropriate type of starch was found (high-amylose starch) and the extrusion parameters and water content (plasticizer) were optimized. In the next part of the project, the potential of the produced system in the formation of a controlled release system was evaluated using different techniques. Water penetration into the system and the possible release mechanisms were evaluated using EPR and NMR relaxometry. Both methods demonstrated fast water penetration into the starch-based implant leading to rapid and complete release of hydrophilic molecules from the system, as observed in different in vitro tests explained within the thesis. The in vitro results confirmed the potential of the starch-based implant in the formation of a controlled drug release system for hydrophobic substances. NMD is a

hydrophobic API with a log P value of 3.1 and very low oral bioavailability, which can vary extensively among patients, ranging from 3% to 30% [85,86]. Therefore, there is a need for a parenteral depot of NMD capable of releasing the drug over the desired duration. With the aim of producing a parenteral depot of NMD and assessing the impact of drug load on the release profile, two different amounts of NMD (20% and 40%) were incorporated into the starch-based implant. The implants were characterized in detail. NMD was released over 3 months from both formulations. Possible changes in NMD modifications were evaluated using different techniques including DSC, IR and Raman Spectroscopy. Changes in NMD modifications were observed in all the mentioned techniques but the quantification of each polymorph was not possible. The impact of NMD on the starch was assessed using various techniques. The findings indicated that the presence of NMD in the formulation enhances the degree of starch gelatinization, and a higher NMD content resulted in a more porous structure and a faster release profile. As the system was intended for parenteral administration, finding an appropriate sterilization method was of utmost importance. E-beam sterilization was found to be an appropriate method for the sterilization of the final product. The potential of the developed system to protect NMD during the sterilization process was confirmed using various methods. Animal studies were conducted to investigate the fate of the implant and the release profiles of fluorescent dyes with different hydrophilicity/hydrophobicity in vivo. For this purpose, the implants loaded with different fluorescent dyes were injected SC in mice and imaged at determined time intervals. The release of ICG as a model of a hydrophilic drug was completed after one day in vivo. This was expected as previous experiments have demonstrated rapid water penetration into the system. The release of DiR as a model of a hydrophobic substance was observed over 4 weeks. After 4 weeks, the experiment was finished and the injection site was examined ex vivo. The implant was completely degraded after 4 weeks, as no residue of the implant could be observed in any of the mice's tissue at the injection site macroscopically. In vitro, the starch extrudate remained as a monolithic extrudate after 4 weeks. These findings suggest a complete degradation of the starch in vivo by enzymes, most likely amylases. Amylases are present in serum at a normal level. The amylose and amylopectin molecules of starch are broken down into dextrins by these enzymes. The dextrins will be further on degraded to fermentable sugars, mainly maltose but some glucose as well [123]. The difference in behavior between in vitro and in vivo environments suggests that nonenzymatic hydrolysis is not the primary mechanism of starch degradation in vivo, in contrast to PLA and PLGA implants, where autocatalytic hydrolysis is the primary mechanism for polymer degradation.

5. Outlook

The following section will discuss future perspectives in the context of this work based on the promising results that were acquired within this thesis. Based on the obtained results, this project can be extended from different aspects:

a) As the potential of the starch-NMD implant in providing sustained release of nimodipine is proven, and an appropriate sterilization method is found, the next phase on this project's horizon is the in vivo evaluation of this formulation using appropriate animal models. Currently, available possibilities are being evaluated to conduct the animal studies. This study will provide valuable insights into the efficacy and potential clinical applications of the starch-NMD implant.

b) In this thesis, the extrusion temperature was chosen to be minimized, with a maximum limit of 70 °C. The potential benefit of elevating the extrusion temperature closer to the melting point of the API, specifically NMD, is intended to be explored. The objective behind this approach is to induce the formation of an amorphous dispersed system within the implant. This amorphous state often leads to enhanced drug solubility and bioavailability. Furthermore, an examination of the possible inhibitory effect of starch on the recrystallization of NMD will be conducted, as it could have a significant impact on the long-term stability and efficacy of the implant in the future.

c) Shape memory characteristics of starch could be utilized to produce implants for other clinical purposes. In a study conducted by Beilvert et al. resorbable starch-based shape-memory stents were produced to keep the salivary duct open after sialendoscopy surgery [124]. They reported fast degradation of the device due to the high amount of amylases in the simulated saliva and suggested that such starch stents might be used in other pathologies implicating restenosis, such as the esophagus after stricture, but also in the bile duct, urinary tract, or in the trachea. The shape memory and controlled release features of starch can be merged to address various clinical needs simultaneously. Further studies are essential to develop such a system.

6. References

[1] T. Kissel, Z. Brich, S. Bantle, I. Lancranjan, F. Nimmerfall, P. Vit, Parenteral depot-systems on the basis of biodegradable polyesters, J. Control. Release. 16 (1991). https://doi.org/10.1016/0168-3659(91)90028-C.

[2] I. Vhora, D. Bardoliwala, S.R. Ranamalla, A. Javia, Parenteral controlled and prolonged drug delivery systems: Therapeutic needs and formulation strategies, in: Nov. Drug Deliv. Technol. Innov. Strateg. Drug Re-Positioning, 2020. https://doi.org/10.1007/978-981-13-3642-3_7.

[3] K. Mäder, Characterization methodologies for long-acting and implantable drug delivery systems, in: Long-Acting Drug Deliv. Syst., 2021. https://www.sciencedirect.com/book/9780128217498/long-acting-drug-delivery-systems.

[4] Y.-S. Rhee, C.-W. Park, P.P. DeLuca, H.M. Mansour, Sustained-release injectable drug delivery, (2010).

[5] S. Kempe, K. Mäder, In situ forming implants - An attractive formulation principle for parenteral depot formulations, J. Control. Release. 161 (2012). https://doi.org/10.1016/j.jconrel.2012.04.016.

[6] A. Göpferich, Bioerodible implants with programmable drug release, J. Control. Release. 44 (1997) 271–281.

[7] E. Lehner, D. Gündel, A. Liebau, S. Plontke, K. Mäder, Intracochlear PLGA based implants for dexamethasone release: Challenges and solutions, Int. J. Pharm. X. (2019). https://doi.org/10.1016/j.ijpx.2019.100015.

[8] D. Pardo-López, E. Francés-Muñoz, R. Gallego-Pinazo, M. Díaz-Llopis, Anterior chamber migration of dexametasone intravitreal implant (Ozurdex®), Graefe's Arch. Clin. Exp. Ophthalmol. 250 (2012) 1703–1704.

[9] A. Wadee, V. Pillay, Y.E. Choonara, L.C. du Toit, C. Penny, V.M.K. Ndesendo, P. Kumar, C.S. Murphy, Recent advances in the design of drug-loaded polymeric implants for the treatment of solid tumors, Expert Opin. Drug Deliv. 8 (2011) 1323–1340.

[10] N. Howard-jones, A critical study of the origins and early development of hypodermic medication, J. Hist. Med. Allied Sci. 2 (1947). https://doi.org/10.1093/jhmas/II.2.201.

[11] J. Folkman, D.M. Long, The use of silicone rubber as a carrier for prolonged drug therapy, J. Surg. Res. 4 (1964). https://doi.org/10.1016/S0022-4804(64)80040-8.

[12] B.B. Pharriss, R. Erickson, J. Bashaw, S. Hoff, V.A. Place, A. Zaffaroni, Progestasert: a uterine therapeutic system for long term contraception: I. Philosophy and clinical efficacy, Fertil. Steril. 25 (1974). https://doi.org/10.1016/s0015-0282(16)40748-x.

[13] I. Sivin, Clinical effects of Norplant subdermal implants for contraception, Long-Acting Steroid Contraception. Adv. Hum. Fertil. Reprod. Endocrinol. 2 (1983) 89–116.

[14] E. Schmitt, R. Polistina, Surgical sutures. US Patent, US Patent 3,297,033, 1967.

[15] J.C. Wright, A.S. Hoffman, Historical Overview of Long Acting Injections and Implants, in: Long Act. Inject. Implant., 2012. https://doi.org/10.1007/978-1-4614-0554-2_2.

[16] F.G. Hutchinson, B.J.A. Furr, Biodegradable polymers for the sustained release of peptides, Biochem. Soc. Trans. 13 (1985). https://doi.org/10.1042/bst0130520.

[17] F.G. Hutchinson, B.J.A. Furr, Biodegradable polymer systems for the sustained release of polypeptides, J. Control. Release. 13 (1990). https://doi.org/10.1016/0168-3659(90)90018-O.

[18] S.S. Lee, P. Hughes, A.D. Ross, M.R. Robinson, Biodegradable implants for sustained drug release in the eye, Pharm. Res. 27 (2010). https://doi.org/10.1007/s11095-010-0159-x.

[19] N. Shore, Introducing Vantas: The First Once-Yearly Luteinising Hormone-Releasing Hormone Agonist, Eur. Urol. Suppl. 9 (2010). https://doi.org/10.1016/j.eursup.2010.08.004.

[20] C. Wischke, S.P. Schwendeman, Principles of encapsulating hydrophobic drugs in PLA/PLGA microparticles, Int. J. Pharm. 364 (2008). https://doi.org/10.1016/j.ijpharm.2008.04.042.

[21] Zoladex approved for prostate cancer, Drug Ther. (NY). 20 (1990).

[22] D. Cuevas-Ramos, M. Fleseriu, Pasireotide: A novel treatment for patients with acromegaly, Drug Des. Devel. Ther. 10 (2016). https://doi.org/10.2147/DDDT.S77999.

[23] S.P. Schwendeman, R.B. Shah, B.A. Bailey, A.S. Schwendeman, Injectable controlled release depots for large molecules, J. Control. Release. 190 (2014) 240–253.

[24] K. Mäder, B. Gallez, K.J. Liu, H.M. Swartz, Non-invasive in vivo characterization of release processes in biodegradable polymers by low-frequency electron paramagnetic resonance spectroscopy, Biomaterials. 17 (1996). https://doi.org/10.1016/0142-9612(96)89664-5.

[25] A. Schädlich, S. Kempe, K. Mäder, Non-invasive in vivo characterization of microclimate pH inside in situ forming PLGA implants using multispectral fluorescence imaging, J. Control. Release. 179 (2014). https://doi.org/10.1016/j.jconrel.2014.01.024.

[26] A.G. Ding, S.P. Schwendeman, Acidic microclimate pH Distribution in PLGA microspheres monitored by confocal laser scanning microscopy, Pharm. Res. (2008). https://doi.org/10.1007/s11095-008-9594-3.

[27] C.F. van der Walle, G. Sharma, M.N. V Ravi Kumar, Current approaches to stabilising and analysing proteins during microencapsulation in PLGA, Expert Opin. Drug Deliv. 6 (2009) 177–186.

[28] M. van de Weert, W.E. Hennink, W. Jiskoot, Protein instability in poly (lactic-co-glycolic acid) microparticles, Pharm. Res. 17 (2000) 1159–1167.

[29] L.R. Brown, Commercial challenges of protein drug delivery, Expert Opin. Drug Deliv. 2 (2005) 29–42.

[30] K. Fu, A.M. Klibanov, R. Langer, Protein stability in controlled-release systems, Nat. Biotechnol. 18 (2000) 24–25.

[31] A. Lucke, J. Kiermaier, A. Göpferich, Peptide acylation by poly(α-hydroxy esters), Pharm. Res. 19 (2002). https://doi.org/10.1023/A:1014272816454.

[32] A. Rawat, U. Bhardwaj, D.J. Burgess, Comparison of in vitro–in vivo release of Risperdal® Consta® microspheres, Int. J. Pharm. 434 (2012) 115–121.

[33] J. Shen, S. Choi, W. Qu, Y. Wang, D.J. Burgess, In vitro-in vivo correlation of parenteral risperidone polymeric microspheres, J. Control. Release. 218 (2015) 2–12.

[34] M. Eerdekens, I. Van Hove, B. Remmerie, E. Mannaert, Pharmacokinetics and tolerability of long-acting risperidone in schizophrenia, Schizophr. Res. 70 (2004) 91–100.

[35] E.D. Knox, G.L. Stimmel, Clinical review of a long-acting, injectable formulation of risperidone, Clin. Ther. 26 (2004) 1994–2002.

[36] FDA, (n.d.). https://www.accessdata.fda.gov/drugsatfda_docs/label/2006/018869s014lbl.pdf.

[37] T. Hickey, D. Kreutzer, D.J. Burgess, F. Moussy, In vivo evaluation of a dexamethasone/PLGA microsphere system designed to suppress the inflammatory tissue response to implantable medical devices, J. Biomed. Mater. Res. 61 (2002). https://doi.org/10.1002/jbm.10016.

[38] S. V. Fulzele, P.M. Satturwar, A.K. Dorle, Study of the biodegradation and in vivo biocompatibility of novel biomaterials, Eur. J. Pharm. Sci. 20 (2003). https://doi.org/10.1016/S0928-0987(03)00168-4.

[39] E.A. Ho, V. Vassileva, C. Allen, M. Piquette-Miller, In vitro and in vivo characterization of a novel biocompatible polymer-lipid implant system for the sustained delivery of paclitaxel, J. Control. Release. 104 (2005). https://doi.org/10.1016/j.jconrel.2005.02.008.

[40] M. Dirauf, I. Muljajew, C. Weber, U.S. Schubert, Recent advances in degradable synthetic polymers for biomedical applications - Beyond polyesters, Prog. Polym. Sci. 129 (2022). https://doi.org/10.1016/j.progpolymsci.2022.101547.

[41] I. Rudnik-Jansen, K. Schrijver, N. Woike, A. Tellegen, S. Versteeg, P. Emans, G. Mihov, J. Thies, N. Eijkelkamp, M. Tryfonidou, L. Creemers, Intra-articular injection of triamcinolone acetonide releasing biomaterial microspheres inhibits pain and inflammation in an acute arthritis model, Drug Deliv. 26 (2019). https://doi.org/10.1080/10717544.2019.1568625.

[42] J. Siepmann, A. Faham, S.D. Clas, B.J. Boyd, V. Jannin, A. Bernkop-Schnürch, H. Zhao, S. Lecommandoux, J.C. Evans, C. Allen, O.M. Merkel, G. Costabile, M.R. Alexander, R.D. Wildman, C.J. Roberts, J.C. Leroux, Lipids and polymers in pharmaceutical technology: Lifelong companions, Int. J. Pharm. 558 (2019).

https://doi.org/10.1016/j.ijpharm.2018.12.080.

[43] M.E. Aulton, K. Taylor, Aulton's pharmaceutics: the design and manufacture of medicines, Elsevier Health Sciences, 2018.

[44] J. Steiner, R. Alaneed, J. Kressler, K. Mäder, Fatty acid-modified poly (glycerol adipate) microparticles for controlled drug delivery, J. Drug Deliv. Sci. Technol. 61 (2021) 102206.

[45] F. Kreye, F. Siepmann, J. Siepmann, Drug release mechanisms of compressed lipid implants, Int. J. Pharm. 404 (2011). https://doi.org/10.1016/j.ijpharm.2010.10.048.

[46] S.S. Jensen, H. Jensen, E.H. Møller, C. Cornett, F. Siepmann, J. Siepmann, J. Østergaard, In vitro release studies of insulin from lipid implants in solution and in a hydrogel matrix mimicking the subcutis, Eur. J. Pharm. Sci. 81 (2016). https://doi.org/10.1016/j.ejps.2015.10.011.

[47] X. Feng, F. Zhang, Twin-screw extrusion of sustained-release oral dosage forms and medical implants, Drug Deliv. Transl. Res. 8 (2018). https://doi.org/10.1007/s13346-017-0461-9.

[48] M. Vollrath, J. Engert, G. Winter, Long-term release and stability of pharmaceutical proteins delivered from solid lipid implants, Eur. J. Pharm. Biopharm. 117 (2017). https://doi.org/10.1016/j.ejpb.2017.04.017.

[49] F. Kreye, F. Siepmann, A. Zimmer, J.F. Willart, M. Descamps, J. Siepmann, Cast lipid implants for controlled drug delivery: Importance of the tempering conditions, J. Pharm. Sci. 100 (2011). https://doi.org/10.1002/jps.22574.

[50] A.-C. Eliasson, Starch in food: Structure, function and applications, CRC press, 2004.

[51] M.A. Araújo, A.M. Cunha, M. Mota, Enzymatic degradation of starch-based thermoplastic compounds used in protheses: Identification of the degradation products in solution, Biomaterials. 25 (2004). https://doi.org/10.1016/j.biomaterials.2003.09.093.

[52] B. Krämer, F. Neis, S.Y. Brucker, S. Kommoss, J. Andress, S. Hoffmann, Peritoneal Adhesions and their Prevention - Current Trends, Surg. Technol. Int. 38 (2021). https://doi.org/10.52198/21.sti.38.hr1385.

[53] S.C. Mendes, R.L. Reis, Y.P. Bovell, A.M. Cunha, C.A. Van Blitterswijk, J.D. De Bruijn, Biocompatibility testing of novel starch-based materials with potential application in orthopaedic surgery: A preliminary study, Biomaterials. 22 (2001). https://doi.org/10.1016/S0142-9612(00)00395-1.

[54] L. Copeland, J. Blazek, H. Salman, M.C. Tang, Food Hydrocolloids Form and functionality of starch, Food Hydrocoll. 23 (2009).

[55] R.F. Tester, J. Karkalas, X. Qi, Starch - Composition, fine structure and architecture, J. Cereal Sci. 39 (2004). https://doi.org/10.1016/j.jcs.2003.12.001.

[56] J. Blazek, L. Copeland, Pasting and swelling properties of wheat flour and starch in relation to amylose content, Carbohydr. Polym. 71 (2008).

https://doi.org/10.1016/j.carbpol.2007.06.010.

[57] E. Bertoft, Understanding starch structure: Recent progress, Agronomy. 7 (2017) 56.

[58] C. Chi, X. Li, S. Huang, L. Chen, Y. Zhang, L. Li, S. Miao, Basic principles in starch multi-scale structuration to mitigate digestibility: A review, Trends Food Sci. Technol. 109 (2021) 154–168.

[59] E. Ojogbo, E.O. Ogunsona, T.H. Mekonnen, Chemical and physical modifications of starch for renewable polymeric materials, Mater. Today Sustain. 7 (2020) 100028.

[60] X. Wang, L. Huang, C. Zhang, Y. Deng, P. Xie, L. Liu, J. Cheng, Research advances in chemical modifications of starch for hydrophobicity and its applications: A review, Carbohydr. Polym. 240 (2020) 116292.

[61] S. Punia, Barley starch modifications: Physical, chemical and enzymatic - A review, Int. J. Biol. Macromol. 144 (2020). https://doi.org/10.1016/j.ijbiomac.2019.12.088.

[62] J. Jane, Y.Y. Chen, L.F. Lee, A.E. McPherson, K.S. Wong, M. Radosavljevic, T. Kasemsuwan, Effects of amylopectin branch chain length and amylose content on the gelatinization and pasting properties of starch, Cereal Chem. 76 (1999). https://doi.org/10.1094/CCHEM.1999.76.5.629.

[63] N. Lindeboom, P.R. Chang, R.T. Tyler, Analytical, biochemical and physicochemical aspects of starch granule size, with emphasis on small granule starches: A review, Starch/Staerke. 56 (2004). https://doi.org/10.1002/star.200300218.

[64] M. Beck, M. Jekle, T. Becker, Starch re-crystallization kinetics as a function of various cations, Starch/Staerke. 63 (2011). https://doi.org/10.1002/star.201100071.

[65] G. Spigno, D.M. De Faveri, Gelatinization kinetics of rice starch studied by non-isothermal calorimetric technique: Influence of extraction method, water coyncentration and heating rate, J. Food Eng. 62 (2004). https://doi.org/10.1016/S0260-8774(03)00248-6.

[66] T. De Pilli, R. Giuliani, A. Buléon, B. Pontoire, J. Legrand, Effects of protein-lipid and starch-lipid complexes on textural characteristics of extrudates based on wheat flour with the addition of oleic acid, Int. J. Food Sci. Technol. 51 (2016). https://doi.org/10.1111/ijfs.13070.

[67] C. Chao, J. Yu, S. Wang, L. Copeland, S. Wang, Mechanisms underlying the formation of complexes between maize starch and lipids, J. Agric. Food Chem. 66 (2018) 272–278.

[68] O. Nimz, K. Gessler, I. Usón, G.M. Sheldrick, W. Saenger, Inclusion complexes of V-amylose with undecanoic acid and dodecanol at atomic resolution: X-ray structures with cycloamylose containing 26 D-glucoses (cyclohexaicosaose) as host, Carbohydr. Res. 339 (2004) 1427–1437.

[69] W.C. Obiro, S. Sinha Ray, M.N. Emmambux, V-amylose structural characteristics, methods of preparation, significance, and potential applications, Food Rev. Int. 28 (2012) 412–438.

[70] G. Rappenecker, P. Zugenmaier, Detailed refinement of the crystal structure of Vh-

amylose, Carbohydr. Res. 89 (1981) 11–19.

[71] T. Carlson, K. Larsson, N. Dinh-Nguyen, N. Krog, A study of the amylose-monoglyceride complex by raman spectroscopy, Starch-Stärke. 31 (1979) 222–224.

[72] M.J. Gidley, S.M. Bociek, Carbon-13 CP/MAS NMR studies of amylose inclusion complexes, cyclodextrins, and the amorphous phase of starch granules: Relationships between glycosidic linkage conformation and solid-state carbon-13 chemical shifts, J. Am. Chem. Soc. 110 (1988) 3820–3829.

[73] J. Kawada, R.H. Marchessault, Solid state NMR and X-ray studies on amylose complexes with small organic molecules, Starch-Stärke. 56 (2004) 13–19.

[74] S. Wang, C. Chao, J. Cai, B. Niu, L. Copeland, S. Wang, Starch–lipid and starch–lipid–protein complexes: A comprehensive review, Compr. Rev. Food Sci. Food Saf. 19 (2020) 1056–1079.

[75] R. Cui, C.G. Oates, The effect of amylose-lipid complex formation on enzyme susceptibility of sago starch, Food Chem. 65 (1999). https://doi.org/10.1016/S0308-8146(97)00174-X.

[76] G.G. Gelders, J.P. Duyck, H. Goesaert, J.A. Delcour, Enzyme and acid resistance of amylose-lipid complexes differing in amylose chain length, lipid and complexation temperature, Carbohydr. Polym. 60 (2005). https://doi.org/10.1016/j.carbpol.2005.02.008.

[77] Y. Huang, W.-G. Dai, Fundamental aspects of solid dispersion technology for poorly soluble drugs, Acta Pharm. Sin. B. 4 (2014). https://doi.org/10.1016/j.apsb.2013.11.001.

[78] G. Esfahani, O. Häusler, K. Mäder, Controlled release starch-lipid implant for the therapy of severe malaria, Int. J. Pharm. 622 (2022). https://doi.org/10.1016/j.ijpharm.2022.121879.

[79] C. Auch, M. Harms, Y. Golitsyn, D. Reichert, K. Mäder, Miniaturized measurement of drug–polymer interactions via viscosity increase for polymer selection in amorphous solid dispersions, Mol. Pharm. 16 (2019) 2214–2225.

[80] V. Malaterre, H. Metz, J. Ogorka, R. Gurny, N. Loggia, K. Mäder, Benchtop-magnetic resonance imaging (BT-MRI) characterization of push–pull osmotic controlled release systems, J. Control. Release. 133 (2009) 31–36.

[81] H. Metz, K. Mäder, Benchtop-NMR and MRI—A new analytical tool in drug delivery research, Int. J. Pharm. 364 (2008) 170–175.

[82] T. De Pilli, K. Jouppila, J. Ikonen, J. Kansikas, A. Derossi, C. Severini, Study on formation of starch–lipid complexes during extrusion-cooking of almond flour, J. Food Eng. 87 (2008) 495–504.

[83] U.S. Food and Drug Administration, (n.d.). https://www.accessdata.fda.gov/drugsatfda_docs/label/2006/018869s014lbl.pdf (accessed September 10, 2023).

[84] Z. He, D. Zhong, X. Chen, X. Liu, X. Tang, L. Zhao, Development of a dissolution medium for nimodipine tablets based on bioavailability evaluation, Eur. J. Pharm. Sci. 21 (2004). https://doi.org/10.1016/j.ejps.2003.11.009.

[85] S.H. Mahmoud, X. Ji, F.A. Isse, Nimodipine Pharmacokinetic Variability in Various Patient Populations, Drugs R D. 20 (2020). https://doi.org/10.1007/s40268-020-00322-3.

[86] K.D. Ramsch, G. Ahr, D. Tettenborn, L.M. Auer, Overview on pharmacokinetics of nimodipine in healthy volunteers and in patients with subarachnoid hemorrhage, Neurochirurgia (Stuttg). 28 (1985). https://doi.org/10.1055/s-2008-1054107.

[87] ICH. Guidance for Industry – Q8 (r2), Pharm. Dev. Food Drug Adm. (2009). http://www.fda.gov/downloads/Drugs/GuidanceComplianceRegulatoryInformation/Guidances/ucm073507.pdf.

[88] J. Zech, S. Leisz, B. Göttel, F. Syrowatka, A. Greiner, C. Strauss, W. Knolle, C. Scheller, K. Mäder, Electrospun Nimodipine-loaded fibers for nerve regeneration: Development and in vitro performance, Eur. J. Pharm. Biopharm. 151 (2020). https://doi.org/10.1016/j.ejpb.2020.03.021.

[89] G. Esfahani, M.-L. Trutschel, D. Reichert, K. Mäder, Characterization of Controlled Release Starch-Nimodipine Implant for Antispasmodic and Neuroprotective Therapies in the Brain, Mol. Pharm. (2023).

[90] G. Esfahani, H. Lucas, F. Syrowatka, K. Mäder, A starch-based implant as a controlled drug release system: Non-invasive in vivo characterization using multispectral fluorescence imaging, J. Control. Release Off. J. Control. Release Soc. (2023) S0168-3659.

[91] S. Bialleck, H. Rein, Preparation of starch-based pellets by hot-melt extrusion, Eur. J. Pharm. Biopharm. 79 (2011). https://doi.org/10.1016/j.ejpb.2011.04.007.

[92] L.M.G. Castro, E.M.C. Alexandre, J.A. Saraiva, M. Pintado, Impact of high pressure on starch properties: A review, Food Hydrocoll. 106 (2020). https://doi.org/10.1016/j.foodhyd.2020.105877.

[93] D. Donmez, L. Pinho, B. Patel, P. Desam, O.H. Campanella, Characterization of starch–water interactions and their effects on two key functional properties: starch gelatinization and retrogradation, Curr. Opin. Food Sci. 39 (2021). https://doi.org/10.1016/j.cofs.2020.12.018.

[94] A. Besheer, K.M. Wood, N.A. Peppas, K. Mäder, Loading and mobility of spin-labeled insulin in physiologically responsive complexation hydrogels intended for oral administration, J. Control. Release. 111 (2006). https://doi.org/10.1016/j.jconrel.2005.12.008.

[95] R.G. Evans, A.J. Wain, C. Hardacre, R.G. Compton, An electrochemical and ESR spectroscopic study on the molecular dynamics of TEMPO in room temperature ionic liquid solvents, ChemPhysChem. 6 (2005). https://doi.org/10.1002/cphc.200500157.

[96] S. Kempe, H. Metz, K. Mäder, Application of Electron Paramagnetic Resonance (EPR)

spectroscopy and imaging in drug delivery research - Chances and challenges, Eur. J. Pharm. Biopharm. 74 (2010). https://doi.org/10.1016/j.ejpb.2009.08.007.

[97] World Health Organization, Guidelines for the treatment of malaria Third edition, Trans. R. Soc. Trop. Med. Hyg. 85 (2015). https://doi.org/10.1016/0035-9203(91)90261-V.

[98] A.-C. Eliasson, N. Krog, Physical properties of amylose-monoglyceride complexes, J. Cereal Sci. 3 (1985) 239–248.

[99] U. Uthumporn, A.A. Karim, A. Fazilah, Defatting improves the hydrolysis of granular starch using a mixture of fungal amylolytic enzymes, Ind. Crops Prod. 43 (2013) 441–449.

[100] X. Liang, J.M. King, F.F. Shih, Pasting property differences of commercial and isolated rice starch with added lipids and β-cyclodextrin, Cereal Chem. 79 (2002) 812–818.

[101] S. Uchida, S. Yamada, K. Nagai, Y. Deguchi, R. Kimura, Brain pharmacokinetics and in vivo receptor binding of 1,4-dihydropyridine calcium channel antagonists, Life Sci. 61 (1997). https://doi.org/10.1016/S0024-3205(97)00881-3.

[102] A. SCRIABINE, W. van den KERCKHOFF, Pharmacology of Nimodipine: A Review, Ann. N. Y. Acad. Sci. 522 (1988). https://doi.org/10.1111/j.1749-6632.1988.tb33415.x.

[103] S. Kazda, B. Garthoff, H.P. Krause, K. Schlossmann, Cerebrovascular effects of the calcium antagonistic dihydropyridine derivative nimodipine in animal experiments, Arzneimittel-Forschung/Drug Res. 32 (1982).

[104] R. Towart, E. Wehinger, H. Meyer, S. Kazda, The effects of nimodipine, its optical isomers and metabolites on isolated vascular smooth muscle, Arzneimittel-Forschung/Drug Res. 32 (1982).

[105] R.W.S. Li, C.M. Tse, R.Y.K. Man, P.M. Vanhoutte, G.P.H. Leung, Inhibition of human equilibrative nucleoside transporters by dihydropyridine-type calcium channel antagonists, Eur. J. Pharmacol. 568 (2007). https://doi.org/10.1016/j.ejphar.2007.04.033.

[106] M.I. Sweeney, Neuroprotective effects of adenosine in cerebral ischemia: Window of opportunity, Neurosci. Biobehav. Rev. 21 (1997). https://doi.org/10.1016/S0149-7634(96)00011-5.

[107] Z. Zhou, Y. Zhang, X. Chen, M. Zhang, Z. Wang, Multi-scale structural and digestion properties of wheat starches with different amylose contents, Int. J. Food Sci. Technol. 49 (2014). https://doi.org/10.1111/ijfs.12593.

[108] Q. Sun, M. Wu, X. Bu, L. Xiong, Effect of the amount and particle size of wheat fiber on the physicochemical properties and gel morphology of starches, PLoS One. 10 (2015). https://doi.org/10.1371/journal.pone.0128665.

[109] X. Zheng, R. Yang, X. Tang, L. Zheng, Part I: Characterization of solid dispersions of nimodipine prepared by hot-melt extrusion, Drug Dev. Ind. Pharm. 33 (2007). https://doi.org/10.1080/03639040601050213.

[110] A. Grunenberg, B. Keil, J.O. Henck, Polymorphism in binary mixtures, as exemplified by nimodipine, Int. J. Pharm. 118 (1995). https://doi.org/10.1016/0378-5173(94)00284-C.

[111] G.Z. Papageorgiou, D. Bikiaris, E. Karavas, S. Politis, A. Docoslis, Y. Park, A. Stergiou, E. Georgarakis, Effect of physical state and particle size distribution on dissolution enhancement of nimodipine/PEG solid dispersions prepared by melt mixing and solvent evaporation, AAPS J. 8 (2006). https://doi.org/10.1208/aapsj080471.

[112] A. Docoslis, K.L. Huszarik, G.Z. Papageorgiou, D. Bikiaris, A. Stergiou, E. Georgarakis, Characterization of the distribution, polymorphism, and stability of nimodipine in its solid dispersions in polyethylene glycol by micro-Raman spectroscopy and powder X-ray diffraction, AAPS J. 9 (2007). https://doi.org/10.1208/aapsj0903043.

[113] M.K. Riekes, R.N. Pereira, G.S. Rauber, S.L. Cuffini, C.E.M. de Campos, M.A.S. Silva, H.K. Stulzer, Polymorphism in nimodipine raw materials: Development and validation of a quantitative method through differential scanning calorimetry, J. Pharm. Biomed. Anal. 70 (2012). https://doi.org/10.1016/j.jpba.2012.06.029.

[114] K.C. Gordon, C.M. McGoverin, Raman mapping of pharmaceuticals, Int. J. Pharm. 417 (2011). https://doi.org/10.1016/j.ijpharm.2010.12.030.

[115] R. Xiong, W. Lu, J. Li, P. Wang, R. Xu, T. Chen, Preparation and characterization of intravenously injectable nimodipine nanosuspension, Int. J. Pharm. 350 (2008). https://doi.org/10.1016/j.ijpharm.2007.08.036.

[116] J. Yu, H.B. He, X. Tang, Formulation and evaluation of nimodipine-loaded lipid microspheres, J. Pharm. Pharmacol. 58 (2010). https://doi.org/10.1211/jpp.58.11.0002.

[117] R. Bunkerd, R. Molloy, R. Somsunan, W. Punyodom, P.D. Topham, B.J. Tighe, Synthesis and Characterization of Chemically-Modified Cassava Starch Grafted with Poly(2-Ethylhexyl Acrylate) for Blending with Poly(Lactic Acid), Starch/Staerke. 70 (2018). https://doi.org/10.1002/star.201800093.

[118] M. yan Wei, X. ping Lei, J. jing Fu, M. yue Chen, J. xia Li, X. yong Yu, Y. lei Lin, J. ping Liu, L. ran Du, X. Li, Y. Zhang, Y. ling Miao, Y. gang Huang, L. Liang, J. jun Fu, The use of amphiphilic copolymer in the solid dispersion formulation of nimodipine to inhibit drug crystallization in the release media: Combining nano-drug delivery system with solid preparations, Mater. Sci. Eng. C. 111 (2020). https://doi.org/10.1016/j.msec.2020.110836.

[119] D.N. Bikiaris, S. Papadimitriou, G.Z. Papageorgiou, F.I. Kanaze, M. Georgarakis, Nanoencapsulation of nimodipine in novel biocompatible poly(propylene-co-butylene succinate) aliphatic copolyesters for sustained release, J. Nanomater. 2009 (2009). https://doi.org/10.1155/2009/716242.

[120] H. Li, H. Li, C. Wei, J. Ke, J. Li, L. Xu, H. Liu, YangYang, S. Li, M. Yang, Biomimetic synthesis and evaluation of histidine-derivative templated chiral mesoporous silica for improved oral delivery of the poorly water-soluble drug, nimodipine, Eur. J. Pharm. Sci. 117 (2018). https://doi.org/10.1016/j.ejps.2018.03.013.

[121] A.J. Salgado, O.P. Coutinho, R.L. Reis, Novel Starch-Based Scaffolds for Bone Tissue Engineering: Cytotoxicity, Cell Culture, and Protein Expression, in: Tissue Eng., 2004. https://doi.org/10.1089/107632704323061825.

[122] X. Zhang, Y. Liu, S. Gong, M. Li, S. Li, Y. Hemar, Probing the biotoxicity of starch nanoparticles in vivo and their mechanism to desensitize β-lactoglobulin, Food Hydrocoll. 135 (2023) 108166.

[123] H.D. Janowitz, D.A. Dreiling, The plasma amylase: source, regulation and diagnostic significance, Am. J. Med. 27 (1959) 924–935.

[124] A. Beilvert, F. Faure, A. Meddahi-Pellé, L. Chaunier, S. Guilois, F. Chaubet, D. Lourdin, A. Bizeau, A resorbable shape-memory starch-based stent for the treatment of salivary ducts under sialendoscopic surgery, Laryngoscope. 124 (2014) 875–881.

7. Appendix

A. Publication list (Related publications to this thesis are marked with*)

1. * **Esfahani G**, Trutschel ML, Reichert D, Mäder K. Characterization of Controlled Release Starch-Nimodipine Implant for Antispasmodic and Neuroprotective Therapies in the Brain. Molecular Pharmaceutics. 2023 Sep 26.

2. * **Esfahani G**, Lucas H, Syrowatka F, Mäder K. A starch-based implant as a controlled drug release system: Non-invasive in vivo characterization using multispectral fluorescence imaging. Journal of Controlled Release. 2023 Jun 1;358:358-67.

3. * **Esfahani G**, Häusler O, Mäder K. Controlled release starch-lipid implant for the therapy of severe malaria. International Journal of Pharmaceutics. 2022 Jun 25;622:121879.

4. Sharif Makhmal Zadeh B, **Esfahani G**, Salimi A. Permeability of ciprofloxacin-loaded polymeric micelles including ginsenoside as P-glycoprotein inhibitor through a Caco-2 cells monolayer as an intestinal absorption model. Molecules. 2018 Jul 31;23(8):1904.

5. Sharif Makhmal Zadeh B, Niro H, Rahim F, **Esfahani G.** Ocular delivery system for propranolol hydrochloride based on nanostructured lipid carrier. Scientia pharmaceutica. 2018;86(2):16.

6. Makhmalzadeh BS, Salimi A, Nazarian A, **Esfahani G**. Formulation, characterization and in vitro/ex vivo evaluation of trolamine salicylate-loaded transfersomes as transdermal drug delivery carriers. International Journal of Pharmaceutical Sciences and Research. 2018 Sep 1;9(9):3725-31.

7. Salimi A, Makhmalzadeh BS, **Esfahani G**. Polymeric micelle as a new carrier in Oral drug delivery systems. Asian J. Pharm. 2017 Oct 1;11(4):704-11.

B. Oral presentations

- G Esfahani, Controlled release starch lipid implant for the therapy of severe malaria, Controlled Release Society Local chapters meeting, 9-11 March 2022, Aachen, Germany

- G Esfahani, Characterization of Controlled release starch lipid implant, 3rd Discussion Meeting of International Graduate School "Functional Polymers", 16-18 May 2022, Lutherstadt Wittenberg, Germany

- G Esfahani, Controlled release starch lipid implant for the therapy of severe malaria, Pharma Research Day, 5th of July 2022, Halle (Saale), Germany

- G Esfahani, A starch-based implant as a controlled drug release system, Pharma Research Day, 10th of July 2023, Halle (Saale), Germany

C. Posters

- G Esfahani, H Lucas, K Mäder, A starch-based implant as a controlled drug release system, ESAO Winter School 2023, 15-18 February, 2023, Lutherstadt Wittenberg, Germany

- G Esfahani, K Mäder, O Häusler, Controlled release starch lipid implant for the therapy of severe malaria, Controlled Release Society EU Local chapters meeting, 2-3 March 2023, Würzburg, Germany

- G Esfahani, H Lucas, K Mäder, A starch-based implant as a controlled drug release system, 4th European Conference on Pharmaceutics, 20 - 21 March 2023, Marseille, France

D. Curriculum vitae

Personal Data

Name	Golbarg Esfahani
Date of birth	21. November 1992
Place of birth	Tehran
Nationality	Iranian

Professional background

09/2022-Current	Researcher Pharmaceutical Technology Department, Pharmacy Institute, Martin Luther University Halle-Wittenberg
05/2019-09/2022	PhD candidate Pharmaceutical Technology Department, Pharmacy Institute, Martin Luther University Halle-Wittenberg
2017-2019	Pharmacist 24/7 Pharmacy, Mehrshahr Clinic, Karaj
2011 – 2017	PharmD (Continous master program in pharmacy) Ahvaz Jundishapur University of Medical Sciences, Ahvaz, Iran (4 years) Shahid Beheshti University of Medical Sciences, Tehran, Iran (2 years as Erasmus student)
2016	Internship during PharmD program, Hakim pharmaceutical company Shariati Street, Gholhak, Tehran
2015	Internship during PharmD program, Iran Hormone Pharmaceutical company District 21, Tehran

Date: 09.02.2024 **Signature:**

E. Acknowledgement

I would like to take this opportunity to sincerely thank everyone who supported me during my PhD project. Above all, I wish to extend my appreciation to my first supervisor, Prof. Dr. Karsten Mäder, for giving me the opportunity to pursue my goals. I am truly grateful for his consistent guidance and support during this project. Furthermore, I would like to extend my thanks to my second supervisor Prof. Dr. Detlef Reichert for all his kind guidance during this project.

I wish to express my sincere gratitude to the following individuals for their invaluable support and guidance during various aspects of my project:

- Dr. Henrike Lucas, for her kind support and precious guidance, especially during in vivo studies.
- Ms. Julia Kollan for her intensive support and guidance during the in vivo studies.
- Dr. Marie-luise Trutschel, for her kind support and valuable guidance, especially during NMR measurements.
- Dr. Olaf Häusler from Roquette Freres Company for his insightful comments and guidance in our first publication.
- Dr. Christoph Wagner from the Chemistry Institute of Martin Luther University Halle-Wittenberg, for his kind assistance with x-ray diffraction measurements.
- Dr. Matthias Schmidt and Ms. Antje Herbrich-Peters, for their generous assistance with HPLC and mass analysis.
- Dr. Stefan Gröger and Dr. Alexey Krushelnitsky for their kind support during NMR measurements.
- Dr. Wolfgang Knolle from the Leibniz Institute of Surface Engineering, for his support in sterilizing the samples.
- Ms. Rudolf, for her kind contributions to the FTIR measurements.
- Mr. Frank Syrowatka and Dr. Frank Heyroth, for their kind support with SEM and Raman Spectroscopy measurements.
- Dr. Hendrik Metz, for his valuable guidance and insightful comments regarding the EPR measurements.
- Ms. Kerstin Schwarz and Ms. Manuela Woik, our previous technical assistants, for their kind support during the analytical measurements.
- Ms. Claudia Bertram, for her kind support with official procedures.

Their contributions have been crucial in the success of this project, and I am deeply appreciative of their assistance.

I'd like to express my appreciation to my former and current colleagues who have been a valuable part of my journey:

Dr. Ligia de Souza, for her kind guidance, the warm atmosphere in our office, and the enjoyable moments we spent together. As for Dr. Henrike Lucas, Dr. Marie-luise Trutschel, Dr. Eric Lehner, Dr. Miriam Klein, Dr. Jonas Steiner, Dr. Martin Kirchberg, Dr. Johanna Zech, Dr. Bennedict Göttel, Dr. Ahmad Hivechi, Julia Kollan, Diana Kujas, Johannes Albrecht, Eike Bussmann, Anne Düminchen, Anastasios Nalbadis, Foozieh Sahne, Finnya Nienau, Lukas Bollenbach, Johanna Weber, Daniel Brucks, Sophie Meinhard, Fitore Mejzini, Linda-Marie Rauch, Julian Marcel Kunert, and Annelie Bading, I am thankful for their presence, which has enriched these years with cherished memories.

Finally, I want to express my gratitude to my family for their unconditional support throughout this journey. I extend my heartfelt thanks to my parents and my sister for their patience in coping with my absence and distance from home. I am particularly thankful to my husband for his unwavering support and his continuous assistance throughout my whole academic career.

Eidesstattliche Erklärung

der

Naturwissenschaftliche Fakultät I

- Biowissenschaften -

Martin-Luther-Universität Halle-Wittenberg

Ich erkläre gemäß § 5 der Promotionsordnung der Naturwissenschaftlichen Fakultäten I, II und III der Martin-Luther-Universität Halle-Wittenberg an Eides statt, dass ich die Arbeit selbstständig und ohne fremde Hilfe verfasst, keine anderen als die von mir angegebenen Quellen und Hilfsmittel benutzt und die den benutzten Werken wörtlich oder inhaltlich entnommenen Stellen als solche kenntlich gemacht habe. Weiterhin erkläre ich, dass ich mich mit der vorliegenden Dissertationsarbeit erstmals um die Erlangung eines Doktorgrades bewerbe.

09.02.2024 _____

Datum Unterschrift

International Journal of Pharmaceutics 622 (2022) 121879

Contents lists available at ScienceDirect

International Journal of Pharmaceutics

journal homepage: www.elsevier.com/locate/ijpharm

Controlled release starch-lipid implant for the therapy of severe malaria

Golbarg Esfahani [a], Olaf Häusler [b], Karsten Mäder [a,*]

[a] Institute of Pharmacy, Martin Luther University Halle-Wittenberg, Kurt-Mothes-Straße 3, 06120 Halle (Saale), Germany
[b] Roquette Freres, route haute loge, 62080 Lestrem, France

ARTICLE INFO

Keywords:
Controlled release
Biodegradable
Starch
Glycerol monostearate
Artesunate
Artemether

ABSTRACT

Parenteral depot systems can provide a constant release of drugs over a few days to months. Poly-(lactic acid) (PLA) and Poly-(lactide-co-glycolide) (PLGA) are the most commonly used polymers in the production of these systems. Finding alternatives to these polymers is of great importance to avoid certain drawbacks of these polymers (e.g. microacidity) and to increase the selection possibilities. In this study, different types of starch in combination with glycerol monostearate (GMS) were developed and investigated for their physicochemical properties and release characteristics. The noninvasive method of electron paramagnetic resonance (EPR) was used to study the release kinetics and mechanisms of nitroxide model drugs. The studies demonstrated the general suitability of the system composed of high amylose starch and GMS to form a controlled release system. For further characterization of the prepared system, formulations with different proportions of starch and GMS, loaded with the antimalarial agents artesunate or artemether were prepared. The implants were characterized with X-ray powder diffraction (XRPD) and texture analysis. The *in vitro* release studies demonstrated the sustained release of artemether over 6 days from a starch-based implant which matches desired kinetic for the treatment of severe malaria. In summary, a starch-based implant with appropriate mechanical properties was produced that can be a potential candidate for the treatment of severe malaria.

1. Introduction

Parenteral depot systems are potential drug delivery systems for the treatment of various diseases. They have several advantages compared to oral administration, because these systems can provide a constant concentration of the drug for a few days to several months. Many of the drugs with low water solubility and short half-life are good candidates to be loaded in these systems (Kempe and Mäder, 2012). In the last two decades, there has been a growing interest in long acting parenteral drug delivery systems. Currently, various types of parenteral depot systems are commercially available on the pharmaceutical market. Most of these products are based on polylactic acid (PLA) and poly(lactic-co-glycolic) acid (PLGA) polymers. PLA and PLGA are biodegradable polymers. However, they degrade to acidic monomers which might cause acidic microenvironments both *in vitro* (Ding and Schwendeman, 2008) and *in vivo* (Mäder et al., 1996; Schädlich et al., 2014). In addition to the development of low PH values inside the degrading polymer matrix, these acidic monomers can also cause autocatalysis and complex and nonlinear release profiles. Also, drug inactivation may happen by the formation of the covalent bond between the drug molecule and the produced monomers (Lucke et al., 2002). Hence, finding alternative biodegradable materials will be beneficial in the formulation of future parenteral depot systems. Starch, as a natural biodegradable polymer can be a candidate to replace these polymers.

Starch (nonmodified form) is in general fully biodegradable. Its degradation in the body produces non-toxic and non-acidic monomers (Araújo et al., 2004). Starch-based materials are already clinically used as bioresorbable medical products for providing hemostasis and to prevent postoperative tissue adhesion (Krämer et al., 2021; Mendes et al., 2001). It is also a major excipient in the pharmaceutical industry. However, there are still some drawbacks in using starch; such as its weak mechanical properties and its fast degradation in the body over a few days. Starch properties can be modified by the presence of other molecules and/or the impact of temperature and pressure. Studies have shown that starch can form complexes with certain lipids (e.g. fatty acids or mono-glycerides) and lipid complexation can be facilitated at higher temperatures utilizing the extrusion process (De Pilli et al., 2016). In this study, the effect of the addition of the lipid to starch and the effect of temperature and pressure on starch was evaluated to modify starch characteristics. In addition, the formation of starch-lipid complexes

* Corresponding author.
E-mail address: karsten.maeder@pharmazie.uni-halle.de (K. Mäder).

https://doi.org/10.1016/j.ijpharm.2022.121879
Received 16 February 2022; Received in revised form 9 May 2022; Accepted 26 May 2022
Available online 29 May 2022

makes the material more resistant against enzymatic digestion (Cui and Oates, 1999; Gelders et al., 2005). Introducing lipids into starch is therefore a rational approach to decrease enzymatic degradation and to slow down the drug release.

Malaria is a life-threatening disease. Despite recent efforts to reduce the malaria burden globally, there were an estimated 229 million clinical cases, 2 million severe malaria cases, and approximately 409 000 deaths due to malaria worldwide in 2019 (World Health Organization, 2020). Artesunate (AS) is the WHO first-line treatment of severe malaria in adults and children. It is a clinically versatile artemisinin derivative but with an extremely short half-life. Per WHO guidelines, this drug should be administered several times per day intravenously in case of treatment of severe malaria. Studies have shown that intravenous artesunate administration is associated with high initial artesunate concentrations which subsequently decline rapidly, with typical artesunate half-life estimates of less than 15 min (Morris et al., 2011). Per WHO guidelines, parenteral artemether (AM) is an alternative option in case injectable artesunate is not available (World Health Organization, 2015). Both of these drugs are metabolized to dihydroartemisinin (DHA), the active metabolite of the drugs, in the human body. Artemether is poorly soluble in water and its parenteral formulation is only available as a premixed oil-based solution for intramuscular injection (Esu et al., 2020). Based on a WHO report, intramuscular injection of artemether results in slow but erratically absorption that leads to a smaller survival benefit than intravenously applied artesunate (World Health Organization, 2015). Therefore, finding a system that provides a sustained release of artesunate or artemether is of great clinical importance to treat severe malaria. The aim of this study was the preparation and characterization of a parenteral depot system based on starch and lipid that can provide a constant release of artesunate or artemether over a few days to a week for the treatment of severe Malaria.

This study is divided into two main parts. In prescreening studies, implants with different types of starch in combination with Glycerol monostearate (GMS) were produced and characterized to find the appropriate type of starch and lipid to be used. The homogeneity of the prepared implants and their physical stability in PBS were the criteria for the selection of the implants for further assessment by Electron Paramagnetic Resonance (EPR). The implant's microenvironment, water penetration into the implants, and release behavior of model drugs from the implants were assessed with EPR. Based on the obtained data from prescreening studies, three formulations were chosen to load antimalarial agents. The prepared implants were characterized by texture analysis, X-ray powder diffraction, and high-pressure liquid chromatography (HPLC).

2. Materials and methods

2.1. Materials

Native pea starch (PEA STARCH N-735) and high amylose starch (MAIZE STARCH AMYLO N-400 (amylose content ≈53%)) were kindly provided by Roquette (Lestrem, France). Hydroxyethyl starch (HES) was kindly provided by Serumwerk Bernburg (Bernburg, Deutschland). Glycerol monostearate (Kolliwax® GMS II) was kindly provided by BASF (Germany). Glycerol monostearate (IMWITOR® 491) was kindly provided by IOI Oleo GmbH (Germany). Tempol (4-Hydroxy-TEMPO) and Tempol Benzoate (4-hydroxy-tempo benzoate) were purchased from SIGMA Aldrich Chemie GmbH (Munich, Germany). Artemether and artesunate were purchased from abcr GmbH. Olive oil was purchased from Caelo (Germany). NMP (1-Methyl-2-pyrrolidone) was purchased from Sigma-Aldrich (USA). Testing media was Phosphate Buffered Saline (Ph.Eur.) plus 1% sodium dodecyl sulfate (SDS), adjusted to pH 7.4. SDS was purchased from Sigma Aldrich Chemie GmbH (Munich, Germany). Acetonitrile (VWR International, Darmstadt, Germany), Formic Acid (Merck, Germany) and, double distilled water were used for the HPLC measurements.

2.2. Prescreening studies

Prescreening studies were conducted to identify the appropriate type of starch that can form a controlled release system in combination with lipid (GMS). Also, the temperature and extrusion speed for the HME process and the amount of water in the formulation were optimized in prescreening studies. Four different types of starch including HES, native pea starch, gelatinized pea starch, and high amylose starch in combination with two commercially available products of Glycerol monostearate (GMS) namely Kolliwax® GMS II and IMWITOR® 491 were examined. Gelatinized pea starch was obtained by adding water to pea starch (1 g pea starch:5 g water) and stirring the mixture at 80 °C for 5 min. The preparation was then dried in an oven at 50 °C overnight. The produced film was cryomilled with two 4 mm grinding media with two cycles each at 25 Hz for 90 s. The implants were prepared by hot-melt extrusion (ZE 5 ECO; Three-Tec GmbH; Seon; Swiss) with different extrusion screw speeds and different temperatures zones, depending on the formulation's components. Thermal measurements were also conducted to assess the thermal behavior of the formulation; the data is shown in the supplementary materials (Fig. S1 and Fig. S2). The homogeneity of the implants was studied with optical light microscopy on the micrometer scale. The physical stability of the prepared implants was assessed by incubating extrudates of 1 cm length in 50 ml PBS, pH 7.4 at 37 °C in the shaker (Memmert GmbH + Co. KG, Schwabach, Germany). The homogeneity of the prepared implants and their physical stability in PBS were the criteria for choosing the implants for further assessment by EPR.

2.3. Optical light microscopy

Light microscopy was used to assess the homogeneity of the prepared implant on the micrometer scale.

2.4. Hot melt extrusion

The following criteria led to the selection of the excipients and the processing conditions of extrusion. In general, extrusion the temperature should not be too high to prevent chemical degradation. However, if the temperature is too low, no extrusion is possible. Prescreening studies showed that a minimum temperature of around 60 °C is needed to obtain homogenous extrudates from starch. As the higher temperature than the melting point of the lipid may lead to the separation of the solid starch and the low viscous oily liquid, IMWITOR 491 with a higher melting point than Kolliwax® GMS ll was chosen as the lipid component. Water which was used as a plasticizer plays a significant role in the extrusion process. Although a certain amount of water is needed to gelatinize the starch (what makes the extrudates more flexible) and make the extrusion possible, an excess amount of water leads to super soft extrudates which are hard to gather or even the formation of foam-like material. Also, it should be noted that the formulations containing a high amount of lipid were only extrudable with a lower amount of water. The water amount was optimized in prescreening studies. Based on the results of the prescreening studies high amylose starch (AMYLO N-400®) and GMS (IMWITOR® 491) were chosen to prepare the implants by hot-melt extrusion (HME) (ZE 5 ECO; Three-Tec GmbH; Seon; Swiss). The components of each formulation and the hot-melt extrusion parameters (including extrusion screw speed and heating zone temperatures) are shown in Table 1 and Table 2 respectively. Before extrusion, components of each formulation were mixed and filled into the grinding chamber of a Retsch CryoMill (Retsch, Haan, Germany) together with two 10 mm grinding media. The cryomilling process scheduled an automatic pre-cooling phase and 2 milling cycles at 30 Hz for 150 s. Each cycle was followed by a 30 s lasting cooling phase at 5 Hz. Extrusion dies with a 1 mm diameter were used. Samples were collected and stored in opaque falcon tubes between 4° and 8 °C.

Table 1
Composition of investigated formulations in gram.

Formulation No	Formulation name	Components [g]				
		High amylose maize Starch	GMS	Artemether	Artesunate	water
1	Starch implant	4	–	–	–	2
2	Starch-lipid implant	4	3	–	–	1
3	Starch-AM implant	5	–	5	–	2.5
4	Starch-AM-Low lipid implant	4	1	5	–	2
5	Starch-AM-High lipid implant	4	3	7	–	1
6	Starch-AS implant	5	–	–	5	2.5
7	Starch-AS-Low lipid implant	4	1	–	5	2
8	Starch-AS-High lipid implant	4	3	–	7	1

Table 2
Used extrusion parameters.

Formulation No.	Temp. heating zone 1 [°C]	Temp. heating zone 2 [°C]	Temp. heating zone 3 [°C]	Screw speed rpm
1	70	80	90	140
2	69	68	67	140
3	60	65	70	140
4	60	65	68	140
5	69	68	67	140
6	60	65	70	140
7	60	65	70	140
8	69	68	67	140

2.5. Electron paramagnetic resonance (EPR)

Electron paramagnetic resonance (EPR) was applied to assess the model drug release behavior, water penetration and the microenvironment in the blank formulations (No 1 and 2). Tempol and Tempol Benzoate (TB) were used as models for hydrophilic and hydrophobic drugs with a concentration of 5 mmol/kg. The implants were incubated in 50 ml PBS in a shaking water bath (50 rpm) at 37 °C. At determined time points, the implants were taken out of the PBS and transferred to the EPR spectrometer. EPR spectra were obtained using an L-Band spectrometer (Magnettech GmbH, Germany), operating at a microwave frequency of about 1.1–1.3 GHz, equipped with a re-entrant resonator. EPR parameters were set to: centre field 49 mT, scan width 12 mT, scan time 60 s, modulation amplitude 0.0625 mT and modulation frequency 100 kHz. The spectral simulation was used to determine the distribution of the spin probe between different phases. The software EPRSIM V.4.99 from the Biophysical laboratory EPR centre (Josef Stefan Institute of Solid State Physics Ljubljana, Slovenia) was used for the evaluation and simulation of the EPR spectra.

2.6. Texture analysis

The mechanical properties of the implants were studied by a texture analyzer (CT3-4500, Brookfield-Rheotec, Germany) with the TexturePro CT V1.6 software. The samples were placed on microscopic slides and adjusted at the base table (TA-RT-KIT) of the analyzer. The TA7 standard probe, which resembles a knife-edge, was utilized. The required force to push the probe with a constant velocity into the samples was measured. Experiments were conducted at 20 °C with a scan velocity of 0.05 mm/s and a trigger force of 0.067 N.

2.7. X-ray powder diffraction

XRPD was applied to determine the state of drugs and GMS inside the implants. As a preparation step for the XRPD measurements, the implants were split into smaller pieces with a scalpel and submitted to cryomilling (Retsch GmbH, Haan, Germany). After an automatic precooling phase, samples were milled with two 4 mm grinding media at 25 Hz for 60 s. XRPD was performed on an STOE STADI MP (STOE & Cie GmbH, Darmstadt, Germany) powder diffractometer, equipped with molybdenum anode (50 kV and 30 mA) and a Ge (1 1 1) monochromator to select the Mo K_α radiation at 0.071073 nm. Data of the rotating samples were collected in the transmission mode from 2°-25° in 1° steps for 60 s each using a DECTRIS MYTHEN 1 K Strip Detector. The diffraction patterns obtained were processed using an STOE WinXPOW software package.

2.8. In vitro artemether and artesunate release

One centimeter implant of each formulation was weighed and placed in 2 ml vials filled with 1.5 ml PBS plus 1% SDS, pH 7.4 and the vials were slightly agitated in a shaker with light protection (Memmert GmbH + Co. KG, Schwabach, Germany) at 37 °C. Total buffer volume was withdrawn at regular time intervals and analyzed according to the described HPLC method. An appropriate volume of fresh PBS plus 1% SDS was replaced after taking samples. Each experiment was conducted in triplicate.

2.9. High performance liquid chromatography

HPLC analysis was performed with a Waters Delta 600 system with 717 plus Auto Sampler, 2996 Photodiode Array Detector, and a ZORBAX Eclipse XDB C8 150x4.6 5 μm column. A sample volume of 40 μl was injected at a flow rate of 1.0 ml/min. The mobile phase was Acetonitrile, water and formic acid with the ratio of 55:45:0.1 and 60:40:0.1 V/V for artesunate and artemether respectively. The retention times were 4.4 and 7.9 min for artesunate and artemether respectively. The quantification was carried out with a UV/VIS detector at 257 nm. Linear calibration curves ($r^2 > 0.999$) were obtained in the range of 50–1000 μg/ml for both drugs. Masslynx V4.1 software was used to analyze the data.

3. Results and discussions

3.1. Prescreening studies

Starch is a widely used pharmaceutical excipient in its native and its modified forms (Sasaki et al., 2000). It can be used e.g. as a binder, disintegrant, diluent, glidant and lubricant (Builders et al., 2013). Native starches are coming from the different botanic origin and own therefore various physical properties, such as different gelatinisation temperatures. Choosing an appropriate starch type for a controlled release system is, therefore, an important goal of prescreening studies. It is also to consider that the pressure and the temperature of the HME process and the water amount, acting as a plasticizer in the formulation can alter the thermal properties of starch significantly (Bialleck and Rein, 2011; Castro et al., 2020; Donmez et al., 2021). This affects the implant mechanical properties. Therefore, finding an optimized temperature and extrusion speed, as well as the right water amount to prepare implants with appropriate mechanical properties, was another important goal of prescreening study.

The homogeneity of the prepared implants and their physical stability in PBS were the main criteria for choosing the right type of starch

and GMS. Results of prescreening studies did show, that more homogenous extrudates were obtained with higher temperatures. GMS (Kolliwax® GMS ll) and GMS (IMWITOR® 491) have melting points of 58 °C and 68 °C respectively. When Kolliwax® GMS ll was used, high temperatures lead to the separation of GMS from the other components and its faster exit from the extruder. This was even worse in formulations with a higher amount of GMS. Therefore, GMS (IMWITOR 491) with a higher melting temperature was used as a lipid part of the formulation. Implants made of high amylose starch (AMYLO N-400®) and GMS (IMWITOR 491) were homogeneous and were physically stable in PBS for more than a month. Therefore, high amylose starch (AMYLO N-400®) and GMS (IMWITOR 491) were chosen to prepare the formulations for further studies.

3.2. Hot melt extrusion

Extrusion temperatures depend on the components of each formulation. The melting point of the GMS, homogeneity of the prepared implant, and drug stability were the determining factors in choosing the appropriate temperature for the process. If the temperature is too low, no extrusion is possible at all or inhomogenous extrudates are formed. High temperatures can cause the formation of separated liquids (for GMS containing extrudates) and drug degradation (both artemether and artesunate are heat sensitive). Pure artemether has a melting point in the range of 86–89 °C (Kuntworbe et al., 2018). In order to prevent drug degradation, the maximum temperature of 70 °C was used for the formulations containing artemether or artesunate. As mentioned in prescreening studies, GMS (IMWITOR 491) with a higher melting point (68 °C) was used to make the extrusion process possible in higher temperatures for GMS containing samples. The finally applied process parameters for HME related to each formulation are listed in the Materials and Methods section in Table 2.

The starch implants loaded with artesunate (left) and artemether (right) are shown in Fig. 1.

3.3. Electron paramagnetic resonance

Electron paramagnetic resonance (EPR) was applied to evaluate the model drug release and the water penetration into the implants. A low frequency spectrometer (1.1 GHz, L-band) was used. L-band has the advantage of the higher penetrating depth of the irradiation (about 5–10 mm) into water-containing samples in comparison to X-band (Kempe et al., 2010). Stable nitroxyl radicals (spin probes) with different physicochemical properties allow the determination of micro-viscosity and micropolarity (Lurie and Mäder, 2005). In this study, Tempol (TL) and Tempol Benzoate (TB) as models of a hydrophilic (TL) and hydrophobic (TB) drug were used. The chemical structures of the spin probes are shown in Fig. 2.

The interaction with the nitrogen nucleus is the primary interaction of the unpaired electron in nitroxide spin probes. This interaction is called ''hyperfine interaction''. Hyperfine interaction produces small changes in the allowed energy levels of the electron that leads to splitting the EPR signal into multiple lines. Tempol and Tempol benzoate

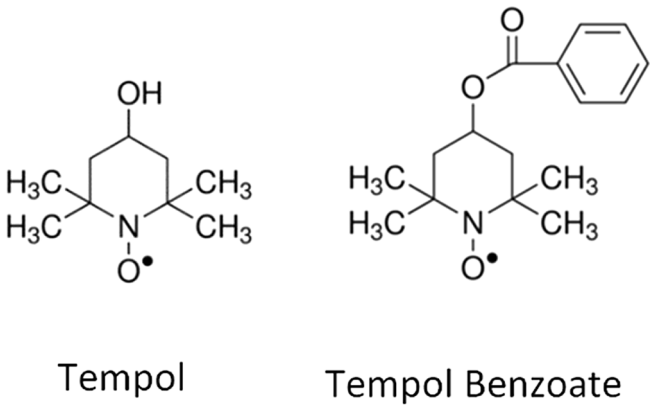

Fig. 2. Chemical structure of Tempol, (4-hydroxy-2,2,6,6-tetramethylpiperidine-N-oxyl, left) and Tempol benzoate (4-Hydroxy-2,2,6,8-tetramethylpiperidin-1-oxyl-benzoat, right).

with the predominant 14 N isotope give rise to a three-line EPR spectrum (Klug and Feix, 2008).

EPR spectra are sensitive to the rotational motion of the spin probes. Polarity and microviscosity are the parameters that affect the spin probe's rotational motion and therefore the shape of the EPR spectra. Higher polarities cause larger distances between the lines of the spectra. As can be seen in Fig. 3, the distance between the outer lines in PBS as a

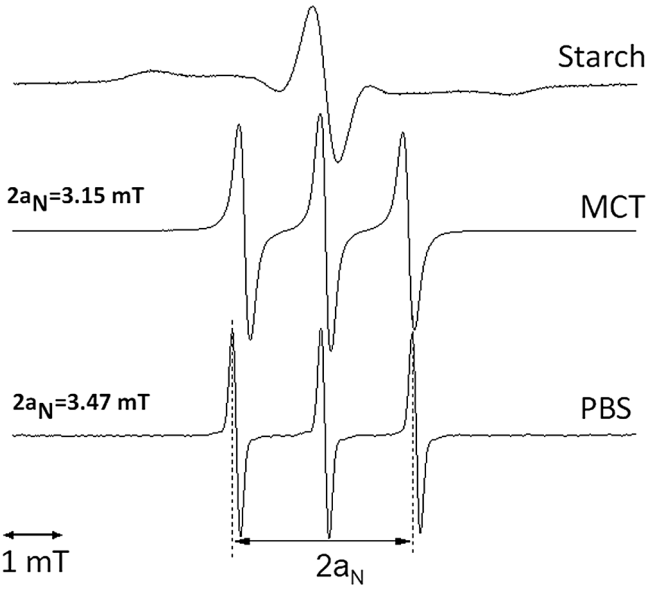

Fig. 3. EPR spectrum of TB in starch (powder-like spectrum), MCT (less polar environment, shorter distance between the outer lines, 2aN = 3.15 mT) and PBS (polar environment with longer distance between the outer lines, 2aN = 3.47 mT).

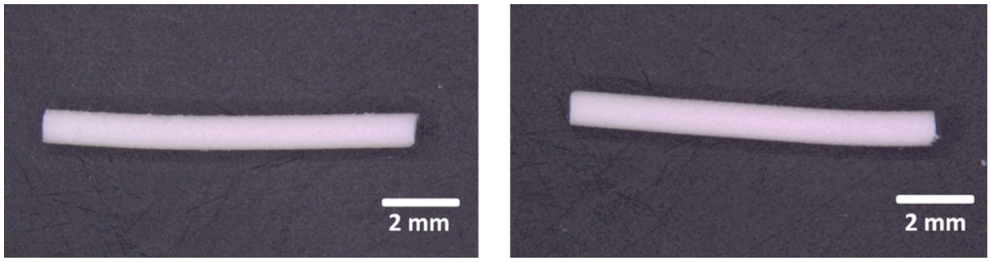

Fig. 1. Starch implants loaded with artesunate (left) and artemether (right) with 1 mm diameter.

polar environment is higher than the distance in medium chain triglyceride (MCT) as a less polar media (Lurie and Mäder, 2005). In low viscous media, the spin probes tumble freely resulting in spectra with three narrow lines of approximately equal height that can be seen in spectra of TB in PBS. As the viscosity increases, due to slower motions, the lines broaden and the signal amplitude decreases (Besheer et al., 2006). In a solution, anisotropic interactions are averaged out and lines widths are more narrow compared to less mobile and more viscous systems. In solid materials, the anisotropy is not averaged and typical "powder spectra" can be recorded (Evans et al., 2005; Kempe et al., 2010). EPR spectrum of TB loaded implant made of starch shows a "powder spectra" due to immobilization of TB inside the solid system.

Fig. 4 shows the EPR spectra of TB loaded implants in the dry state and after different times of exposure to PBS. The EPR spectra of TB in different components of the formulations were also obtained to achieve more details (Fig. S3). The EPR spectra are magnified by the mentioned number next to each signal to make the comparison easier. A decrease in signal amplitude of both implants was observed over two weeks shows the extended release of the TB from both implants. Comparing the two implants, it can be seen that the starch implant signal amplitude is almost one third after 9 days, while the signal amplitude of starch-lipid implant is about half after 15 days of PBS exposure. Therefore, as it was expected, a longer release time was observed in a formulation containing lipid (GMS). This is probably due to slower water penetration into the starch-lipid system in comparison to the starch system. The release of TB from the starch implant was almost completed after 14 days. After this time, only a very noisy signal was observed, due to the very low remaining amount of TB inside the implant. In contrast, no more decrease in the signal amplitude of starch-lipid implant was observed after the 15th day. This is probably due to some part of the TB that is trapped in the lipid part of the implant and it is not released from the system during this time period *in vitro*. Therefore, the addition of the lipid to the formulation could help to have the release of TB over a longer period of time.

To have a better understanding of the water penetration into the implant and also to determine the distribution of the spin probe between different phases, spectral simulations were carried out. The EPR spectra of TB in different environments and the simulations (dashed line) of the spectral pattern are shown in the supplementary in Fig. S4. Fig. 5 shows EPR spectra of TB loaded starch-lipid implant exposed to PBS (black line) after different exposure times to PBS and simulations (dashed line) of the mobile and immobile spectral pattern. A superposition of two species within the spectra was detectable. At all times, some part of TB is immobilised within the implant and its mobility is so restricted that so-called powder-like spectra result. In addition, a second species with higher mobility is observed which shows a three line spectrum with broad lines. The spectral shape indicates a "moderate" mobility which means that the molecule is sufficient mobile to give some averaging of the anisotropic hyperfine splitting. However, the different amplitudes and broad line widths indicate much less mobility compared to low viscous systems (e.g. TB in water). After 5 min about 28% of the total amount of TB in the implant is moderate mobile and 72% of TB is still immobile. Over time, the amount of partially mobile TB inside the implant is increased due to the diffusion of water into the implant. Since the mobile TB is released from the implant into the PBS over time, a decrease in the amount of mobile TB was observed after 48 h. It should be noted that the mobile species of TB is still much less mobile compared to mobile Tempol in the corresponding starch and starch/lipid extrudates (Fig. 6). This can be concluded by comparison in the line width of the two spectra (Fig. 7). The three lines are much broader in TB mobile species spectra in comparison to the lines of the Tempol loaded implant spectra. As mentioned previously, slower motions of the spin probe broaden the lines of the EPR spectra.

In the next step, Tempol, as a hydrophilic spin probe was used to assess the water penetration into the implants in more detail. The EPR spectra of TL in olive oil (less polar environment, shorter distance between the outer lines), NMP and PBS (polar environment with longer distance between the outer lines) are shown in Fig. S5 (supplementary materials) as controls to show the effect of environment polarity and viscosity on TL mobility and 2aN value.

Fig. 6 shows the EPR spectra of the TL loaded implants in the dry state and after different exposure times to PBS. The EPR spectrum of the Tempol in PBS is shown to make the comparison easier.

As can be seen in Fig. 6, the EPR spectra of the TL loaded implants in the dry state do not show real powder like spectra like what was observed in the dry state of TB loaded implants. The three broad lines of these spectra show that most part of TL shows moderate mobility (indicating mobility in a viscous environment) even before exposure to buffer. Due to their different hydrophilicities, TL and TB will localize in different environments in heterogeneous media. TL is much more hydrophilic and we hypothesised that three line spectrum of TL arises from the localization in viscous microregions of high polarity (e.g. adsorbed water). This assumption has been confirmed by the evaluation of the hyperfine splitting values.

The distance between the first and the third line (2aN) is sensitive to the polarity of the environment. The 2aN values for both TL loaded implants in the dry state are 3.43 mT which is close to the 2aN value of TL in PBS (=3.46 mT), but much higher than the 2aN values for TL in olive oil (2aN = 3.15 mT) and NMP (2aN = 3.21 mT) (Fig. 7). After exposure of both TL loaded extrudates to PBS, a continuous decrease in the width of all three lines was observed over the whole time period, but the most remarkable change was already observed only after 5 min.

These results prove a very fast water penetration into both systems (Fig. 7). These results are in line with the results obtained from the EPR

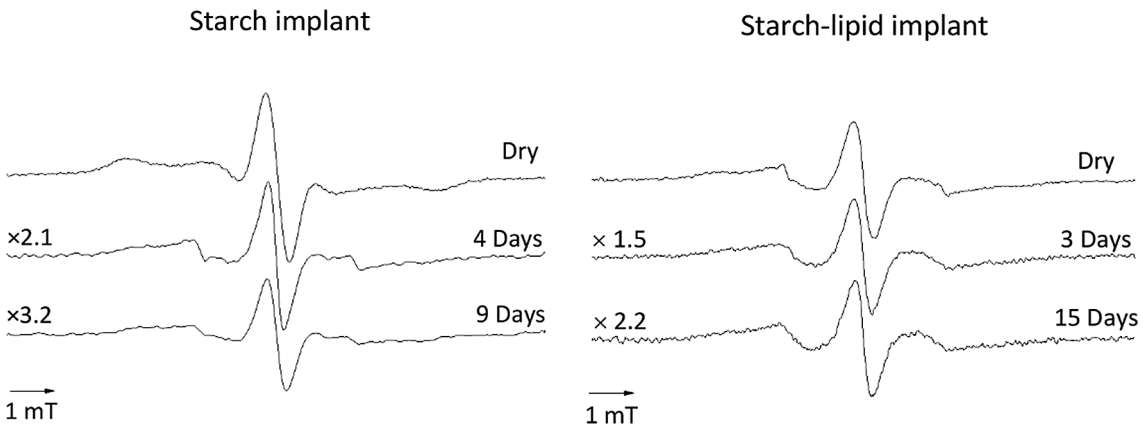

Fig. 4. EPR-Spectra of Tempol benzoate (TB) loaded implants. Starch implant on the left, and, starch-lipid implant on the right, after different times of exposure to PBS.

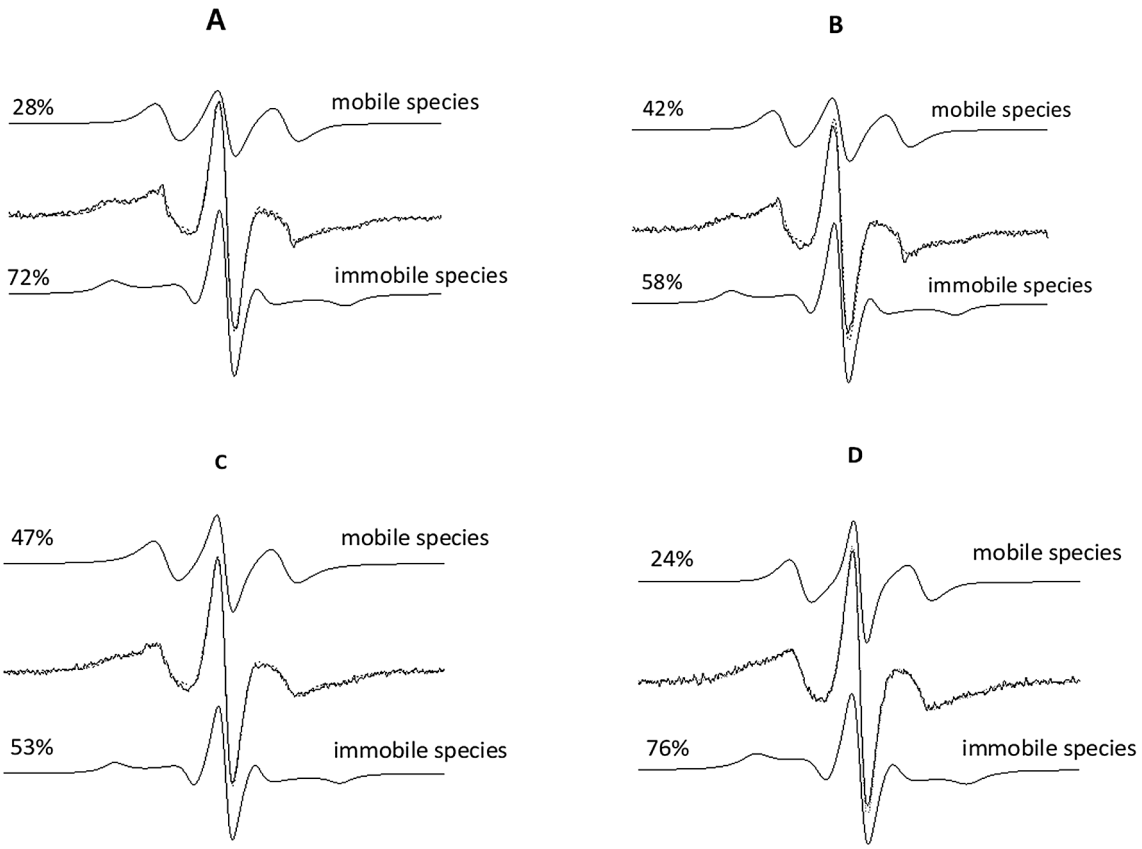

Fig. 5. EPR spectra of TB loaded starch-lipid implant exposed to PBS (black) after different exposure times to PBS and simulation (dashed line) of the mobile and immobile spectral pattern. The figure shows EPR spectra of the implant after: 5 min (a), 15 min (b), 24 h (c) and, 48 h (d) exposure to PBS.

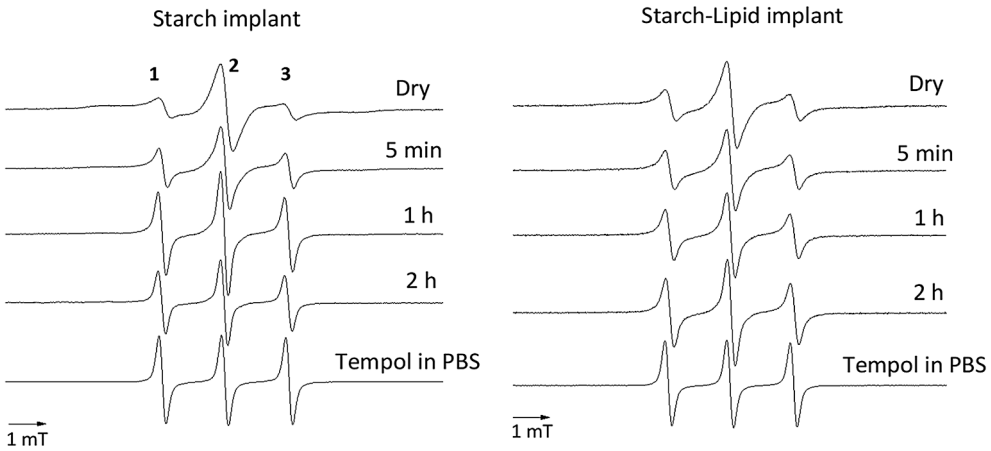

Fig. 6. EPR-Spectra of TL loaded implants (starch implant on the left and starch-lipid implant on the right) after different times of exposure to PBS.

spectra simulation. Both experiments demonstrated a fast water diffusion into the systems in the first 5 min and a subsequent increase in the amount of solubilized spin probe inside the implant that is released over time.

Based on the results of EPR experiments, both the starch implant and starch-lipid implant demonstrated the potential to be used as a controlled release system for more lipophilic drugs. Hydrophilic small molecules are expected to be released similar to TL. The EPR spectra of the TL extrudates prove a fast water penetration and solubilization of hydrophilic molecules both in GMS loaded extrudates and GMS free extrudates.

In order to assess the effect of the amount of lipid (GMS) on the system's characteristics, three formulations including starch implant, starch-low lipid implant, and, starch-high lipid implant were produced and characterized. The exact components of each formulation are shown in Table 1.

3.4. Texture analysis

Subcutaneous injection is a possible route of administration for the prepared implants. For subcutaneous injection, it is important to have an implant with sufficient flexibility and mechanical resistance. A brittle implant may break during insertion, therefore, sufficient strength is required to withstand the insertion process. Breakage or cracks in the

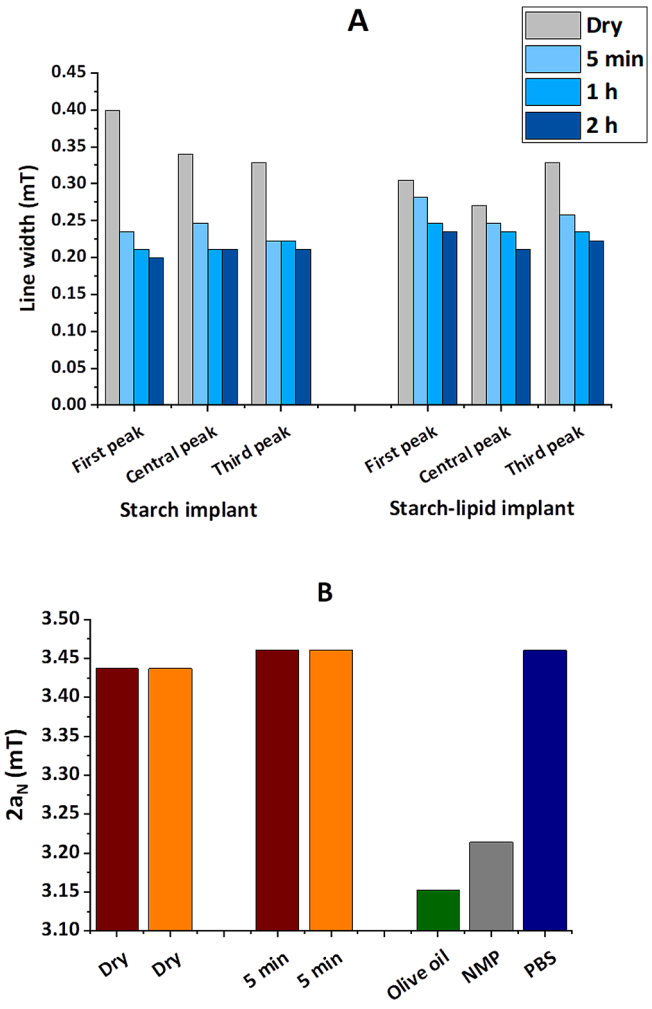

Fig. 7. A: Impact of buffer incubation time on EPR line widths. B: The 2aN hyperfine splitting values for TL loaded starch implant and starch-lipid implant in the dry state (2aN = 3.43 mT) and after 5 min exposure to PBS (2aN = 3.46 mT). The 2aN values for TL in olive oil (2aN = 3.15 mT), NMP (2aN = 3.21 mT) and PBS (2aN = 3.46 mT). Typical standard deviations in the determination of the 2aN values and the line widths were below 1% and 5% respectively.

implant may lead to faster release of drug and undesirable side effects in the patient. Different mechanical tests have been reported to assess the mechanical properties of medical devices. A test similar to the performed test in this study has been done by Lehner et al. to evaluate the mechanical strength of intracochlear PLGA based implants for dexamethasone release (Lehner et al., 2019). In a study done by Stewart et al. a three-point bending test was performed to find the maximum force required to break the 3D printed biodegradable subcutaneous implants for prolonged drug delivery (Stewart et al., 2020). In this study, the mechanical properties of the implants were studied by texture analysis. A small blade was forced to penetrate over a distance of 0.3 mm into the implant and the resulting force was measured. Fig. 8 shows the force path diagrams of the different implants. All implants cracked before reaching the 0.3 mm penetration distance. Testing of starch implants resulted in a fast increase of force, indicating a higher mechanical resistance in comparison to lipid containing formulations. The maximum forces for the artesunate and artemether loaded starch implants were 5.15 N and 4.50 N respectively. The found maximum forces for lipid containing formulations were much lower than for the starch-based implants. They were for starch-low lipid and starch-high lipid implants 0.51 N and 1.98 N for artemether loaded implants, and 2.2 N and 1.38 N for artesunate loaded implants respectively. These formulations were all cracked before reaching a distance of 0.15 mm. As the results show, the addition of the lipid to the formulation makes the implants more brittle. The observed increase in the standard deviations at the final points of the graph is due to crack formation and breakage of the implants.

3.5. X-ray powder diffraction

Fig. 9 shows the x-ray pattern of the powdered samples. X-ray diffractograms of powdered samples of starch are shown in the supplementary (Fig. S6). Fig. 9 shows the diffractograms of artesunate, GMS and the formulations loaded with artesunate on the left and diffractograms of artemether, GMS and the formulations loaded with artemether on the right. Both antimalarial agents are crystalline powder. The diffractograms show the identical peaks of artesunate (Lisgarten et al., 2002) and artemether (Luo et al., 1984). The strong diffraction peaks of artesunate and artemether were observed in all formulations. Therefore, both drugs exist in their crystalline state in all formulations. The diffraction patterns of artesunate prove no polymorphic transformation to the second crystalline form. There are some changes in the diffraction patterns of artemether loaded starch implant and starch-low lipid implant. Further studies are needed to prove whether transformation to another crystalline form of artemether has occurred due to the heat, pressure and existence of water in the extrusion process (Gao et al., 2013; Zhang et al., 2011). Observed peaks with 2 Theta values of 8.9, 10.63 and 11.15° in GMS diffractogram correspond to d spacing values of 0.46, 0.38 and 0.37 nm that are the typical peaks of the beta crystalline form of the GMS, usually seen in the raw GMS powder (Himawan et al., 2006; Metin and Hartel, 2005). The x-ray diffractograms of the

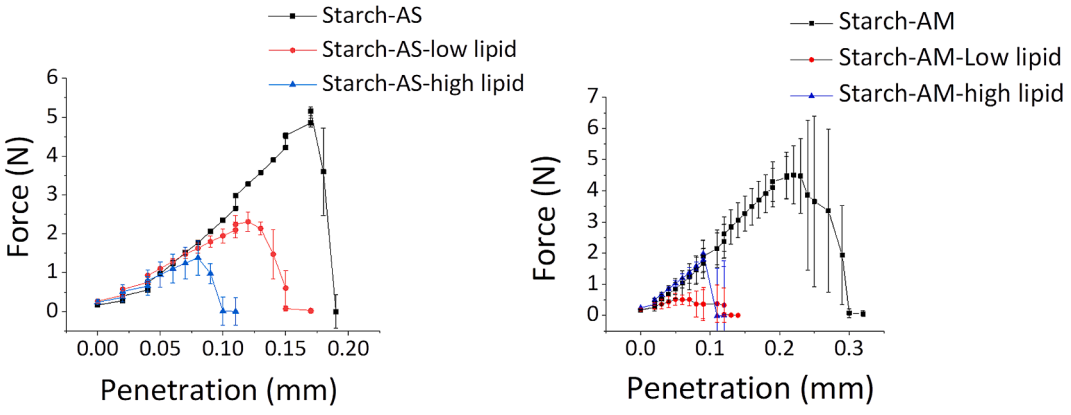

Fig. 8. Penetration test – Force path diagrams of implants loaded with artesunate (left) and artemether (right) with the same diameter of 1 mm; n = 3; the error bars indicate the standard deviation.

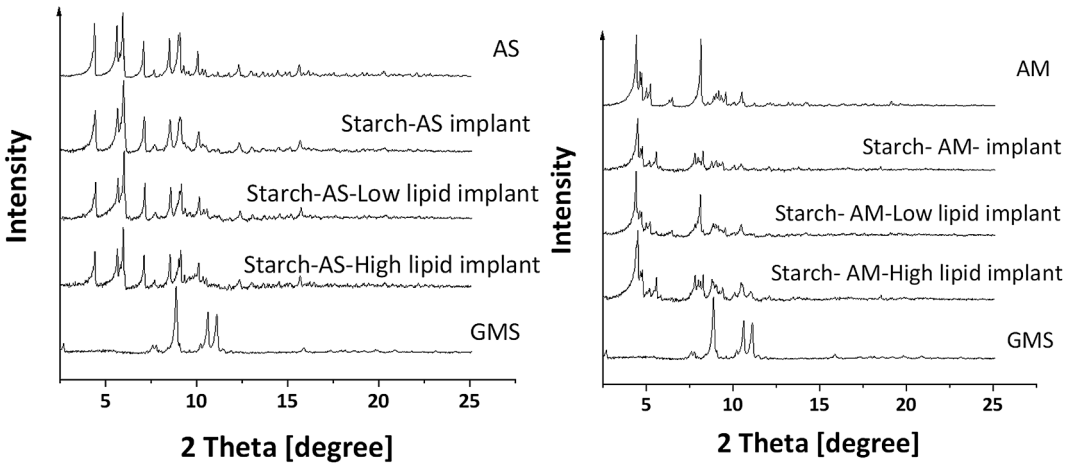

Fig. 9. XRPD-diffractograms of powdered samples of artesunate, artesunate loaded implants and GMS (left) and artemether, artemether loaded implants and GMS (right). The measurements were carried out at room temperature.

physical mixture of the GMS and other components of the formulation before the extrusion were also obtained which are shown in supplementary materials (Fig. S7 and Fig. S8). The GMS peaks were not clearly detectable in the physical mixture. Therefore, although the GMS peaks were not observed after the extrusion process, it cannot be concluded whether the GMS exist in its beta crystalline state after the extrusion process.

3.6. *In vitro* artesunate and artemether release

The release of artesunate and artemether from different formulations was investigated at 37 °C in PBS pH 7.4. Fig. 10 shows the artesunate and artemether release kinetics. As can be seen in the graphs, the release of the artesunate was completed after 2 days in all three formulations. No significant difference between the release behaviors can be seen. The addition of the lipid to the formulation did not cause significant changes in the release behaviour of artesunate. This is probably due to the effect of lipid (GMS), preventing the full starch gelatinization during the extrusion process. It might therefore also prevent possible interactions between the drug and the starch. Further studies are needed to understand the possible interactions between the components of the formulation. The total amount of released artesunate was equal to 3.0 mg ± 0.14 mg, 3.0 mg ± 0.20 mg and 3.1 mg ± 0.31 mg for the starch implant, starch-low lipid implant and starch-high lipid implant respectively. As can be seen in the graph, the released amount of the drug has not reached 100 percent of the loaded drug. This is probably due to the hydrolysis of artesunate to dihydroartemisinin during the *in vitro* study. Several studies have shown that, in aqueous solutions, artesunate hydrolyzes to dihydroartemisinin (DHA), depending on the environmental conditions, including temperature and pH (Agnihotri et al., 2013; Batty et al., 1996; Gabriëls and Plaizier-Vercammen, 2004). Simultaneous quantification of artesunate and dihydroartemisinin in plasma by HPLC has been done by several studies (Chutvirasakul et al., 2021; Geditz et al., 2014). DHA co-exists in two forms and is shown as DHA-1 and DHA-2 in the chromatogram in supplementary (Fig. S9). Related peaks to DHA were observed in chromatograms of release media of all artesunate loaded implants (Fig. S9). Regarding the formulations loaded with artemether, the starch-high lipid implant was unstable in PBS plus 1% SDS and it was completely destroyed after a few hours. Therefore, the release behavior of this formulation was not assessed. Per WHO guidelines, treatment of severe malaria with artemether starts with a relatively high initial dose and continues with a maintenance dose for another 2 days. Both formulations of artemether showed a relatively high initial release continued with the constant release of the drug over several days. The drug was released from the starch-low lipid implant in 3 days, while the release was prolonged to 6 days from the starch implant. The total amount of released artemether from the implants were equal to 4.0 mg ± 0.08 mg and 4.0 mg ± 0.02 mg respectively which is of relevance to the therapeutics dose in preclinical studies in mice (Lin et al., 1994; Zech et al., 2021). The release profiles of both formulations match with a desired kinetic profile for the treatment of severe malaria per WHO guidelines (World Health Organization, 2015).

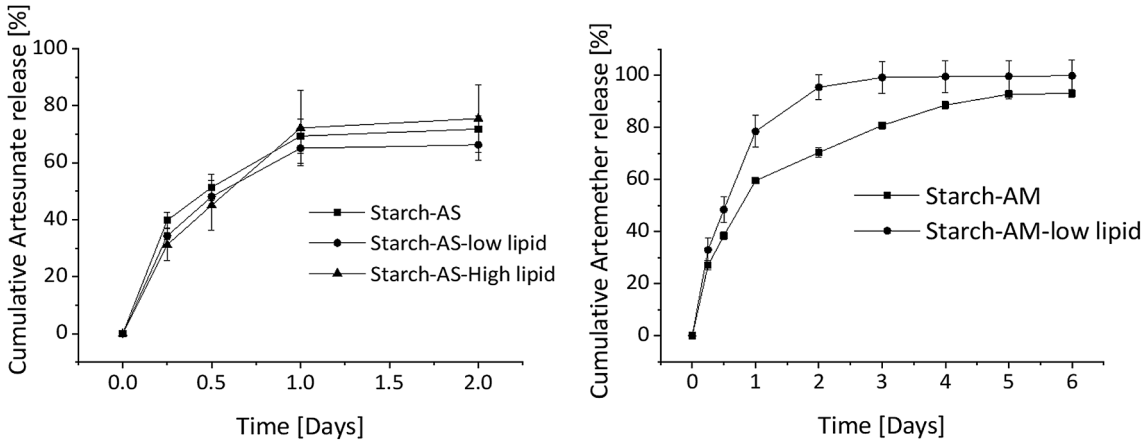

Fig. 10. Cumulative release of artesunate (left) and artemether (right) from different implants in PBS plus 1% SDS pH 7.4; n = 3; the error bars indicate the standard deviation.

Both Artemether and artesunate metabolize to the same active metabolite dihydroartemisinin in the human body. Also, per WHO guidelines artemether is the drug of choice for the treatment of severe malaria, in case parenteral artesunate is not available. Therefore, both artemether loaded implants (starch-AM implant and starch-AM-low lipid implant) are potential candidates for the treatment of severe malaria.

Based on the obtained data for the release kinetics, the addition of lipid to the formulations could not provide longer drug release from the implants. This is probably due to the high amount of drug loading (50%) that reduced the interactions between the lipid and starch and could also lead to porogenic effects. Further studies are needed to assess the possible interactions between the drug, starch and lipid in more detail. The EPR results and the drug release studies confirmed that the degree of benefit of combining starch and GMS will depend on (i) the selected ratio starch/GMS, the (ii) the drug properties and (iii) the drug load. The best benefit will be for drugs which are molecular dispersed in the lipid phase. This scenario is expected for lipophilic molecules at low loadings (e.g. as observed for TB in our study). Solid lipids are, due to their partially crystalline structure, only able to accommodate a limited amount of foreign molecules, even if they are hydrophobic. High drug loadings with hydrophobic drugs will therefore lead to phase separation and the formation of at least three different domains: (i) phase separated drug molecules, (ii) GMS phase with drug molecules dissolved and (iii) starch phase with an expected low amount of hydrophobic drug molecules.

4. Conclusion

This study investigates the possibility to combine different types of starch with GMS to produce a parenteral depot system, that can provide a sustained release of antimalarial agents over a few days to a week. In prescreening studies, the extrudability of the different starch varieties, formulated with different GMS proportions, were studied, in order to choose an appropriate starch, that can form a controlled release system complying with predefined characteristics. These characteristics include the implant's homogeneity, the physical stability in PBS and the release profile of the drug model (spin probes) from the prepared implant. Also, the temperature, the extrusion screw speed and the optimal water amount for the HME were optimized in prescreening studies. These studies showed the general feasibility to make a controlled release system as an implant, using high amylose starch and GMS. EPR studies confirmed the potential of the prepared system to provide a sustained release of the drug model over a period of a few days to weeks depending on the physicochemical properties of the loaded drug model. Therefore, three formulations including starch, starch-low lipid and starch-high lipid, loaded with antimalarial agents, artesunate and artemether, were produced and characterized. The results of the texture analysis demonstrated that, for both artesunate and artemether loaded formulations, starch implants had the maximum mechanical resistance and the addition of the lipid to the formulations makes the implant more brittle. The XRPD confirmed the crystalline state of both artesunate and artemether in all prepared implants. Artemether was released over a longer period of time in comparison to the artesunate. The release was completed after 3 days in starch-low lipid implant while it was prolonged to 6 days in starch implant. The release kinetics of both implants match the desired release profile for the treatment of severe malaria. Artemether and artesunate both metabolize to the same active metabolite dihydroartemisinin in the human body. Also, per WHO guidelines artemether is the drug of choice for the treatment of severe malaria, in case parenteral artesunate is not available (World Health Organization, 2015). Therefore, both formulations are potential candidates to be used in the treatment of severe malaria.

In summary, the study shows the general suitability of biodegradable starch-based implants in forming a sustained release system with desired mechanical properties.

CRediT authorship contribution statement

Golbarg Esfahani: Conceptualization, Methodology, Validation, Investigation, Writing – original draft. **Olaf Häusler:** Conceptualization, Writing – review & editing. **Karsten Mäder:** Conceptualization, Writing – review & editing, Resources, Supervision, Funding acquisition.

Declaration of Competing Interest

The authors declare that they have no known competing financial interests or personal relationships that could have appeared to influence the work reported in this paper: [Golbarg Esfahani reports financial support was provided by the European Union and the Federal State of Saxony-Anhalt. Karsten Mäder reports material supply (starch) was provided by Roquette Freres. Olaf Häusler reports a relationship with Roquette Freres that includes: employment.].

Acknowledgements

This study was supported by the IGS "Functional polymers" as a part of the AGRIPOLY program with funding from the European Social Fund (ESF). Additionally, we kindly thank Dr Christoph Wagner from the Chemistry Institute of Martin Luther University Halle-Wittenberg for his supports in x-ray diffraction measurements. As well, we would like to express our gratitude to the companies Roquette (Lestrem, France), BASF (Germany) and IOI Oleo GmbH (Germany) for providing us with the materials.

Appendix A. Supplementary material

Supplementary data to this article can be found online at https://doi.org/10.1016/j.ijpharm.2022.121879.

References

Agnihotri, J., Singh, S., Bigonia, P., 2013. Formal chemical stability analysis and solubility analysis of artesunate and hydroxychloroquinine for development of parenteral dosage form. J. Pharm. Res. 6 (1), 117–122.

Klayman, D.L., Lin, A.J., Ager, A.L., 1994. Antimalarial activity of dihydroartemisinin derivatives by transdermal application. Am. J. Trop. Med. Hyg. 50 (6), 777–783.

Alberta Araújo, M.A., Cunha, A.M., Mota, M., 2004. Enzymatic degradation of starch-based thermoplastic compounds used in protheses: identification of the degradation products in solution. Biomaterials 25 (13), 2687–2693.

Batty, K.T., Ilett, K.F., Davis, M.E., 1996. Chemical stability of artesunate injection and proposal for its administration by intravenous infusion. J. Pharm. Pharmacol. 48 https://doi.org/10.1111/j.2042-7158.1996.tb05870.x.

Besheer, A., Wood, K.M., Peppas, N.A., Mäder, K., 2006. Loading and mobility of spin-labeled insulin in physiologically responsive complexation hydrogels intended for oral administration. J. Control. Release 111 (1-2), 73–80.

Bialleck, S., Rein, H., 2011. Preparation of starch-based pellets by hot-melt extrusion. Eur. J. Pharm. Biopharm. 79 (2), 440–448.

Builders, P.F., Anwunobi, P.A., Mbah, C.C., Adikwu, M.U., 2013. New direct compression excipient from tigernut starch: physicochemical and functional properties. AAPS PharmSciTech 14 (2), 818–827.

Castro, L.M.G., Alexandre, E.M.C., Saraiva, J.A., Pintado, M., 2020. Impact of high pressure on starch properties: a review. Food Hydrocoll 106, 105877.

Chutvirasakul, B., Joseph, J.F., Parr, M.K., Suntornsuk, L., 2021. Development and applications of liquid chromatography-mass spectrometry for simultaneous analysis of anti-malarial drugs in pharmaceutical formulations. J. Pharm. Biomed. Anal. 195, 113855.

Cui, R., Oates, C.G., 1999. The effect of amylose-lipid complex formation on enzyme susceptibility of sago starch. Food Chem. 65 (4), 417–425.

De Pilli, T., Giuliani, R., Buléon, A., Pontoire, B., Legrand, J., 2016. Effects of protein-lipid and starch-lipid complexes on textural characteristics of extrudates based on wheat flour with the addition of oleic acid. Int. J. Food Sci. Technol. 51 (5), 1063–1074.

Ding, A.G., Schwendeman, S.P., 2008. Acidic microclimate pH Distribution in PLGA microspheres monitored by confocal laser scanning microscopy. Pharm. Res. 25 (9), 2041–2052.

Donmez, D., Pinho, L., Patel, B., Desam, P., Campanella, O.H., 2021. Characterization of starch–water interactions and their effects on two key functional properties: starch gelatinization and retrogradation. Curr. Opinion Food Sci. 39, 103–109.

Esu, E.B., Effa, E.E., Opie, O.N., Meremikwu, M.M., Berbenetz, N., 2020. Artemether for severe malaria. Emergencias. https://doi.org/10.1002/14651858.CD010678.pub3.

Evans, R.G., Wain, A.J., Hardacre, C., Compton, R.G., 2005. An electrochemical and ESR spectroscopic study on the molecular dynamics of TEMPO in room temperature ionic liquid solvents. ChemPhysChem 6 (6), 1035–1039.
Gabriëls, M., Plaizier-Vercammen, J., 2004. Experimental designed optimisation and stability evaluation of dry suspensions with artemisinin derivatives for paediatric use. Int. J. Pharm. 283 (1-2), 19–34.
Gao, H., Chen, L., Chen, W., Bao, S., 2013. Thermal stability evaluation of β-artemether by DSC and ARC. Thermochim. Acta 569, 134–138.
Geditz, M.C.K., Heinkele, G., Ahmed, A., Kremsner, P.G., Kerb, R., Schwab, M., Hofmann, U., 2014. LC-MS/MS method for the simultaneous quantification of artesunate and its metabolites dihydroartemisinin and dihydroartemisinin glucuronide in human plasma. Anal. Bioanal. Chem. 406 (17), 4299–4308.
Gelders, G.G., Duyck, J.P., Goesaert, H., Delcour, J.A., 2005. Enzyme and acid resistance of amylose-lipid complexes differing in amylose chain length, lipid and complexation temperature. Carbohydr. Polym. 60 (3), 379–389.
Himawan, C, Starov, V.M, Stapley, A.G.F, 2006. Thermodynamic and kinetic aspects of fat crystallization. Adv. Colloid Interface Sci. 122 (1–3) https://doi.org/10.1016/j.cis.2006.06.016.
Kempe, S., Mäder, K., 2012. In situ forming implants - An attractive formulation principle for parenteral depot formulations. J. Control. Release. 161 (2), 668–679.
Kempe, S., Metz, H., Mäder, K., 2010. Application of Electron Paramagnetic Resonance (EPR) spectroscopy and imaging in drug delivery research - Chances and challenges. Eur. J. Pharm. Biopharm. 74 (1), 55–66.
Klug, C.S., Feix, J.B., 2008. Methods and applications of site-directed spin labeling EPR spectroscopy. Methods Cell Biol. https://doi.org/10.1016/S0091-679X(07)84020-9.
Krämer, B., Neis, F., Brucker, S.Y., Kommoss, S., Andress, J., Hoffmann, S., 2021. Peritoneal Adhesions and their Prevention. Curr. Trends Surg. Technol. Int. https://doi.org/10.52198/21.sti.38.hr1385.
Kuntworbe, N., Acquah, F.A., Johnson, R., Ofori-Kwakye, K., 2018. Comparison of the physicochemical properties and in vivo bioavailability of generic and innovator artemether-lumefantrin tablets in Kumasi, Ghana. J. Pharm. Pharmacogn. Res. 6.
Lehner, E., Gündel, D., Liebau, A., Plontke, S., Mäder, K., 2019. Intracochlear PLGA based implants for dexamethasone release: challenges and solutions. Int. J. Pharm.: X 1, 100015.
Lisgarten, J.N., Potter, B., Palmer, R.A., Chimanuka, B., Aymami, J., 2002. Structure, absolute configuration, and conformation of the antimalarial drug artesunate. J. Chem. Crystallogr. 32 https://doi.org/10.1023/A:1015696306812.
Lucke, A., Kiermaier, J., Göpferich, A., 2002. Peptide acylation by poly(α-hydroxy esters). Pharm. Res. 19 https://doi.org/10.1023/A:1014272816454.
Luo, X.-D., Yeh, H.J.C., Brossi, A., Flippen-Anderson, J.L., Gillardi, R., 1984. The chemistry of drugs part IV, Configurations of antimalarials derived from qinghaosu: dihydroqingyhaosu, artemether, and artesunic acid. Helv. Chim. Acta 67 (6), 1515–1522.
Lurie, D., Mader, K., 2005. Monitoring drug delivery processes by EPR and related techniques - Principles and applications. Adv. Drug Deliv. Rev. 57 (8), 1171–1190.
Mäder, K., Gallez, B., Liu, K.J., Swartz, H.M., 1996. Non-invasive in vivo characterization of release processes in biodegradable polymers by low-frequency electron paramagnetic resonance spectroscopy. Biomaterials 17 (4), 457–461.
Mendes, S.C., Reis, R.L., Bovell, Y.P., Cunha, A.M., van Blitterswijk, C.A., de Bruijn, J.D., 2001. Biocompatibility testing of novel starch-based materials with potential application in orthopaedic surgery: a preliminary study. Biomaterials 22 (14), 2057–2064.
Metin, S., Hartel, R.W., 2005. Crystallization of Fats and Oils. Bailey's Industrial Oil and Fat Products. doi:10.1002/047167849x.bio021.
Morris, C.A., Duparc, S., Borghini-Fuhrer, I., Jung, D., Shin, C.-S., Fleckenstein, L., 2011. Review of the clinical pharmacokinetics of artesunate and its active metabolite dihydroartemisinin following intravenous, intramuscular, oral or rectal administration. Malar. J. 10 (1) https://doi.org/10.1186/1475-2875-10-263.
Sasaki, T., Yasui, T., Matsuki, J., 2000. Effect of amylose content on gelatinization, retrogradation, and pasting properties of starches from waxy and nonwaxy wheat and their F1 seeds. Cereal Chem. 77 (1), 58–63.
Schädlich, A., Kempe, S., Mäder, K., 2014. Non-invasive in vivo characterization of microclimate pH inside in situ forming PLGA implants using multispectral fluorescence imaging. J. Control. Release 179, 52–62.
Stewart, S., Domínguez-Robles, J., McIlorum, V., Mancuso, E., Lamprou, D., Donnelly, R., Larrañeta, E., 2020. Development of a biodegradable subcutaneous implant for prolonged drug delivery using 3D printing. Pharmaceutics 12 (2), 105.
World Health Organization, 2020. World Malaria Report: 20 years of global progress and challenges, World Health.
World Health Organization, 2015. Guidelines for the treatment of malaria Third edition. Trans. R. Soc. Trop. Med. Hyg. 85. https://doi.org/10.1016/0035-9203(91)90261-V.
Zech, J., Dzikowski, R., Simantov, K., Golenser, J., Mäder, K., 2021. Transdermal delivery of artemisinins for treatment of pre-clinical cerebral malaria. Int. J. Parasitol. Drugs Drug Resist. 16, 148–154.
Zhang, Y., Liu, Q., Zhang, D., Jiang, Y., 2011. Polymorphism, crystal structure and crystal habit of β-artemether. Huagong Xuebao/CIESC J. 62 https://doi.org/10.3969/j.issn.0438-1157.2011.10.040.

molecular pharmaceutics

pubs.acs.org/molecularpharmaceutics

Article

Characterization of Controlled Release Starch-Nimodipine Implant for Antispasmodic and Neuroprotective Therapies in the Brain

Golbarg Esfahani, Marie-Luise Trutschel, Detlef Reichert, and Karsten Mäder*

Cite This: https://doi.org/10.1021/acs.molpharmaceut.3c00618

Read Online

ACCESS | Metrics & More | Article Recommendations | Supporting Information

ABSTRACT: Parenteral depot systems can provide a constant release of drugs over a few days to months. Most of the parenteral depot products on the market are based on poly(lactic acid) and poly(lactide-*co*-glycolide) (PLGA). Studies have shown that acidic monomers of these polymers can lead to nonlinear release profiles or even drug inactivation before release. Therefore, finding alternatives for these polymers is of great importance. Our previous study showed the potential of starch as a natural and biodegradable polymer to form a controlled release system. Subarachnoid hemorrhage (SAH) is a life-threatening type of stroke and a major cause of death and disability in patients. Nimotop® (nimodipine (NMD)) is an FDA-approved drug for treating SAH-induced vasospasms. In addition, NMD has, in contrast to other Ca antagonists, unique neuroprotective effects. The oral administration of NMD is linked to variable absorption and systemic side effects. Therefore, the development of a local parenteral depot formulation is desirable. To avoid the formation of an acidic microenvironment and autocatalytic polymer degradation, we avoided PLGA as a matrix and investigated starch as an alternative. Implants with drug loads of 20 and 40% NMD were prepared by hot melt extrusion (HME) and sterilized with an electron beam. The effects of HME and electron beam on NMD and starch were evaluated with NMR, IR, and Raman spectroscopy. The release profile of NMD from the systems was assessed by high-performance liquid chromatography. Different spectroscopy methods confirmed the stability of NMD during the sterilization process. The homogeneity of the produced system was proven by Raman spectroscopy and scanning electron microscopy images. In vitro release studies demonstrated the sustained release of NMD over more than 3 months from both NMD systems. In summary, homogeneous nimodipine-starch implants were produced and characterized, which can be used for therapeutic purposes in the brain.

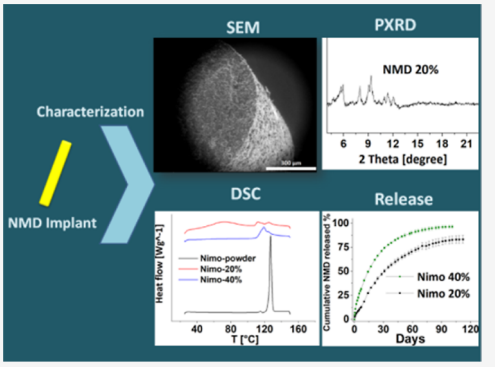

KEYWORDS: *parenteral, controlled release, biodegradable, starch, nimodipine*

1. INTRODUCTION

Achieving a constant concentration of a drug in the blood or target tissue is a requirement for the treatment of many diseases. Many of the orally administered drugs have limited water solubility or a short half-life, which leads to low oral bioavailability. Reaching a constant concentration of these drugs requires a high dose of the drug administered several times per day. Parenteral depot systems, first introduced in 1981 by Shoupe et al., are designed to provide sustained release of drugs over several days, weeks, or even years.[1] Currently, various types of parenteral depot systems are commercially available. Poly(lactic acid) and poly(lactide-*co*-glycolide) (PLGA) polymers are the dominant polymers used in the pharmaceutical industry to produce parenteral depot systems.[1−3] These polymers are biodegradable; however, their degradation results in the formation of highly acidic monomers and nonlinear release profiles.[2−5] This underlines the need to find alternative materials.[4,5] Starch, as a natural, biodegradable, and cheap polymer with nontoxic and nonacidic degradation products, is widely used in the pharmaceutical industry but mainly for oral drug products.[6−9] In our previous study, the potential of starch in forming a parenteral controlled drug release system for a hydrophobic drug was shown by different in vitro and in vivo tests.[10] Nimodipine (NMD) is a hydrophobic API with very low oral bioavailability.[11] Nimotop (nimodipine 30 mg capsule, Bayer) is an FDA-approved drug for the treatment of subarachnoid hemorrhage (SAH)-induced vasospasms.[12] SAH is a serious, life-threatening type of stroke where cerebral vasospasm remains a serious complication and a major cause of death and disability in these patients. Based on FDA guidelines, 60 mg (two capsules) of NMD should be administered every 4 h for 21 continuous days.[12] As the administration dosing regimen shows, NMD has very low oral bioavailability due to slow dissolution and decomposition in stomach acid.[11] NMD oral bioavailability is reported from 3 to

Received: July 15, 2023
Revised: September 13, 2023
Accepted: September 14, 2023

30%, which can be extensively variable among patients.[13,14] Therefore, a parenteral depot of NMD with the ability to release the drug over a desired period will be the ideal scenario. One notable benefit attributed to NMD is its demonstrated neuroprotective capability. The neuroprotective effect of NMD against different types of stress-induced neuronal damage during surgery or various neurodegenerative diseases has been reported in several studies.[15−17]

In our previous study, the release of Artemether (AM), with the log p-value of 3, the same as NMD, was observed over 6 days from a starch-based system. Our investigations clarified that some critical changes in the native structure of starch are needed to achieve a controlled release system.[18] These changes are mainly formed by gelatinization of starch during the extrusion process. The plasticizer effect of NMD during the hot melt extrusion (HME) process has been previously reported.[19] The possible plasticizer effect of NMD might lead to better cohesiveness of the system through physical interactions with starch and a longer release profile. Exploring the biodegradability of the system after implantation, our research group conducted an in vivo study to investigate the fate of the starch implant. For this purpose, a starch implant loaded with a hydrophobic molecule as a model of a hydrophobic drug was injected subcutaneously in mice. The implant was totally degraded after 4 weeks, with no residual material observable in the mice's injection site tissues upon macroscopic examination.[10] These results suggest complete degradation of starch in vivo by enzymes, most likely amylases. Amylases are produced by salivary glands, pancreas, liver, and other tissues and exist in serum at a normal level.[20] Also, the existence of alpha-amylases in the brain has been suggested by several recent studies.[21−23] Hence, we anticipate that the starch-based implant will undergo biodegradation after implantation in the brain.

Within this study, NMD-loaded starch implants were prepared and characterized. To assess the impact of drug load on the system, two formulations with 20 and 40% NMD loads were prepared. NMR relaxometry was implemented to evaluate the water penetration into the system, which helps us with a better understanding of the possible release mechanism. As NMD has different modifications, different techniques, including differential scanning calorimetry (DSC), Raman spectroscopy, and infrared (IR) spectroscopy, were applied to investigate possible changes in the modifications during the extrusion process. In addition, different techniques were utilized to assess the potential effects of the API on the polymeric system and vice versa. As the system is designed for parenteral administration, finding an appropriate sterilization method was of the utmost importance. Challenges in finding the appropriate method for the sterilization of the NMD-loaded system have been reported previously due to the instability of NMD during the sterilization process.[24] The ability of the developed system to protect NMD during the sterilization process was evaluated by different techniques. Furthermore, we tried to gain insights into potential interactions between the drug and polymer through a variety of approaches.

2. MATERIALS AND METHODS

2.1. Materials. High amylose starch (MAIZE STARCH AMYLO N-400) was kindly provided by Roquette (Lestrem, France). Nimodipine was purchased from BIOSYNTH. The testing media was phosphate buffered saline (PBS) (Ph.Eur.) plus 1% sodium dodecyl sulfate (SDS), adjusted to pH 7.4. SDS was purchased from Sigma-Aldrich Chemie GmbH (Munich, Germany). Acetonitrile (VWR International, Darmstadt, Germany), formic Acid (Merck, Germany), and double distilled water were used for the high-performance liquid chromatography (HPLC) measurements.

2.2. Implant Preparation. The implants were prepared by HME (ZE 5 ECO; Three-Tec GmbH; Seon; Swiss). Water was used as a plasticizer. The components of each formulation are listed in Table 1. The heating zone's temperatures were 60, 65, and 70 °C for all formulations with a screw speed of 140 rpm. Before the extrusion, components of each formulation were mixed and filled into the grinding chamber of a Retsch CryoMill (Retsch, Haan, Germany) together with two 10 mm grinding media. The cryomilling process scheduled an automatic precooling phase and 2 milling cycles at 30 Hz for 150 s. Each cycle was followed by a 30 s lasting cooling phase at 5 Hz. Extrusion dies with a 1 mm diameter were used. The samples were collected and stored in opaque falcon tubes between 4° to 8 °C. Figure 1 shows the Nimo 40% implant prepared by HME.

Table 1. Composition of the Investigated Formulations

		components [g]		
formulation no	formulation name	starch	nimodipine	Water
1	starch implant	4		2
2	nimo 20%	8	2	4
3	nimo 40%	6	4	3

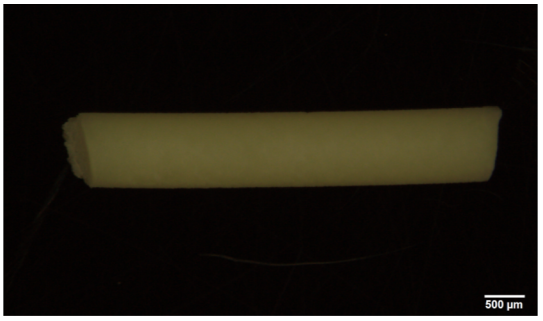

Figure 1. Nimo 40% implant with a 1 mm diameter.

2.3. Release Studies. One centimeter implant of each formulation (1 cm) was weighed and placed in 20 mL amber glass vials filled with 20 mL of PBS plus 1% SDS, pH 7.4, and the vials were slightly agitated in a shaker with light protection (Memmert GmbH + Co. KG, Schwabach, Germany) at 37 °C. The total buffer volume was withdrawn at regular time intervals and analyzed according to the described HPLC method. The withdrawn media was replaced by fresh PBS and 1% SDS. Each experiment was conducted in triplicate.

2.4. High-Performance Liquid Chromatography. The HPLC analysis was performed with a Waters Delta 600 system with 717 plus Auto Sampler, 2996 Photodiode Array Detector, and a Purospher STAR RP-18 end-capped 250 × 4 column (Merck KGaA, Germany). A sample volume of 20 μL was injected at a flow rate of 1.0 mL/min and a column temperature of 40 °C. The mobile phase was acetonitrile, water, and formic acid with a ratio of 65:35:0.1. The retention time was 5.8 min. The quantification was carried out with a

https://doi.org/10.1021/acs.molpharmaceut.3c00618
Mol. Pharmaceutics XXXX, XXX, XXX−XXX

UV/vis detector at 238 nm. Linear calibration curves (r^2 > 0.999) were obtained in the range of 1−100 μg/mL of drug in PBS plus 1% SDS. Masslynx V4.1 software was used to analyze the data.

2.5. E Beam Sterilization. The implants were sealed in glass vials under an argon atmosphere. The samples were then irradiated by a 10 MeV linear accelerator MB 10−30 MP (Mevex, Stittsville, Ontario, Canada) on a moving tray (95 cm/min). The total dose of 25 kGy was achieved by administering two separate doses of 12.5 kGy each (beam current 250 mA, PPS = 450 Hz). Control samples were stored under an argon atmosphere at 4 °C without sterilization. The amount of nimodipine in both the control and sterilized samples was measured via HPLC. ^{1}H NMR, ^{13}C NMR, and IR spectra of the Nimo 40% sample before and after sterilization were acquired to monitor possible drug degradation.

2.6. Powder X-ray Diffraction. Powder X-ray diffraction (PXRD) was applied to determine the state of nimodipine inside the implants. As a preparation step for the PXRD measurements, the implants were split into smaller pieces with a scalpel and submitted to cryo-milling (Retsch GmbH, Haan, Germany). After an automatic precooling phase, the samples were milled with two 10 mm grinding media at 25 Hz for 60 s. PXRD was performed on an STOE STADI MP (STOE & Cie GmbH, Darmstadt, Germany) powder diffractometer, equipped with a molybdenum anode (50 kV and 30 mA) and a Ge(111) monochromator to select the Mo Kα radiation at 0.071073 nm. Data of the rotating samples were collected in the transmission mode from 2−30° in 1° steps for 60 s each using a DECTRIS MYTHEN 1 K Strip Detector. The diffraction patterns obtained were processed using an STOE WinXPOW software package.

2.7. Differential Scanning Calorimetry. DSC measurements for different samples were recorded with a Mettler Toledo DSC 823e module (Mettler Toledo, Gieβen, Germany) in standard aluminum sample pans. Every sample was kept at 25 °C for 2 min and then heated to 150 °C with a 10 K/min heating rate. All samples were kept at 150 °C for 1 min and then cooled down to 25 °C and kept at this temperature for 2 min and then heated up again up to 150 °C with a 10 K/min heating rate. Data recording and processing of the first heating cycles were carried out with the software STARe V15.00 (Mettler Toledo, Gieβen, Germany) as no thermal events were observed during cooling and the second heating.

2.8. Fourier Transform IR Spectroscopy. The Fourier transform infrared (FTIR) spectra were recorded by using a Bruker FTIR spectrophotometer (Model Vertex 70, Bruker, Germany) equipped with a DLaTGS detector. Tablets of the samples were prepared using 1 mg of each sample and 300 mg of KBr. Measurements were performed in the scanning range of 400−4000 cm^{-1} at ambient temperature. Measurements were obtained by using 32 scans at a 2 cm^{-1} resolution.

2.9. Raman Spectroscopy. Raman studies were performed using a Dilor Raman spectrometer (model: LabRam) equipped with a 632 nm He/Ne laser source and an Olympus BX41 microscope system. The collection of spectra was performed at room temperature under the following conditions: ×100 microscope objective, 350 μm pinhole size, 250 μm slit width, and 10 s exposure time. Thirty measurements were taken from each sample.

2.10. NMR Relaxometry. The extrudates were cut into pieces of 1 cm in length and stacked in a 10 mm NMR tube. The transverse relaxation time (T_2) was measured with magic sandwich echo (MSE) and flame ionization detector sequences on a Bruker Miniscope mq20 with 20 MHz resonance frequency and 90° pulse length of 2.8 μs at 37 °C. Measurements were performed primarily on dry samples. Then, 1 mL of PBS was added to each sample. The second measurement was done after 1 h of exposure of the sample to PBS following the elimination of PBS from the tube.

The evaluation of the transverse relaxation was done by fitting mono and double exponential decay curves:

1. mono exponential: $y = A1 \times \exp(-x/t1) + y0$
2. double exponential: $y = A1 \times \exp(-x/t1) + A2 \times \exp(-x/t2) + y0$

The fitting was performed using OriginPro 2019.

2.11. NMR Spectroscopy. Samples were dissolved in deuterated dimethyl sulfoxide (DMSO). ^{1}H and ^{13}C spectra were acquired with a Bruker AVANCE III 800 MHz spectrometer and a cryogenic triple resonance probe. The NMR data were processed using TopSpin 3.6.4.

2.12. Environmental Scanning Electron Microscopy and Scanning Electron Microscopy. Two different instruments were used to obtain the electron microscopy images. To prevent possible changes in the internal structure of the system due to the fast water evaporation, environmental scanning electron microscopy (ESEM) with low vacuum was used. The samples were broken into tiny pieces, and the breakage surface was imaged using an XL 30 ESEM device, with a GSE detector and 12.0 kV electron beam, in wet modules, under low vacuum and pressure of 1 mbar. Also, the scanning electron microscopy (SEM) images of the samples were obtained under high vacuum using a Gemini 500 from Zeiss Microscopy GmbH to obtain images with higher resolution. The acceleration voltage was 1 kV (EHT = 1.00 kV). The imaging was done with secondary electrons (signal A = SE2).

3. RESULTS AND DISCUSSION

3.1. Water Penetration into the Implant and NMD Release. NMR relaxometry is a sensitive and fast method that has been widely used to characterize molecular dynamics in polymers.[25,26] The transverse or spin−spin relaxation time T_2 is the dephasing of the magnetization transverse to the static magnetic field direction (xy-plane).[27] MSE is an advanced refocusing sequence that is often used for avoiding the dead time problem. MSE can be used in systems with rigid phase molecular fragments that have mobility in the microsecond-millisecond range (intermediate-motional effect).[28,29] In this study, the so obtained MSE was fitted with a mono and double exponential function to calculate the T_2 of different components. The weight of each component is then translated into a rigid proton fraction (part of the system with a shorter T_2) or a mobile proton fraction (part of the system with a longer T_2).[30] In this study, we used this method to assess the water penetration into the systems to predict the release profile of NMD.

As can be seen in Figure 2, in the dry state, NMD 20% showed two different T_2. A longer T_2 indicates a part of the system with slower motions due to the existing water in the system, and the shorter T_2 corresponds to the rigid part of the system. NMD 40%, in a dry state, showed a homogeneous rigid system with a single short T_2. After 1 h of exposure of the systems to PBS, both samples show a significant increase in the slow motion region with longer T_2 which corresponds to the

https://doi.org/10.1021/acs.molpharmaceut.3c00618
Mol. Pharmaceutics XXXX, XXX, XXX−XXX

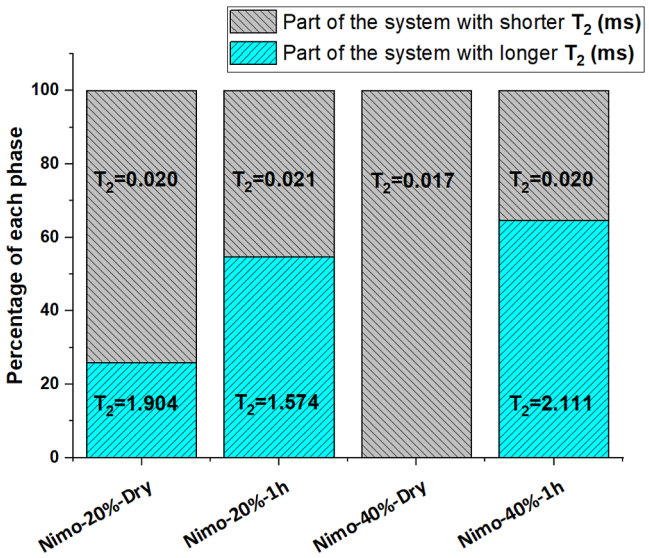

Figure 2. T_2 values of each system calculated by fitting mono- and double exponential decay curves.

part of the system in close contact to water which results in polymer chains mobility and change in T_2. If we look at the T_2 values of both systems after exposure to PBS, it can be seen that the 40% NMD shows a significantly larger T_2 in comparison to the 20% NMD. This shows the closer contact of water molecules to polymer chains in NMD 40% in comparison to NMD 20%, which is probably due to the more porous structure of NMD 40%, which is shown in the SEM image (Figure 12).

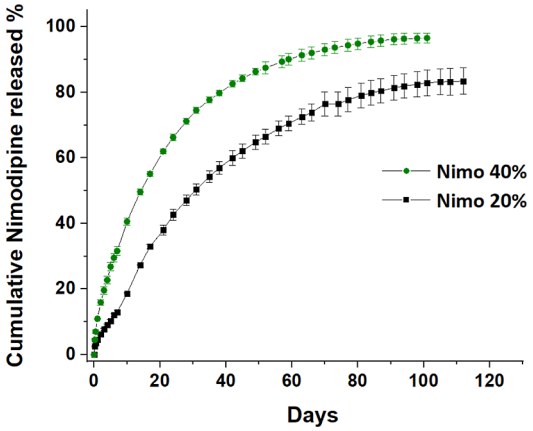

Figure 3. Cumulative release of NMD from NMD 40% (green) and NMD 20% (black) in PBS plus 1% SDS pH 7.4; n = 3; the error bars indicate the standard deviation.

This result is in line with the release profile of NMD from both systems (Figure 3). The release from the 40% drug-loaded implant during the first week of release (32%) is almost 3 times higher than that from the implant with a lower drug load (13%). After 101 days, 96.3% of the drug is released from a higher-loaded implant, and the release is almost completed, while this value is 83% for the implant with a lower drug load. We assume that part of NMD in the NMD 20% system remained inaccessible to the media, and therefore the drug could not be released from the system completely. However, in the formulation with a higher drug load, NMD is released

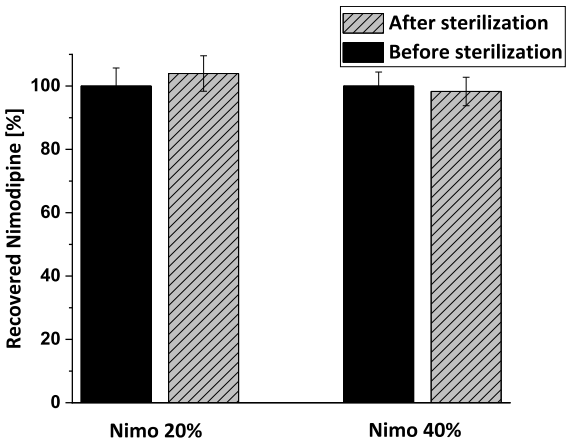

Figure 4. Effect of the electron beam on drug content in 20 and 40% implants before (black) and after (dashed) sterilization, assessed with HPLC; n = 3; the error bars indicate the standard deviation.

almost completely due to the internal porous structure of the system formed by the complete gelatinization of starch.

3.2. Effect of e Beam on Nimodipine. Sterilization is of utmost importance and an important requirement for the development of parenteral drug delivery systems. Sterilization of NMD-loaded formulations has been reported by several studies previously, but the stability of NMD is rarely investigated after the sterilization process.[31,32] In a study conducted by Zech et al., partial degradation of NMD was reported after electron irradiation sterilization.[24] In this study, the effect of the electron beam on NMD and the polymer was assessed by HPLC, IR, and NMR spectroscopy and mass spectroscopy (Supporting Information).

3.2.1. High-Performance Liquid Chromatography. As can be seen in Figure 4, in both formulations, NMD 40 and 20%, no significant decrease in the drug amount was observed. A slight increase in NMD amount in the NMD 20% formulation is probably due to water evaporation during the sterilization process. The stability of the NMD content during the sterilization process is also proved by NMR and IR spectroscopy. In a previous study conducted by Zech et al.,[24] partial degradation of NMD (about 20%) was reported after the electron beam sterilization of NMD-loaded PLGA nanofibers. As they used the same sterilization technique and the same HPLC method for the quantification of NMD, it can be concluded that starch is a better polymeric matrix in comparison to PLGA for the preservation of NMD during sterilization. The same protective effect of the polymer was also observed in our previous study, where we used the electron beam to sterilize the implants loaded with fluorescent dyes.[10]

3.2.2. Infrared. The starch spectrum shows the common signals for polysaccharides, with glucopyranose rings with a C−H band at 2928 cm^{-1}, C−O bands between 1000−1150 cm^{-1}, tightly bounded water signals at 1648 cm^{-1}, and an extremely broad band at 3297 cm^{-1} corresponding to hydrogen-bonded hydroxyl groups which are associated with free, inter, and intramolecular bound hydroxyl groups making up the structure of starch.[33−37] The effect of γ radiation on starch was evaluated in a study by Kizil et al.[35] by evaluation of the peak between 900 and 950 cm^{-1}, showing the glycosidic bond of the starch. In this study, electron beam sterilization was used. As can be seen in Figure 5, this peak is detectable in the sample before

https://doi.org/10.1021/acs.molpharmaceut.3c00618
Mol. Pharmaceutics XXXX, XXX, XXX−XXX

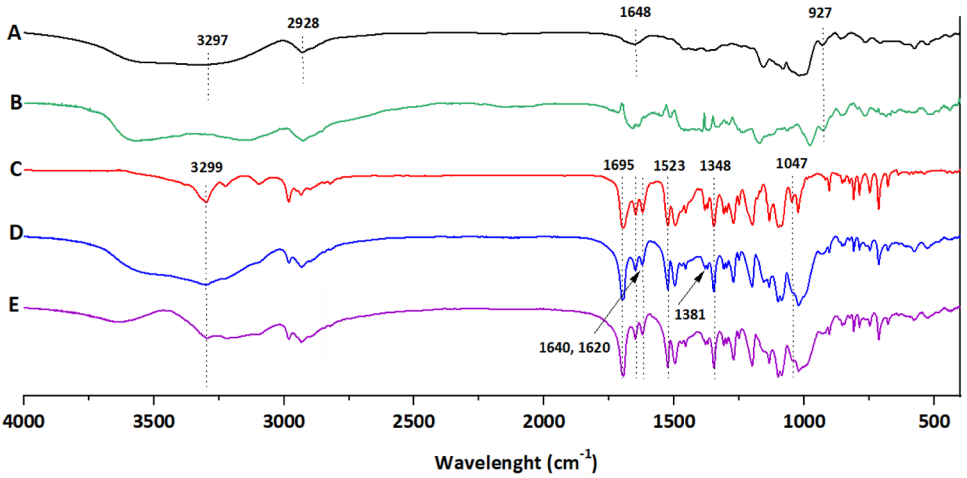

Figure 5. FTIR spectra of the samples. (A) Starch powder, (B) sterilized starch implant, (C) NMD powder, (D) NMD 40% implant, and (E) sterilized NMD 40% implant.

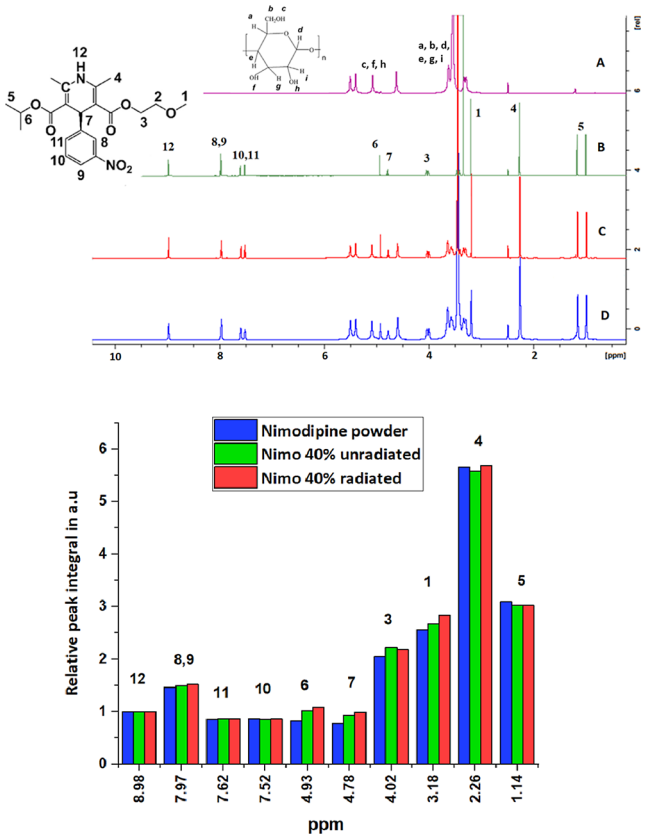

Figure 6. ^{1}H NMR spectra of (A) starch, (B) nimodipine, (C) nimo 40%, and (D) nimo 40% after electron beam sterilization (top), the calculated relative integral value of peaks of 1H NMR spectrum of the different samples. (The integration of peak 12 was considered as 1) (bottom).

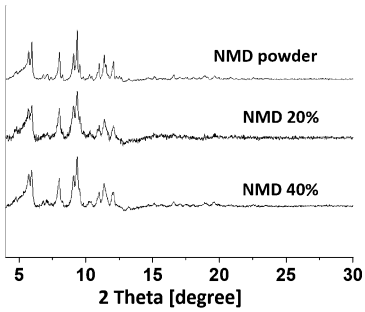

Figure 7. XRPD-diffractograms of powdered samples of NMD, NMD 20% and NMD 40%. The measurements were carried out at room temperature.

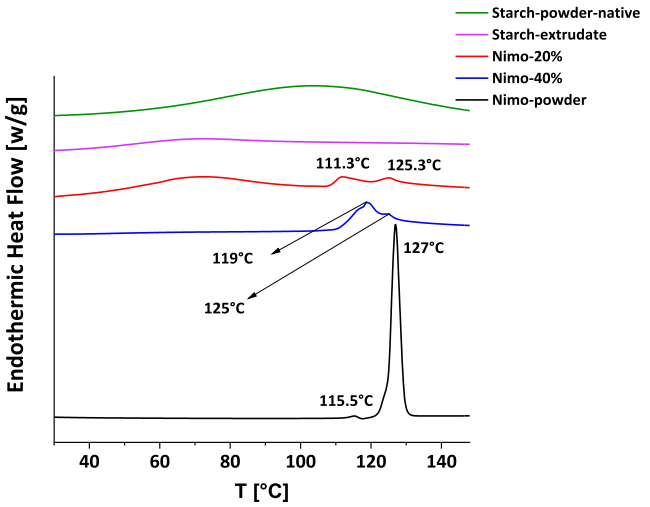

Figure 8. Thermograms of different samples. Measurements were carried out with a heating rate of 10 K/min between 25 and 150 °C.

and after the sterilization which can be proof of no significant degradation of starch during the sterilization process. Although partial degradation of starch is expected due to the broadening of peaks in the NMR spectrum of the sterilized samples, which can be caused by the dissolution of smaller starch degradation products that leads to an increase in the viscosity of the sample (Figure 5). As can be seen in Figure 5, the characteristic peaks of NMD, C−CH_3 at 1381 cm^{-1}, NO_2 group at 1523 cm^{-1}, carbonyl group at 1695 cm^{-1}, C=C stretching of dihydropyridine at 1640 cm^{-1}, and C=C stretches of the aromatic ring at 1620 cm^{-},[138,39] were detectable in samples before and after the sterilization process, which proves the stability of NMD during the sterilization process. Also, no distinct shift was observed in the peaks, meaning that there were no chemical interactions between NMD and the starch as was expected. But it should be noted that the observed N−H stretching at 3300 cm^{-1} in

https://doi.org/10.1021/acs.molpharmaceut.3c00618
Mol. Pharmaceutics XXXX, XXX, XXX−XXX

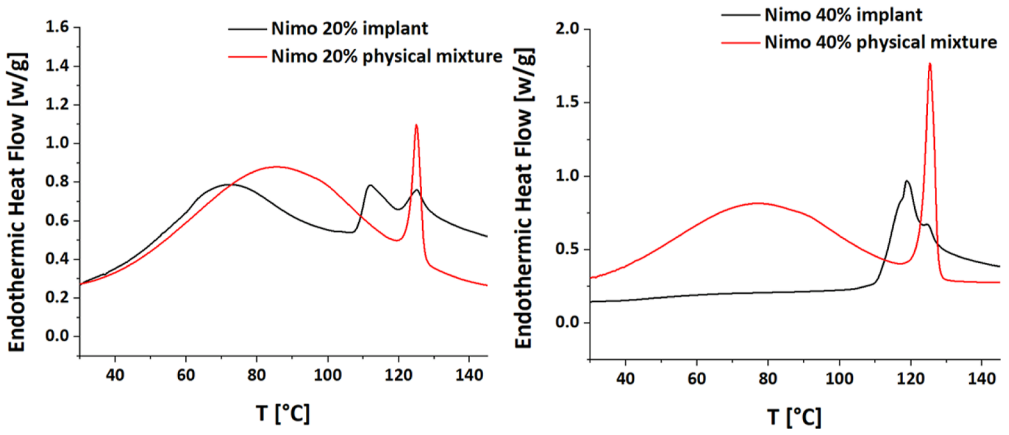

Figure 9. DSC curves of samples before and after the extrusion process.

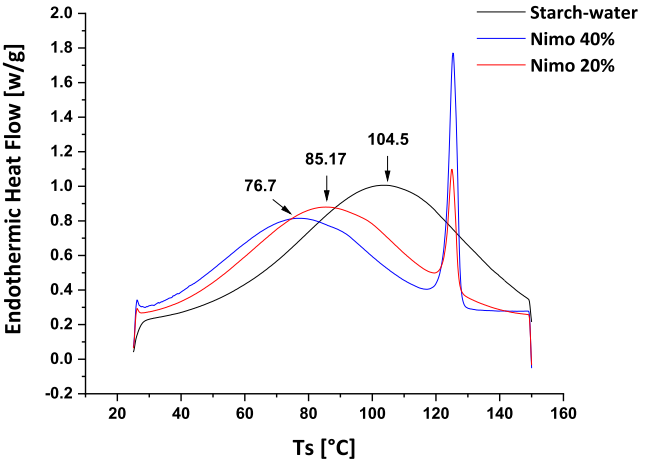

Figure 10. Thermograms of samples with different NMD load. Measurements were carried out with a heating rate of 10 K/min between 25 and 150 °C.

NMD powder is significantly weakened in extruded samples, which can be proof of hydrogen bonds between the O−H of the starch and N−H of NMD.[40] Looking at the IR spectrum of the NMD powder, a peak at 1047 cm^{-1} can be seen, which is significantly weakened in the NMD 40% sample. A study conducted by Calvo et al. reported this peak as the fingerprint region for differentiation between two modifications of NMD. Based on their report, this peak was only observed in mod I of NMD and was absent in the IR spectrum of mod II.[41] The existence of this peak in NMD powder and its change in the NMD 40% sample can be due to possible changes in modifications of NMD during the extrusion process, which was also observed by DSC.

3.2.3. NMR Spectroscopy. Investigation of NMD chemical structure and its polymorphism by ^{1}H NMR and ^{13}C NMR has been previously reported by several studies.[42,43] Comparing the NMR spectra of NMD powder and NMD 40% before and after sterilization (Figure 6), it can be seen that the important peaks arising from NMD[43] are detectable, which proves the nimodipine stability during the production and the sterilization process. As it was expected for the starch, the peaks of starch can be seen in both samples.[44] The peak of H number 2 of NMD is covered by the peak of water. Looking closer at the NMR spectra of the sterilized sample, it can be seen that the peaks are broader, which is probably due to the partial degradation of starch into smaller parts, which makes the dissolved sample more viscous. In all samples, the peak at 2.5 and 3.5 ppm is related to the DMSO. To evaluate possible changes in NMD peaks after sterilization, the relative integration of the peaks is calculated and compared (Figure 6).

As can be seen in Figure 6, there were no significant changes in the peak area after the sterilization process. The slight changes observed could be due to the precision of the NMR device. Regarding peak 1, although a decrease in peak intensity is observed in the NMR spectra of sterilized NMD 40%, the integrated area shows a larger value due to the broadening of the peaks in this spectrum and the overlapping of this peak with the neighboring peak. As no new peaks have appeared in the NMR spectra, no degradation products have formed. This result confirms the stability of NMD during the sterilization process. A similar effect was observed in ^{13}C NMR (Supporting Information).

3.3. X-ray Diffraction. As can be seen in Figure 7, the crystalline state of NMD was observed in the NMD powder as it was received and in both samples after the extrusion process.

3.4. Differential Scanning Calorimetry. *3.4.1. Nimodipine State inside the Formulations.* NMD has two different modifications: modification I, the metastable form with a melting point of around 124 °C, and modification II, the stable form with a melting point of around 116 °C.[45] As can be seen in Figure 8, the NMD powder is mostly composed of modification I. After the extrusion process, a significant change in NMD peaks can be seen. To make the comparison easier, the DSC curves of the NMD starch mixture before and after the extrusion are shown in Figure 9. As can be seen in this figure, the sharp peak of NMD is still clear in the mixture of NMD and starch before the extrusion process, while it is replaced by two wide peaks in both formulations after the extrusion process. As it was previously reported by Papageorgiou et al., NMD crystallizes slowly, and therefore no crystallization peak can be seen during the cooling cycle. But crystallization of glassy NMD during storage at room temperature is not preventable and can lead to the formation of mod II crystals which are less soluble.[46] We assume that part of the NMD powder could become amorphous due to the existence of water and high pressure during the extrusion process, which later formed the mod II crystals during the cooling at room temperature and storage in the fridge.

In order to get more information about the existing modifications of NMD in powder and after the extrusion process, Raman Spectroscopy was used.

https://doi.org/10.1021/acs.molpharmaceut.3c00618
Mol. Pharmaceutics XXXX, XXX, XXX−XXX

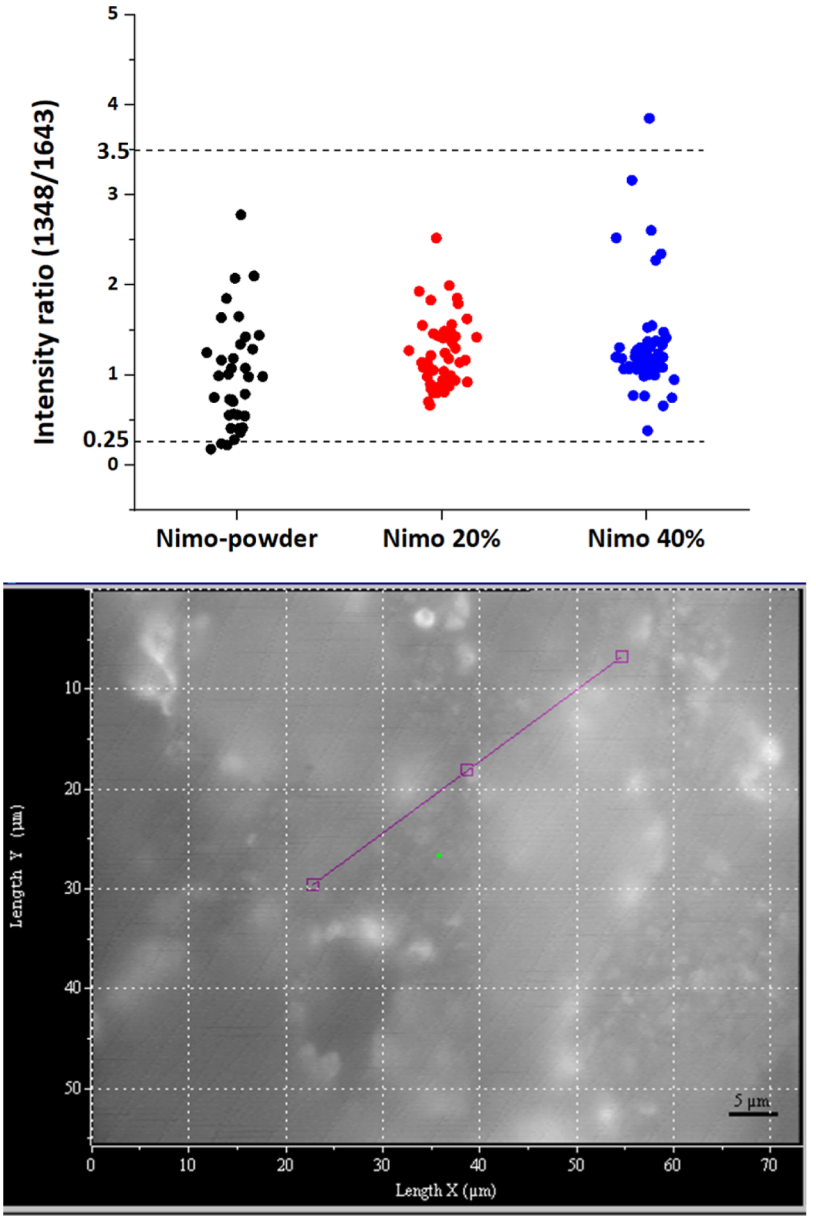

Figure 11. Calculated values of the peak intensity ratio of each sample at 1347/1642 cm^{-1}. Thirty measurements were performed for each sample (top), and the image of the sample under a Raman microscope during measurement (bottom).

3.4.2. Effect of Nimodipine on Starch. Figure 10 shows the DSC curve of the physical mixture of samples. As can be seen in the DSC curves, there is a broad peak starting at 40 °C in all three samples. These peaks are related to water evaporation and the partial gelatinization of starch during the heating cycle. The maximum peaks of gelatinization are 76.7, 85.17, and 104.5 °C for nimo-40%, nimo-20%, and starch-water samples, respectively. As the amount of water in all samples was constant and half of the weight of the starch (starch/water, 2:1), it can be concluded that the existence of nimodipine decreased the gelatinization temperature of the starch. Zheng et al.; reported a similar plasticizer effect of nimodipine on polyvinylpyrrolidone/vinyl acetate copolymer.[19] This result is in line with the observed structure of the sample in SEM images (Figure 12), where the complete gelatinization of starch and, as a result, a porous structure of 40% NMD was observed.

3.5. Raman Spectroscopy. The objective of using Raman spectroscopy was to evaluate the polymorphism of NMD, as well as its dispersion in a polymer matrix (Starch). The differentiation between different polymorphs of NMD by Raman spectroscopy has been reported previously.[42,46−49] In these studies, the intensity ratio of the NO_2 group stretch at 1347 cm^{-1} to the C double bond C stretch of the dihydropyridine ring at 1642 cm^{-1} was used to differentiate among the three solid states of nimodipine. These studies concluded that the values below 0.25 and above 3.5 definitely correspond to modification II and modification I, respectively, but the determination of modification for the values between 0.25 and 3.5 is more complicated, and these values correspond to the regions with submicron crystal size and/or amorphous regions.[49] The results of Raman spectroscopy are listed in Figure 11. As can be seen in the figure, the intensity ratio value of all three samples is mostly between 0.25 and 3.5. Therefore, NMD in all samples exists in the form of submicron size crystals and/or in its amorphous state. This result is in line with the SEM image of the NMD sample (Figure S5,

https://doi.org/10.1021/acs.molpharmaceut.3c00618
Mol. Pharmaceutics XXXX, XXX, XXX−XXX

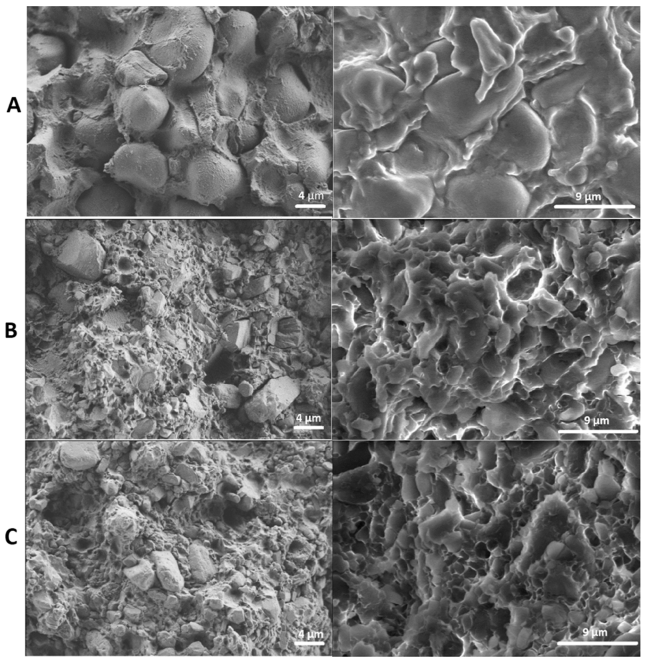

Figure 12. SEM image of the starch implant taken under high vacuum (left) and low vacuum (right) (A) starch implant, (B) NMD 20%, and (C) NMD 40%.

supplementary), where the heterogeneity of the NMD powder as a mixture of small (below 1 μm) and large crystals could be observed. Looking closer at Figure 11, a slight change in the dispersion of the calculated values can be observed between the different samples, which is in line with the result of DSC thermograms of the samples after the extrusion process (Figure 8). Although it was not possible to quantitatively show the change in NMD modifications, the results confirm the appeared change in modifications observed with other methods.

Figure 11 (bottom) shows an example of Raman measurements. For each group measurement, a line in the sample was chosen, and then 15 different points of the line were measured automatically by the device. In all of the obtained measurements from both samples, the peaks corresponding to NMD were observed. This proves the homogeneous dispersion of NMD inside the whole implant.

3.6. Electron Microscopy. Figure 12 shows the SEM image of the starch implant. As it was previously reported by several studies, granules of high amylose-containing starch samples may stay in their native form even after the cooking process.[50] Looking at the SEM image of the starch implant, it seems that the granule content is leaked out to a large extent, but many granules are still in their native form.

Looking at the SEM image of the NMD 20% implant (Figure 12, B), it can be seen that most of the granules are completely gelatinized, and a granule with its native form can hardly be seen. Some large particles can be seen, which are the drug crystals (Figure S5 (Supporting Information), SEM image of NMD powder).

As can be seen in the SEM image of the NMD 40% implant (Figure 12, C), the granules are completely destroyed, and the formed structure seems similar to the honeycomb structure of the gelatinized starch gel.[51] Comparing SEM images of NMD 20 and 40%, the significant effect of NMD on the starch gelatinization degree during the same extrusion procedure can be clearly seen. The porous structure of this system can explain the faster release profile of NMD from this system in comparison to NMD 20%.

4. CONCLUSIONS

In this study, starch-based implants with different NMD loads (20% and 40%) were prepared and characterized. Both formulations showed a sustained release of NMD over 100 days in vitro. Due to the neuroprotective effect of NMD, the long−release profile of NMD from the system could be beneficial in the treatment of different brain diseases, including SAH.[15,24] The system was characterized by different methods to assess the possible changes in the NMD modifications. DSC thermograms of both NMD-loaded implants showed significant changes in NMD modifications after the extrusion process. Although quantification of the change between different modifications of NMD was not possible with different methods, the observed change in modifications was also observed by IR and Raman spectroscopy. E beam sterilization was used to sterilize the implants. HPLC, IR, and NMR spectroscopy confirmed the stability of NMD during the electron beam sterilization. This confirms the ability of the starch-based system to protect NMD and other sensitive active substances during electron beam sterilization.

In summary, the study shows the suitability of the NMD-loaded starch implant as a parenteral controlled release system for local delivery of NMD in the brain. Further studies are needed to evaluate the formulation using in vivo models.

■ ASSOCIATED CONTENT

Supporting Information

The Supporting Information is available free of charge at https://pubs.acs.org/doi/10.1021/acs.molpharmaceut.3c00618.

Raman spectra of nimodipine powder; ^{13}C NMR spectra of starch, NMD powder, and the Nimo 40% sample before and after the electron beam sterilization; SEM image of the NMD powder; and mass spectrum of nimodipine powder and NMD 40% after sterilization (PDF)

■ AUTHOR INFORMATION

Corresponding Author

Karsten Mäder − *Institute of Pharmacy, Martin Luther University Halle-Wittenberg, Halle 06120 Saale, Germany;* orcid.org/0000-0003-1613-6976; Email: karsten.maeder@pharmazie.uni-halle.de

Authors

Golbarg Esfahani − *Institute of Pharmacy, Martin Luther University Halle-Wittenberg, Halle 06120 Saale, Germany*

Marie-Luise Trutschel − *Institute of Pharmacy, Martin Luther University Halle-Wittenberg, Halle 06120 Saale, Germany*

Detlef Reichert − *Institute of Physics, Martin Luther University Halle-Wittenberg, Halle D-06120 Saale, Germany;* orcid.org/0000-0002-6876-1901

Complete contact information is available at: https://pubs.acs.org/10.1021/acs.molpharmaceut.3c00618

Notes

The authors declare no competing financial interest.

https://doi.org/10.1021/acs.molpharmaceut.3c00618
Mol. Pharmaceutics XXXX, XXX, XXX−XXX

■ ACKNOWLEDGMENTS

This study was supported by the IGS "Functional Polymers" as a part of the AGRIPOLY program with funding from the European Social Fund (ESF). We kindly thank Dr Christoph Wagner from the Chemistry Institute of Martin Luther University Halle-Wittenberg for his support in x-ray diffraction measurements. For the kind support with the HPLC and mass analysis, we extend our sincere gratitude to Dr Matthias Schmidt and Ms Antje Herbrich-Peters from the Pharmacy Institute of Martin Luther University Halle-Wittenberg. We are grateful for the help from Ms. Rudolf for the FTIR measurements. Also, we would like to appreciate the kind support from Dr. Stefan Gröger during NMR spectroscopy measurements. As well, we would like to express our gratitude to the company Roquette (Lestrem, France) for providing us with the material. Finally, we would like to thank Dr Frank Heyroth and Mr Frank Syrowatka for their kind supports with SEM and Raman Spectroscopy measurements.

■ REFERENCES

(1) Shoupe, D.; Mishell, D. R. Norplant: Subdermal Implant System for Long-Term Contraception. *Am. J. Obstet. Gynecol.* **1989**, *160*, 1286−1292.
(2) Ding, A. G.; Schwendeman, S. P. Acidic Microclimate PH Distribution in PLGA Microspheres Monitored by Confocal Laser Scanning Microscopy. *Pharm. Res.* **2008**, *25*, 2041−2052.
(3) Lucke, A.; Kiermaier, J.; Göpferich, A. Peptide Acylation by Poly(α-Hydroxy Esters). *Pharm. Res.* **2002**, *19*, 175−181.
(4) Mäder, K.; Gallez, B.; Liu, K. J.; Swartz, H. M. Non-Invasive in Vivo Characterization of Release Processes in Biodegradable Polymers by Low-Frequency Electron Paramagnetic Resonance Spectroscopy. *Biomaterials* **1996**, *17*, 457−461.
(5) Schädlich, A.; Kempe, S.; Mäder, K. Non-Invasive in Vivo Characterization of Microclimate PH inside in Situ Forming PLGA Implants Using Multispectral Fluorescence Imaging. *J. Controlled Release* **2014**, *179*, 52−62.
(6) Garcia, M. A. V. T.; Garcia, C. F.; Faraco, A. A. G. Pharmaceutical and Biomedical Applications of Native and Modified Starch: A Review. *Starch/Staerke* **2020**, *72*, 1900270.
(7) Builders, P. F.; Arhewoh, M. I. Pharmaceutical Applications of Native Starch in Conventional Drug Delivery. *Starch/Staerke* **2016**, *68*, 864−873.
(8) Rowe, R. C.; Sheskey, P. J.; Quinn, M. E. *Handbook of Pharmaceutical Excipients Sixth ed.*, 6th ed., Rev. des Nouv. Technol. l'Information; Pharmaceutical Press, 2018.
(9) Araújo, M. A.; Cunha, A. M.; Mota, M. Enzymatic Degradation of Starch-Based Thermoplastic Compounds Used in Protheses: Identification of the Degradation Products in Solution. *Biomaterials* **2004**, *25* (13), 2687−2693.
(10) Esfahani, G.; Lucas, H.; Syrowatka, F.; Mäder, K. A Starch-Based Implant as a Controlled Drug Release System: Non-Invasive in Vivo Characterization Using Multispectral Fluorescence Imaging. *J. Contr. Release* **2023**, *358*, 358−367.
(11) He, Z.; Zhong, D.; Chen, X.; Liu, X.; Tang, X.; Zhao, L. Development of a Dissolution Medium for Nimodipine Tablets Based on Bioavailability Evaluation. *Eur. J. Pharm. Sci.* **2004**, *21*, 487−491.
(12) U.S. Food and Drug Administration. https://www.accessdata.fda.gov/drugsatfda_docs/label/2006/018869s014lbl.pdf (accessed Sep 10, 2023).
(13) Mahmoud, S. H.; Ji, X.; Isse, F. A. Nimodipine Pharmacokinetic Variability in Various Patient Populations. *Drugs R&D* **2020**, *20*, 307−318.
(14) Ramsch, K. D.; Ahr, G.; Tettenborn, D.; Auer, L. M. Overview on Pharmacokinetics of Nimodipine in Healthy Volunteers and in Patients with Subarachnoid Hemorrhage. *Neurochirurgia* **1985**, *28*, 74−78.
(15) Leisz, S.; Simmermacher, S.; Prell, J.; Strauss, C.; Scheller, C. Nimodipine-Dependent Protection of Schwann Cells, Astrocytes and Neuronal Cells from Osmotic, Oxidative and Heat Stress Is Associated with the Activation of AKT and CREB. *Int. J. Mol. Sci.* **2019**, *20*, 4578.
(16) Scheller, K.; Scheller, C. Nimodipine Promotes Regeneration of Peripheral Facial Nerve Function after Traumatic Injury Following Maxillofacial Surgery: An off Label Pilot-Study. *J. Cranio-Maxillofacial Surg.* **2012**, *40*, 427−434.
(17) Mattsson, P.; Frostell, A.; Björck, G.; Persson, J. K. E.; Hakim, R.; Zedenius, J.; Svensson, M. Recovery of Voice After Reconstruction of the Recurrent Laryngeal Nerve and Adjuvant Nimodipine. *World J. Surg.* **2018**, *42*, 632−638.
(18) Esfahani, G.; Häusler, O.; Mäder, K. Controlled Release Starch-Lipid Implant for the Therapy of Severe Malaria. *Int. J. Pharm.* **2022**, *622*, 121879.
(19) Zheng, X.; Yang, R.; Tang, X.; Zheng, L. Part I: Characterization of Solid Dispersions of Nimodipine Prepared by Hot-Melt Extrusion. *Drug Dev. Ind. Pharm.* **2007**, *33*, 791−802.
(20) Janowitz, H. D.; Dreiling, D. A. The Plasma Amylase: Source, Regulation and Diagnostic Significance. *Am. J. Med.* **1959**, *27*, 924−935.
(21) Byman, E.; Martinsson, I.; Haukedal, H.; Bank, N. B.; Gouras, G.; Freude, K. K.; Wennström, M. Neuronal A-amylase Is Important for Neuronal Activity and Glycogenolysis and Reduces in Presence of Amyloid Beta Pathology. *Aging Cell* **2021**, *20* (8), No. e13433.
(22) Byman, E.; Schultz, N.; Blom, A. M.; Wennström, M. A Potential Role for α-Amylase in Amyloid-β-Induced Astrocytic Glycogenolysis and Activation. *J. Alzheimer's Dis.* **2019**, *68*, 205−217.
(23) Byman, E.; Schultz, N.; Fex, M.; Wennström, M.; Wennström, M. Brain Alpha-amylase: A Novel Energy Regulator Important in Alzheimer Disease? *Brain Pathol.* **2018**, *28*, 920−932.
(24) Zech, J.; Leisz, S.; Göttel, B.; Syrowatka, F.; Greiner, A.; Strauss, C.; Knolle, W.; Scheller, C.; Mäder, K. Electrospun Nimodipine-Loaded Fibers for Nerve Regeneration: Development and in Vitro Performance. *Eur. J. Pharm. Biopharm.* **2020**, *151*, 116−126.
(25) Litvinov, V. M.; Penning, J. P. Phase Composition and Molecular Mobility in Nylon 6 Fibers as Studied by Proton NMR Transverse Magnetization Relaxation. *Macromol. Chem. Phys.* **2004**, *205*, 1721−1734.
(26) Maus, A.; Hertlein, C.; Saalwächter, K. A Robust Proton NMR Method to Investigate Hard/Soft Ratios, Crystallinity, and Component Mobility in Polymers. *Macromol. Chem. Phys.* **2006**, *207*, 1150−1158.
(27) Adams, A. Analysis of Solid Technical Polymers by Compact NMR. *TrAC, Trends Anal. Chem.* **2016**, *83*, 107−119.
(28) Bärenwald, R.; Champouret, Y.; Saalwächter, K.; Schäler, K. Determination of Chain Flip Rates in Poly(Ethylene) Crystallites by Solid-State Low-Field 1H NMR for Two Different Sample Morphologies. *J. Phys. Chem. B* **2012**, *116*, 13089−13097.
(29) Bärenwald, R.; Goerlitz, S.; Godehardt, R.; Osichow, A.; Tong, Q.; Krumova, M.; Mecking, S.; Saalwächter, K. Local Flips and Chain Motion in Polyethylene Crystallites: A Comparison of Melt-Crystallized Samples, Reactor Powders, and Nanocrystals. *Macromolecules* **2014**, *47*, 5163−5173.
(30) Besghini, D.; Mauri, M.; Simonutti, R. Time Domain NMR in Polymer Science: From the Laboratory to the Industry. *Appl. Sci.* **2019**, *9* (9), 1801.
(31) Xiong, R.; Lu, W.; Li, J.; Wang, P.; Xu, R.; Chen, T. Preparation and Characterization of Intravenously Injectable Nimodipine Nanosuspension. *Int. J. Pharm.* **2008**, *350*, 338−343.
(32) Yu, J.; He, H. B.; Tang, X. Formulation and Evaluation of Nimodipine-Loaded Lipid Microspheres. *J. Pharm. Pharmacol.* **2010**, *58*, 1429−1435.
(33) Musa, M. B.; Yoo, M. J.; Kang, T. B.; Kolawole, E. G.; Ishiaku, U. S.; Yakubu, M. K.; Whang, D. J. Characterization and Thermomechanical Properties of Thermoplastic Potato Starch. *J. Eng. Technol.* **2013**, *2*, 9−16.

https://doi.org/10.1021/acs.molpharmaceut.3c00618
Mol. Pharmaceutics XXXX, XXX, XXX−XXX

(34) Lomelí-Ramírez, M. G.; Barrios-Guzmán, A. J.; García-Enriquez, S.; Rivera-Prado, J. D. J.; Manríquez-González, R. Chemical and Mechanical Evaluation of Bio-Composites Based on Thermoplastic Starch and Wood Particles Prepared by Thermal Compression. *BioResources* **2014**, *9*, 2960−2974.
(35) Kizil, R.; Irudayaraj, J.; Seetharaman, K. Characterization of Irradiated Starches by Using FT-Raman and FTIR Spectroscopy. *J. Agric. Food Chem.* **2002**, *50*, 3912−3918.
(36) Zhang, Y.; Han, J. H. Plasticization of Pea Starch Films with Monosaccharides and Polyols. *J. Food Sci.* **2006**, *71*, E253−E261.
(37) Fang, J. M.; Fowler, P. A.; Tomkinson, J.; Hill, C. A. S. The Preparation and Characterisation of a Series of Chemically Modified Potato Starches. *Carbohydr. Polym.* **2002**, *47*, 245−252.
(38) Papadimitriou, S.; Papageorgiou, G. Z.; Kanaze, F. I.; Georgarakis, M.; Bikiaris, D. N. Nanoencapsulation of Nimodipine in Novel Biocompatible Poly(Propylene-Co- Butylene Succinate) Aliphatic Copolyesters for Sustained Release. *J. Nanomater.* **2009**, *2009*, 1−11.
(39) Li, H.; Li, H.; Wei, C.; Ke, J.; Li, J.; Xu, L.; Liu, H.; Li, S.; Yang, M. Biomimetic Synthesis and Evaluation of Histidine-Derivative Templated Chiral Mesoporous Silica for Improved Oral Delivery of the Poorly Water-Soluble Drug, Nimodipine. *Eur. J. Pharm. Sci.* **2018**, *117*, 321−330.
(40) Skrovanek, D. J.; Howe, S. E.; Painter, P. C.; Coleman, M. M. Hydrogen Bonding in Polymers: Infrared Temperature Studies of an Amorphous Polyamide. *Macromolecules* **1985**, *18*, 1676−1683.
(41) Calvo, N. L.; Balzaretti, N. M.; Antonio, M.; Kaufman, T. S.; Maggio, R. M. Chemometrics-Assisted Study of the Interconversion between the Crystalline Forms of Nimodipine. *J. Pharm. Biomed. Anal.* **2018**, *158*, 461−470.
(42) Grunenberg, A.; Keil, B.; Henck, J. O. Polymorphism in Binary Mixtures, as Exemplified by Nimodipine. *Int. J. Pharm.* **1995**, *118*, 11−21.
(43) Wei, M. y.; Lei, X. p.; Fu, J. j.; Chen, M. y.; Li, J. x.; Yu, X. y.; Lin, Y. l.; Liu, J. p.; Du, L. r.; Li, X.; et al. The Use of Amphiphilic Copolymer in the Solid Dispersion Formulation of Nimodipine to Inhibit Drug Crystallization in the Release Media: Combining Nano-Drug Delivery System with Solid Preparations. *Mater. Sci. Eng., C* **2020**, *111*, 110836.
(44) Bunkerd, R.; Molloy, R.; Somsunan, R.; Punyodom, W.; Topham, P. D.; Tighe, B. J. Synthesis and Characterization of Chemically-Modified Cassava Starch Grafted with Poly(2-Ethylhexyl Acrylate) for Blending with Poly(Lactic Acid). *Starch/Staerke* **2018**, *70*, 1800093.
(45) Guo, Z.; Ma, M.; Wang, T.; Chang, D.; Jiang, T.; Wang, S. A Kinetic Study of the Polymorphic Transformation of Nimodipine and Indomethacin during High Shear Granulation. *AAPS PharmSciTech* **2011**, *12*, 610−619.
(46) Papageorgiou, G. Z.; Bikiaris, D.; Karavas, E.; Politis, S.; Docoslis, A.; Park, Y.; Stergiou, A.; Georgarakis, E. Effect of Physical State and Particle Size Distribution on Dissolution Enhancement of Nimodipine/PEG Solid Dispersions Prepared by Melt Mixing and Solvent Evaporation. *AAPS J.* **2006**, *8*, E623−E631.
(47) Docoslis, A.; Huszarik, K. L.; Papageorgiou, G. Z.; Bikiaris, D.; Stergiou, A.; Georgarakis, E. Characterization of the Distribution, Polymorphism, and Stability of Nimodipine in Its Solid Dispersions in Polyethylene Glycol by Micro-Raman Spectroscopy and Powder X-Ray Diffraction. *AAPS J.* **2007**, *9*, E361−E370.
(48) Riekes, M. K.; Pereira, R. N.; Rauber, G. S.; Cuffini, S. L.; de Campos, C. E. M.; Silva, M. A. S.; Stulzer, H. K. Polymorphism in Nimodipine Raw Materials: Development and Validation of a Quantitative Method through Differential Scanning Calorimetry. *J. Pharm. Biomed. Anal.* **2012**, *70*, 188−193.
(49) Gordon, K. C.; McGoverin, C. M. Raman Mapping of Pharmaceuticals. *Int. J. Pharm.* **2011**, *417*, 151−162.
(50) Zhou, Z.; Zhang, Y.; Chen, X.; Zhang, M.; Wang, Z. Multi-Scale Structural and Digestion Properties of Wheat Starches with Different Amylose Contents. *Int. J. Food Sci. Technol.* **2014**, *49*, 2619−2627.
(51) Sun, Q.; Wu, M.; Bu, X.; Xiong, L. Effect of the Amount and Particle Size of Wheat Fiber on the Physicochemical Properties and Gel Morphology of Starches. *PLoS One* **2015**, *10*, No. e0128665.

https://doi.org/10.1021/acs.molpharmaceut.3c00618
Mol. Pharmaceutics XXXX, XXX, XXX−XXX

Journal of Controlled Release 358 (2023) 358–367

Contents lists available at ScienceDirect

Journal of Controlled Release

journal homepage: www.elsevier.com/locate/jconrel

A starch-based implant as a controlled drug release system: Non-invasive *in vivo* characterization using multispectral fluorescence imaging.

Golbarg Esfahani [a], Henrike Lucas [a], Frank Syrowatka [b], Karsten Mäder [a,*]

[a] Institute of Pharmacy, Martin Luther University Halle-Wittenberg, Kurt-Mothes-Straße 3, 06120 Halle (Saale), Germany
[b] Interdisciplinary Center of Materials Science, Martin-Luther-University Halle-Wittenberg, Halle (Saale), Germany

ARTICLE INFO

Keywords:
Fluorescence imaging
In vitro
In vivo
Release kinetics
NIR dyes
Starch
Biodegradable implants
Optical imaging

ABSTRACT

Solid implants are parenteral depot systems that can provide a controlled release of drugs in the desired body area over a few days to months. Finding an alternative for the two most commonly used polymers in the production of parenteral depot systems, namely Poly-(lactic acid) (PLA) and Poly-(lactide-*co*-glycolide) (PLGA), is of great importance due to their certain drawbacks. Our previous study showed the general suitability of starch-based implants for controlled drug release system. In this study, the system is further characterized and the release kinetics are investigated *in vitro* and *in vivo* by fluorescence imaging (FI). ICG and DiR, two fluorescent dyes with different hydrophobicity serving as a model for hydrophilic and hydrophobic drugs, have been used. In addition to 2D FI, 3D reconstructions of the starch implant were also used to assess the release kinetics in 3D mode. The *in vitro* and *in vivo* studies showed a fast release of ICG and a sustained release of DiR over 30 days from the starch-based implant. No treatment-related adverse effects were observed in mice. Our results indicate the promising potential of the biodegradable biocompatible starch-based implant for the controlled release of hydrophobic drugs.

1. Introduction

Parenteral controlled release drug delivery systems (CR-DDS) have gained significant attention during the last decades due to their high potential to improve drug therapy. CR-DDS can provide a constant concentration of drugs in the desired area of the body over several days, weeks, or even months. Currently, Poly-(lactic acid) (PLA) and Poly-(lactide-*co*-glycolide) (PLGA) are the most commonly used polymers in the pharmaceutical industry to produce parenteral depot systems [1–3]. However, these polymers degrade into acidic monomers which might lead to autocatalytic processes and drug degradation prior to release. Market products show often nonlinear release profiles with burst release or lag times [4–6]. Starch as a natural and abundant polymer with non-toxic and non-acidic degradation products might be a potential alternative for PLA and PLGA [7]. Starch is stable in a prolonged period of storage in the dry state. It is mostly used in solid preparations for oral delivery such as powders and tablets with various functions such as diluent, binder, disintegrant and lubricant [8–10]. Versatility in starch uses coupled with its low cost makes it an attractive excipient in the pharmaceutical industry [11]. Starch-based materials are already clinically used as bioresorbable medical products for providing hemostasis [12]. The biosafety of starch in different formulations is proven by several studies [13,14]. Despite all these advantages, there are certain limitations in using starch as the main component of a controlled release system. The most important drawback is its weak mechanical stability and the rapid biodegradation of starch by amylases in the body [15]. Chemical modification of starch has been widely investigated to slow down starch biodegradation and to improve its mechanical stability [8]. Physical modifications are simple, cost-effective and eco-friendly compared to chemical modifications [16]. In our previous study, a physically modified starch based implant was produced by means of high temperature and high pressure during the hot melt extrusion process. The appropriate mechanical properties of the system were proved by texture analysis. The *in vitro* release from the system was assessed by different methods. The results confirmed the general suitability of the system in providing a sustained release of a hydrophobic active substance over a few days to a few weeks [17]. As *in vitro* release kinetics might differ from *in vivo*, the aim of this study was to assess the release behavior from the implant and the fate of the implant *in vivo*. As far as we are concerned, no previous study has reported the fate of parenterally

* Corresponding author.
E-mail addresses: golbarg.esfahani@pharmazie.uni-halle.de (G. Esfahani), henrike.lucas@pharmazie.uni-halle.de (H. Lucas), frank.syrowatka@cmat.uni-halle.de (F. Syrowatka), karsten.maeder@pharmazie.uni-halle.de (K. Mäder).

https://doi.org/10.1016/j.jconrel.2023.05.006
Received 3 March 2023; Received in revised form 16 April 2023; Accepted 5 May 2023
Available online 12 May 2023

administered solid implant based on starch *in vivo*. There are only a few techniques to assess the *in vivo* release kinetics non-invasively. In a recent study conducted by Collantes et al., radiolabeling as a non-invasive method is used for intranasal implant studies development. However, this technique is very expensive and needs special facilities for the use of radioactive material [18]. Optical imaging (OI) is one of the most commonly used techniques in the visualization of *in vivo* processes. In contrast to radiolabeling which is based on ionizing radiation associated with potentially negative side effects, OI uses nonionizing radiation ranging from ultraviolet to infrared light that enables longterm or repetitive observations [19,20]. Due to the higher penetration depth, longer wavelengths are preferred. It requires the presence of a suitable fluorescent molecule with the following desired properties:

- absorption and emission at longer wavelengths for better tissue penetration of the light
- high quantum yield (high intensity)
- long-term stability (no bleaching)
- long-range of linear correlation between dye concentration and signal intensity

In this study, the release kinetics from starch implant is investigated by OI both *in vitro* and *in vivo*. The near-infrared (NIR) dyes ICG and DiR were loaded into the implants as examples of hydrophilic and hydrophobic molecules. The NIR dyes have the advantage of fast clearance from the body and minimal retention in nontargeted organs [21]. ICG is the only FDA approved NIR dye for clinical studies and DiR is widely used in preclinical studies [22–24]. The implants were injected subcutaneously (SC) in mice and evaluated over time with OI. Also, the possibility to quantify and assess the release kinetics by 3D reconstructions of implants was evaluated and compared to 2D OI.

2. Materials and methods

2.1. Materials

The fluorescent dye 1,10-Dioctadecyl-3,3,30,30-Tetramethylindotricarbocyanine Iodide (DiR), was purchased from Thermo Fisher Scientific Inc. (Waltham, MA, USA). The starch (MAIZE STARCH AMYLO N-400) was kindly provided by Roquette (Lestrem, France). Testing media was Phosphate Buffered Saline (PBS) (Ph. Eur.) plus 1% sodium dodecyl sulfate (SDS), adjusted to pH 7.4. SDS was purchased from Sigma Aldrich Chemie GmbH (Munich, Germany). Indocyanine green (ICG) was purchased from Carl Roth GmbH, Karlsruhe, Germany.

2.2. Preparation of implant

The implants were prepared by a hot melt extruder (HME), (ZE 5 ECO; Three-Tec GmbH; Seon; Swiss). Water was used as a plasticizer with a ratio of 1 g to 2 g of the starch. Water and starch were mixed gently and the mixture was used in the extruder. Extrusion die with a 0.3 mm diameter was used. The chamber heating zone's temperatures were 70, 80 and 90 °C. The samples were collected and stored in opaque falcon tubes between 4 and 8 °C.

2.3. Implant characterization

2.3.1. Thermogravimetric analysis

The samples' moisture content was assessed by thermogravimetric analysis with a TG 209 instrument (Netzsch, Selb, Germany). The samples were heated up to 105 °C at a heating rate of 10 K/min and kept at this temperature for 90 min. Nitrogen was used as a flushing gas with a flow rate of 20 ml/min.

2.3.2. Differential scanning calorimetry

DSC measurements were recorded with a Mettler Toledo DSC 823e module (Mettler Toledo, Gießen, Germany) in standard aluminium sample pans. Every sample was kept at 25 °C for 2 min and then heated up to 150 °C with a 10 K/min heating rate. All samples were kept at 150 °C for 1 min and then cooled down to 25 °C and kept at this temperature for 2 min and then heated up again up to 150 °C with a 10 K/min heating rate. Data recording and processing of the first heating cycle were carried out with the software STARe V15.00 (Mettler Toledo, Gießen, Germany) as no thermal event was observed during the cooling and second heating cycles.

2.3.3. Scanning electron microscopy

The samples were broken into tiny pieces and the breakage surface was imaged using an XL 30 ESEM device, with a GSE detector and 12.0 kV electron beam, in wet modules, under low vacuum and pressure of 1 mbar to prevent possible changes in the internal structure of the system due to the fast water evaporation.

2.4. ICG loaded implant preparation

The implants were prepared by a hot melt extruder (HME), (ZE 5 ECO; Three-Tec GmbH; Seon; Swiss). Fluorescent dye, ICG, which was dissolved in water, was added to the starch to reach the concentration of 8 μg per g of the implant. Water was used as a plasticizer with a ratio of 1 g to 2 g of the starch. Water and starch were mixed gently and the mixture was used in the extruder. Extrusion die with a 0.3 mm diameter was used. The chamber heating zone's temperatures were 70, 80 and 90 °C. The samples were collected and stored in opaque falcon tubes between 4 and 8 °C.

2.5. DiR loaded implant preparation

The implants were prepared by a hot melt extruder (HME), (ZE 5 ECO; Three-Tec GmbH; Seon; Swiss). Fluorescent dye, DiR, was dissolved in Ethanol. The required amount was added to the starch to reach a concentration of 1.5 μg per g of the implant. The organic solvent was evaporated under the vacuum. Water was used as a plasticizer with a ratio of 1 g to 2 g of the starch. Water and starch were mixed gently and the mixture was used in the extruder. Extrusion die with a 0.3 mm diameter was used. The chamber heating zone's temperatures were 70, 80 and 90 °C. The samples were collected and stored in opaque falcon tubes between 4 and 8 °C.

2.6. DiR loaded MCT oil as a control

A solution of the DiR with the same concentration of 1.5 μg per g of MCT oil was prepared by simply dissolving the required amount of DiR in MCT oil. This solution was used as a control for DiR implant to confirm that the prolonged release of DiR from DiR implant is not due to retention of the dye in the surrounding tissue at the injection site.

2.7. E-beam sterilization

Electron beam irradiation was chosen as the sterilization process. The extrudates were irradiated by a 10 MeV linear accelerator MB 10–30 MP (Mevex, Stittsville, Ontario, Canada) on a moving tray (95 cm/min). The total dose of 25 kGy was achieved by administering two separate doses of 12.5 kGy each (beam current 250 mA, PPS = 450 Hz).

2.8. In vitro release studies

2.8.1. ICG release

The extrudates were cut into implants with 0.5 cm length and 0.3 mm diameter ($n = 6$). Each implant was put in one well of a six-well plate. PBS was used as a release media (4 ml in each well). The plate was slightly agitated in a shaker with light protection (Memmert GmbH + Co. KG, Schwabach, Germany) at 37 °C. Before each imaging, the

media was withdrawn completely. After the imaging, an appropriate volume of fresh PBS was replaced. First imaging was carried out from the implant in a dry state as a D0 time point and then repeated on D1/2/4/7.

2.8.2. DiR release

The extrudates were cut into implants with 0.5 cm length and 0.3 mm diameter ($n = 6$). Each implant was put in one well of a six-well plate. PBS plus 1% SDS was used as a release media to ensure the sink condition (4 ml in each well). The plate was slightly agitated in a shaker with light protection (Memmert GmbH + Co. KG, Schwabach, Germany) at 37 °C. Before each imaging, the media was withdrawn completely. After the imaging, an appropriate volume of fresh PBS plus 1% SDS was replaced. First imaging was carried out from the implant in a dry state as a D0 time point and then repeated on D1/2/4/7/10/14/17/21/24/28/31.

2.9. In vivo release studies

All animal experiments were approved by local authorities of Saxony-Anhalt, Germany, and complied with the guidelines of the Federation for Laboratory Animal Science Associations (FELASA) [25,26]. Hairless SKH1 mice with albino background were used to avoid fluorescence signal absorption and scattering by hairs. Mice were kept under controlled standard conditions (12 h day/night cycle, 24 °C) in individually ventilated cages in groups of 2–5 individuals with food and water *ad libitum*. Mice condition and body weight were monitored over time. After the experiment, the mice were sacrificed by cervical dislocation. Tissue at the injection site was fixed in 5% formalin in PBS for histology investigations (FFPE–formalin fixed paraffin embedded). The FFPE samples were cut into 3 to 4 μm thin tissue sections on a microtome (Leica Biosystems Nussloch GmbH, Nussloch, Germany). Afterwards, dewaxation and rehydration were performed in a decreasing alcohol series from xylene to water. Standard hematoxylin and eosin (HE) staining followed using a ready-to-use hematoxylin solution and an acetic-acidic 0.1% eosin solution. After a series of increasing alcohol solutions from water to xylene, the sections were covered by Entellan© finally. Microscopic analysis was performed on an Axio Lab microscope (Zeiss, Jena, Germany) using a bright field. Pictures were taken with software Axiovision and camera Axiocam MRm (both Zeiss, Jena, Germany) in 10- to 40-fold magnification (Fig. 13) [27].

2.9.1. ICG implant in vivo release

The implants with 0.5 cm length and 0.3 mm diameter were implanted in anaesthetized mice subcutaneously (SC) in the loose skin overlying the upper back and shoulders into the nuchal fold. A 24G needle filled with an implant was inserted firmly through the skin from caudal to cranial. When correctly placed, the extrudate was pushed out of the needle with an ethanol sanitized plunger made out of wire. Finally, the needle was slowly removed by pulling back with one hand under slight skin fixation using the thumb and forefinger of the other hand ($n = 7$). First imaging was carried out directly after the SC injection of the samples as a D0 time point and then repeated on D1/2/4/7.

2.9.2. DiR implant in vivo release

The implants with 0.5 cm length and 0.3 mm diameter were implanted in anaesthetized mice SC in the loose skin overlying the upper back and shoulders into the nuchal fold. The 24G needle filled with an implant was inserted firmly through the skin from caudal to cranial. When correctly placed, the extrudate was pushed out of the needle with an ethanol sanitized plunger made out of wire. Finally, the needle was slowly removed by pulling back with one hand under slight skin fixation using the thumb and forefinger of the other hand ($n = 7$). First imaging was carried out directly after the SC injection of the samples as a D0 time point and then repeated on D1/2/4/7/10/14/17/21/24/28/31.

2.9.3. DiR solution (MCT) in vivo release

The DiR solution (10 μL) was injected subcutaneously (SC) in the loose skin overlying the upper back and shoulders into the nuchal fold ($n = 3$). First imaging was carried out directly after the SC injection of the samples as a D0 time point and then repeated on D1/2/4/7.

2.10. Fluorescence imaging: data acquisition and analysis

For *in vitro* and *in vivo* fluorescence imaging (FI), the IVIS Spectrum FI system (PerkinElmer, Inc., Waltham, MA, USA) was used. Mice were anaesthetized by inhalation anaesthesia (initially: 2.5% *v*/v isoflurane (Forene, Abbott, Wiesbaden, Germany) in oxygen at 3 L/min, maintenance: 2.5% at 0.3 L/min) in an XGI-8 narcosis system, Caliper Life Sciences (Runcorn, Cheshire, UK) and imaged at 37 °C in the IVIS Spectrum FI system. The FI system was equipped with a 150 W quartz wolfram halogen lamp. Grayscale and FI signals were recorded with a 4.1 megapixel (2048 × 2048) CCD camera at a working temperature of −90 °C. Analysis of *in vitro* and *in vivo* images was performed with Living Image® software, version 4.7.3.20616, PerkinElmer, Inc. (Waltham, MA, USA). The imaging was done with an epi-illumination system in which the source and detectors reside on the same side of the tissue. The respective experimental parameters are presented in the supplements (Table S1). For both *in vitro* and *in vivo* studies, the region of interest (ROI) was defined as an ellipsoid area with dimensions of a longitudinal axis of 1.2 cm and a transversal axis of 0.6 cm. Total radiant efficiency (TRE) was assessed. It takes into account the exposure time and area, quantity of detected photons, a fixed spatial angle (steradian) and the

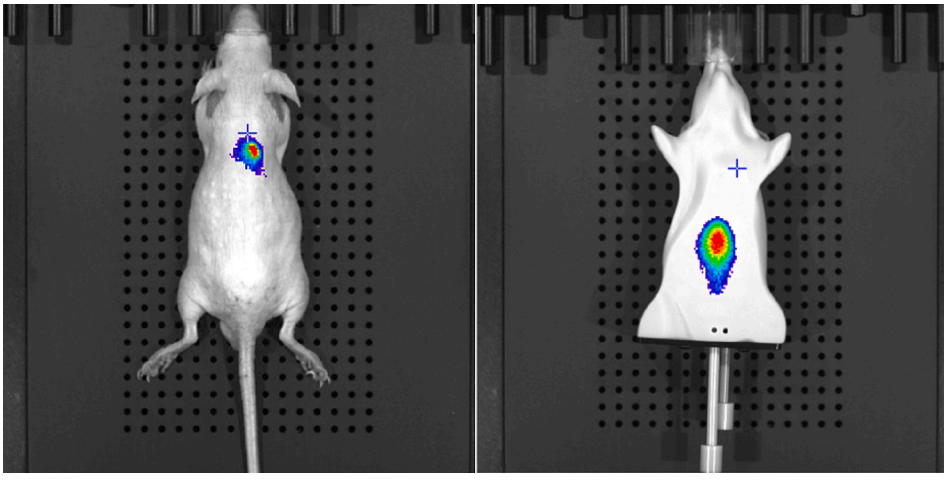

Fig. 1. Image examples obtained with the FLIT sequences acquired in dorsal (mouse) and ventral (mouse phantom) positions.

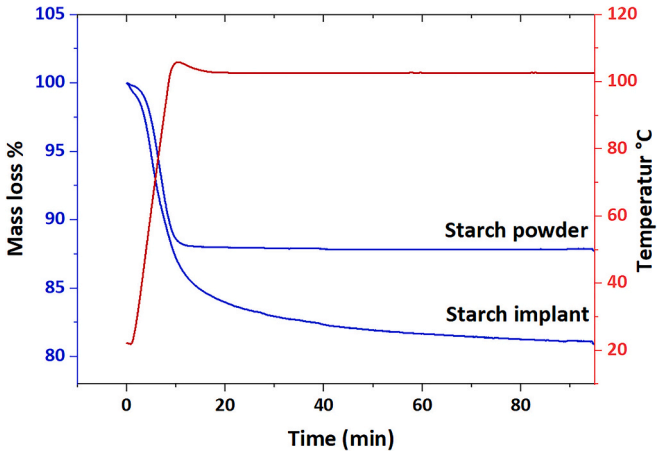

Fig. 2. Curves of different sample mass loss (in blue) and temperature of the chamber (in red) plotted against time. The blue curves show the average value for each sample ($n = 3$). (For interpretation of the references to colour in this figure legend, the reader is referred to the web version of this article.)

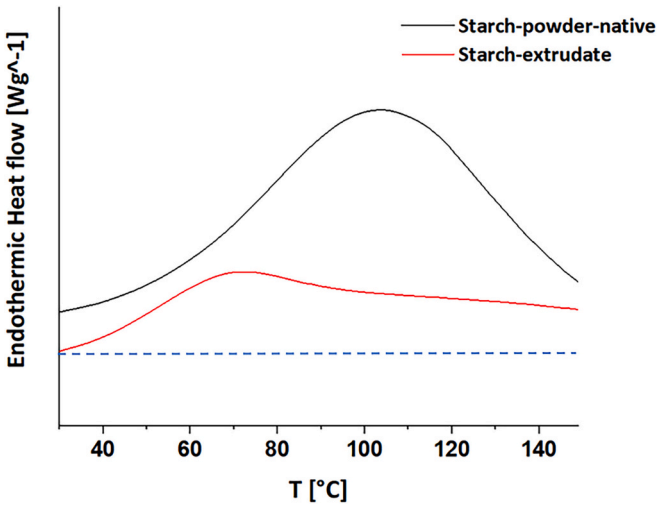

Fig. 3. Differential scanning thermograms of starch powder before (Black) and after (Red) the extrusion process. (For interpretation of the references to colour in this figure legend, the reader is referred to the web version of this article.)

exposure intensity, allowing quantitative comparisons between different implants, mice and time points. To determine the background signal of the mouse body, a region of interest (ROI) was set on the untreated area at the lower back in the lumbar-sacral region of each mouse. The TRE of the untreated area (background area) was subtracted from the TRE of the injection area. In principle, quantification in fluorescence imaging can be approached only through a combination of light transport modelling, data normalization and calibration. In this study, the approach of normalized data was used as the signal has travelled more or less the same tissue path length and the impact of the normalization is to approximately cancel out geometrical and heterogeneity effects that cannot be controlled experimentally [9–11]. For the normalization, TRE at D0 was defined as 1.

2.11. 3D reconstruction of the implant

The Imaging Wizard was used to acquire the Fluorescent Tomography (FLIT) sequence. Always four points (surrounding the injection site) were chosen as the transillumination locations. The low lamp level was used to acquire the FLIT sequences. The surface of the mouse or phantom mouse (XFM-2×) was generated automatically by the software. The XFM-2× Phantom Mouse is made to mimic tissue properties. The colour of the surface of the phantom emulates the behavior of tissue autofluorescence [28]. The phantom mouse is a good tool to optimize the sample composition (*e.g.* dye concentration) and measuring conditions *in vitro* to prepare *in vivo* experiments. It was not made for *in vitro* release experiments in pharmaceutics. Best 3D reconstructions were obtained by Normalized Transmission Fluorescence (NTF) by manual reconstruction.

As can be seen in Fig. S1, there are two different holes in the mouse phantom. In order to simulate the subcutaneously injected implant the upper hole close to the surface of the mouse phantom (in ventral position) was used.

As for the *in vivo* studies the implants were injected in the loose skin overlying the upper back of the mice, the FLIT sequences were acquired with a dorsal position whereas a ventral position was used for mouse phantom (Fig. 1). For the measurement of the signal in 3D fluorescent sources, a 3D region of interest (ROI) with the dimensions of 5*5*10 mm was used. The fluorescence yield summed over the 3D ROI (Total pmol M^{-1} cm^{-1}) was calculated by the software automatically.

2.12. In vivo release 2D vs 3D

As DiR loaded implant showed a sustained release over a month, this implant was used to assess the possibility of using FLIT 3D reconstruction in the quantification of *in vivo* release. To ensure a linear concentration/intensity relation and to monitor the release at a later time point, two different concentrations of the DiR dye 1.5 and 50 μg/g were used. The implants were injected subcutaneously as mentioned previously and the mice were imaged with both epi-illumination (2D) and FLIT (3D). Imaging was performed directly after the injection as D0 and then repeated on D1/2/5/8/12/15/19/22/26/33/40 for 2D and on D2/5/8/12/15/19/22/26/33/40 for 3D. FLIT measurement on day 1 was not performed to prevent mice's long exposure to anaesthesia gas for three continuous days. The FLIT measurement takes longer than epi-illumination (2D).

3. Results and discussion

3.1. Thermogravimetric analysis

As can be seen in Fig. 2, starch powder showed a total mass loss of 12% which corresponds to the water content of the sample. The value is in the normal range of starch samples [29]. Looking at the starch implant TGA curve, it can be seen that, the system had a total mass loss of 20%. As before the extrusion process, water was added to the starch (1 g water to 2 g starch), it can be concluded that a significant part of the water is removed from the system during the extrusion process.

3.2. Differential scanning calorimetry

Figure 3 shows the DSC graph of starch powder and starch implant. The water evaporation peak can be seen in the DSC curve of the starch powder sample, with the maximum peak around 100 °C. As the starch implant is gelatinized during the extrusion process and later on retrograded during cooling of the implant at room temperature, a thermal transition peak of retrograded starch can be seen in the starch extrudate DSC curve with maximum peak around 69 °C [30].

3.3. Scanning electron microscopy (SEM)

The SEM image (Fig. 4) shows the broken surface of the implant. Looking closer at the breakage surface, it can be seen that the starch granules are gelatinized and the content of the granules is leaked out.

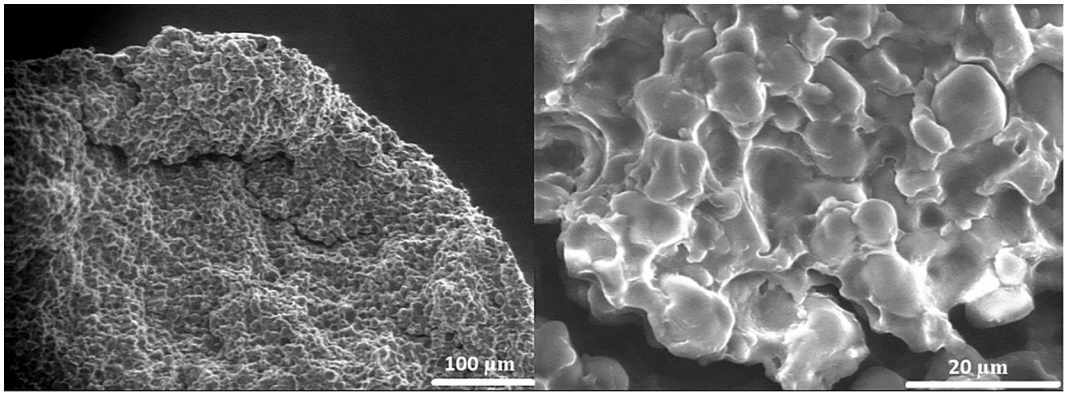

Fig. 4. SEM image of the broken surface of the implant: (**a**) scale bar shows 100 µm; (b) scale bar shows 20 µm.

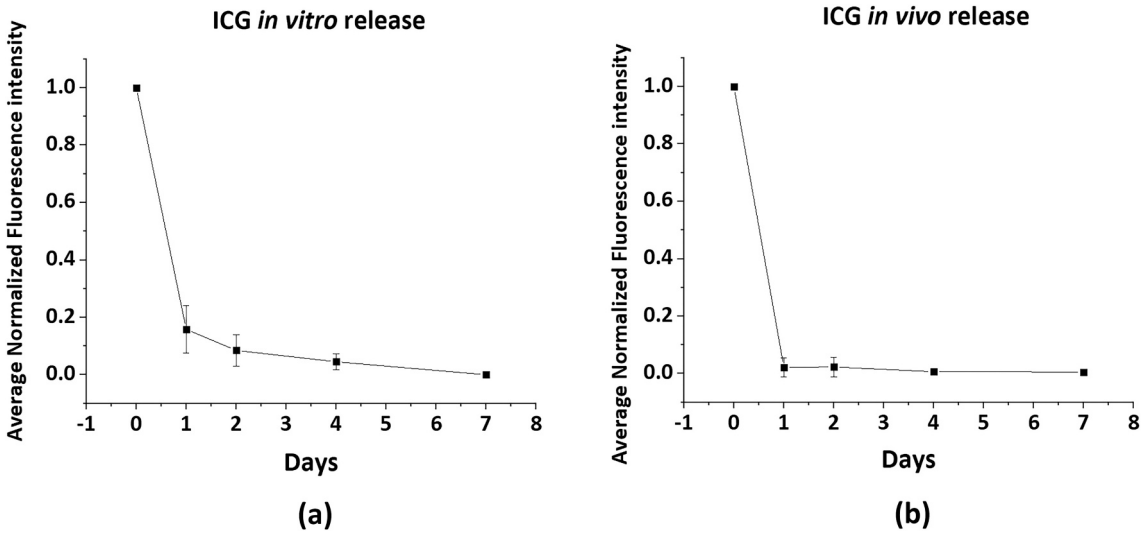

Fig. 5. Kinetics of ICG signals from starch extrudates after: (**a**) incubation in buffer, (*in vitro)*; (**b**) injection into mice, (*in vivo);* (Mean ± SD, $n = 7$).

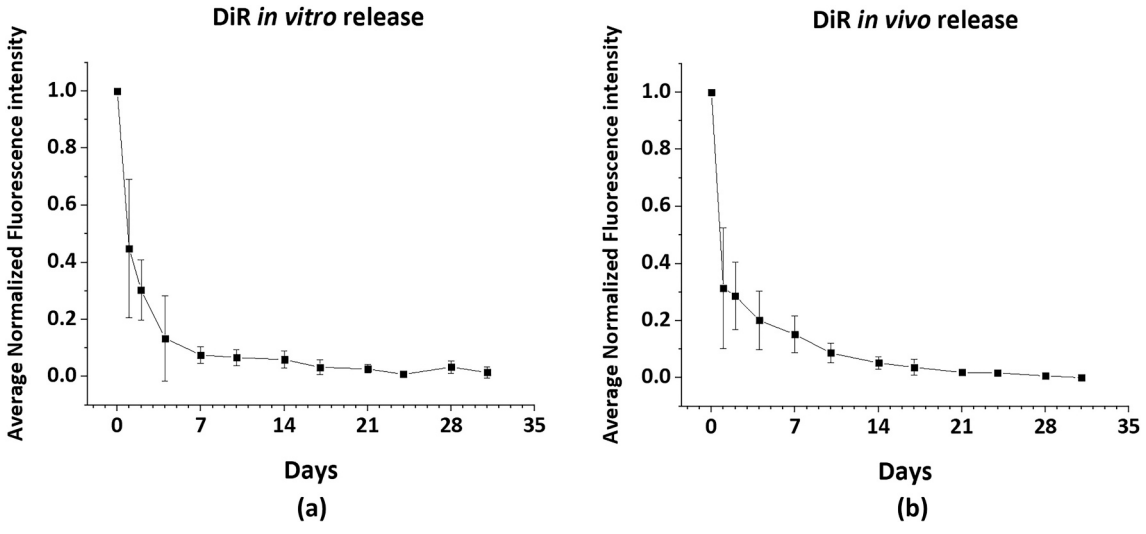

Fig. 6. Kinetics of DiR signals from starch extrudates after: (**a**) incubation in buffer, (*in vitro)*; (**b**) injection into mice, (*in vivo);* (Mean ± SD, $n = 7$).

3.4. ICG in vitro/in vivo release (2D)

As can be seen in Fig. 5, the signal intensity is significantly decreased after the first day, which proves the fast release of ICG from the system both *in vitro* and *in vivo*. The *in vitro* results are in line with the results of our previous publication, where Electron Paramagnetic Resonance (EPR) was implemented to assess the mobility of the drug models (spin probes) and polarity inside the system. This study showed that the water

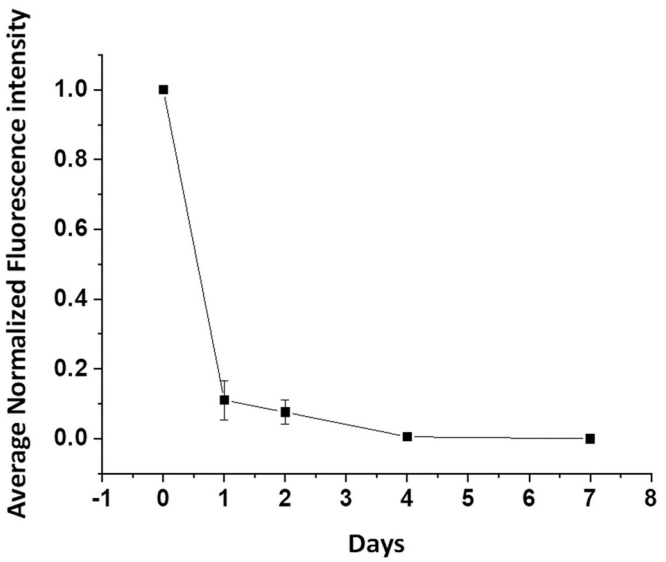

Fig. 7. Kinetics of DiR signals after administration of a DiR loaded MCT solution (Mean ± SD, $n = 3$).

penetration into the starch implant is very fast (a few minutes). Therefore, the existence of water inside the system leads to fast release of hydrophilic substance by diffusion from the system. Tempol as a model of a hydrophilic drug showed fast solubilization after buffer exposure and a similar release behavior as ICG *in vitro* [17]. FI as a more sensitive method than the EPR, enabled us to assess the biodegradability of the implant and release of a hydrophilic drug model from the implant *in vivo* non-invasively.

3.5. DiR in vitro/in vivo release (2D)

Figure 6 shows the *in vitro* and *in vivo* release of the lipophilic dye DiR. As can be seen in the figure, DiR signals could be detected over a period of 30 days. Therefore, compared to ICG, the release time of DiR is much longer. Most part of the DiR dye is released from the system over two weeks both *in vitro* and *in vivo*. The results are in line with the results of our previous *in vitro* EPR study, where Tempol Benzoate (TB) as a model of a hydrophobic drug showed a sustained release over two weeks from starch implant [17].

The *in vitro* and *in vivo* release profiles of DiR are very similar, which was not expected prior to the experiments. After 4 weeks, the experiment was finished and the implantation side was inspected *ex vivo*. The implant was completely degraded after 4 weeks, as no residue of the implant could be observed in any of the mice's tissue at the injection site macroscopically. *In vitro*, the starch extrudate was still present as a monolithic extrudate after 4 weeks. These findings suggest a complete degradation of the starch *in vivo* by enzymes, most likely amylases. Amylases are produced not only by salivary glands, pancreas and liver but also by other tissues and exist in serum at a normal level. The amylose and amylopectin molecules of starch are broken down into dextrins by these enzymes. The dextrins will be further on degraded to fermentable sugars, mainly maltose but some glucose as well [15]. Because of the different behavior *in vitro* and *in vivo*, nonenzymatic hydrolysis is not the major mechanisms of starch degradation *in vivo*. This is in contrast to PLA and PLGA implants, where (autocatalytic) hydrolysis is the major mechanism for polymer degradation.

3.6. DiR in MCT as a control

A possible artifact for the observed kinetics of the DiR could be an intrinsic strong association of the dye with the surrounding tissue. In this case, the DiR would remain for prolonged times at the side of injection (suggesting a "controlled release"), even after the administration of a solution. Therefore, an oily solution of DiR in MCT was injected as a control. As can be seen in Fig. 7, DiR signals were detectable for four days. This finding confirms that the DiR signals observed 4 weeks after implantation of the starch extrudates are due to the controlled release properties of the starch matrix and no the intrinsic properties of the DiR dye.

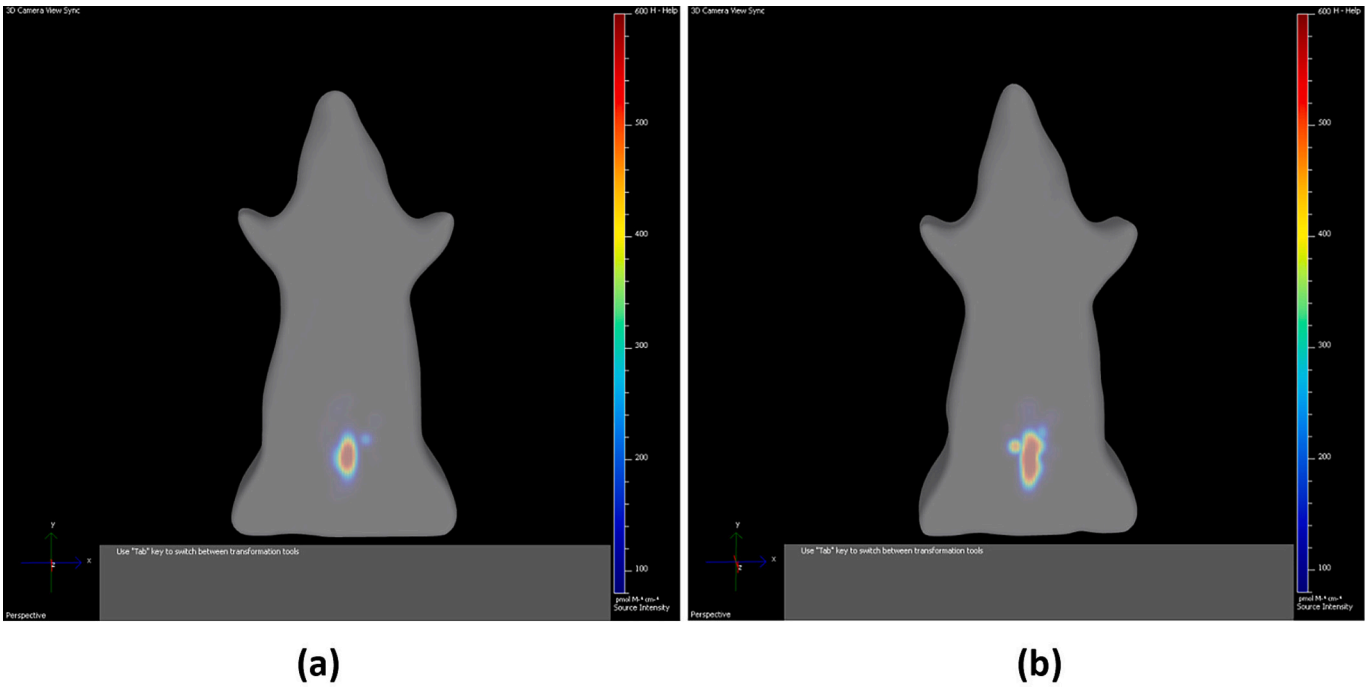

Fig. 8. The 3D reconstruction of the ICG loaded implant with different dimensions in the mouse phantom: (a) Implant with a diameter of 0.3 mm and length of 5 mm; (b)) Implant with a diameter of 0.3 mm and length of 10 mm.

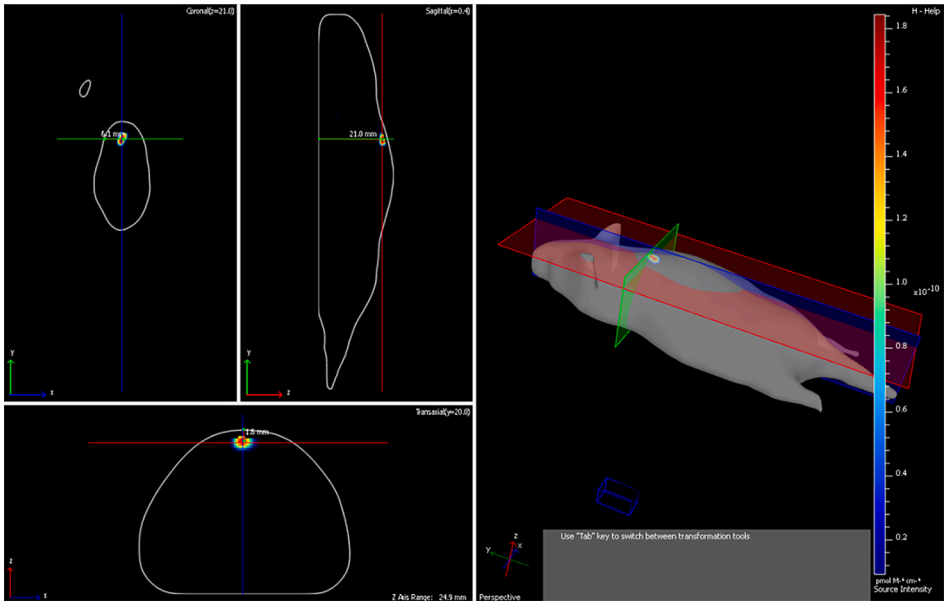

Fig. 9. The 3D reconstruction of the DiR loaded implant subcutaneously injected in the mouse.

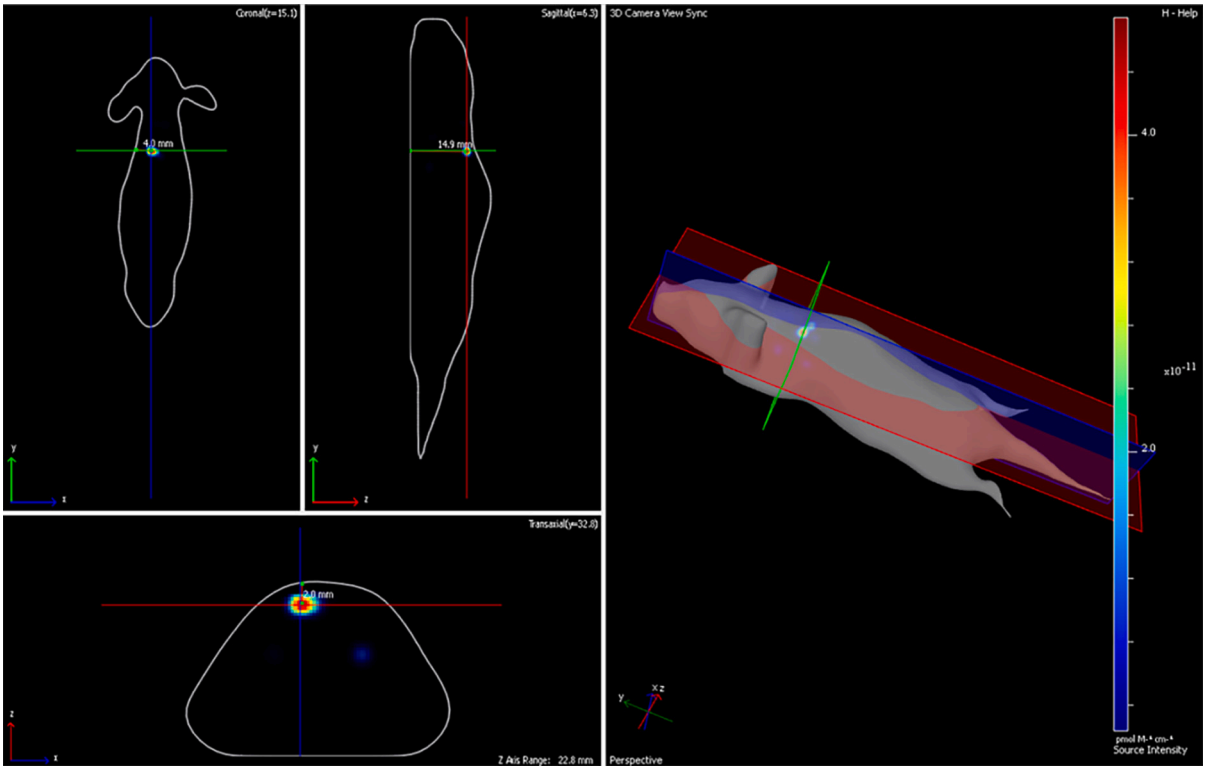

Fig. 10. The 3D reconstruction of the ICG loaded implant subcutaneously injected in the mouse.

3.7. 3D reconstruction of the implant

3D reconstruction of the fluorescent sources has been widely used in optical imaging. Several studies have demonstrated the positive correlation between the fluorescence signal intensity and tumor weights and volume (in our case size of the implant) [31–35]. In this study, this method was used to assess the fate of the fluorophore-loaded implant and the release of the fluorescent dyes as drug models from this implant. A possible problem in the 3D reconstruction of the fluorescent signal is the appearance of the artifacts due to model mismatch and out-of-plane effects [36]. Implants with different diameters were evaluated to assess the positive correlation between the fluorescence signal intensity and implant size and also to discriminate between the signal responsible for the implant and the artifacts. Fig. 8 shows the 3D reconstruction of the ICG loaded implants with different dimensions in the mouse phantom.

Figs. 9 and 10 show the 3D reconstructions of the SC injected implants in mice.

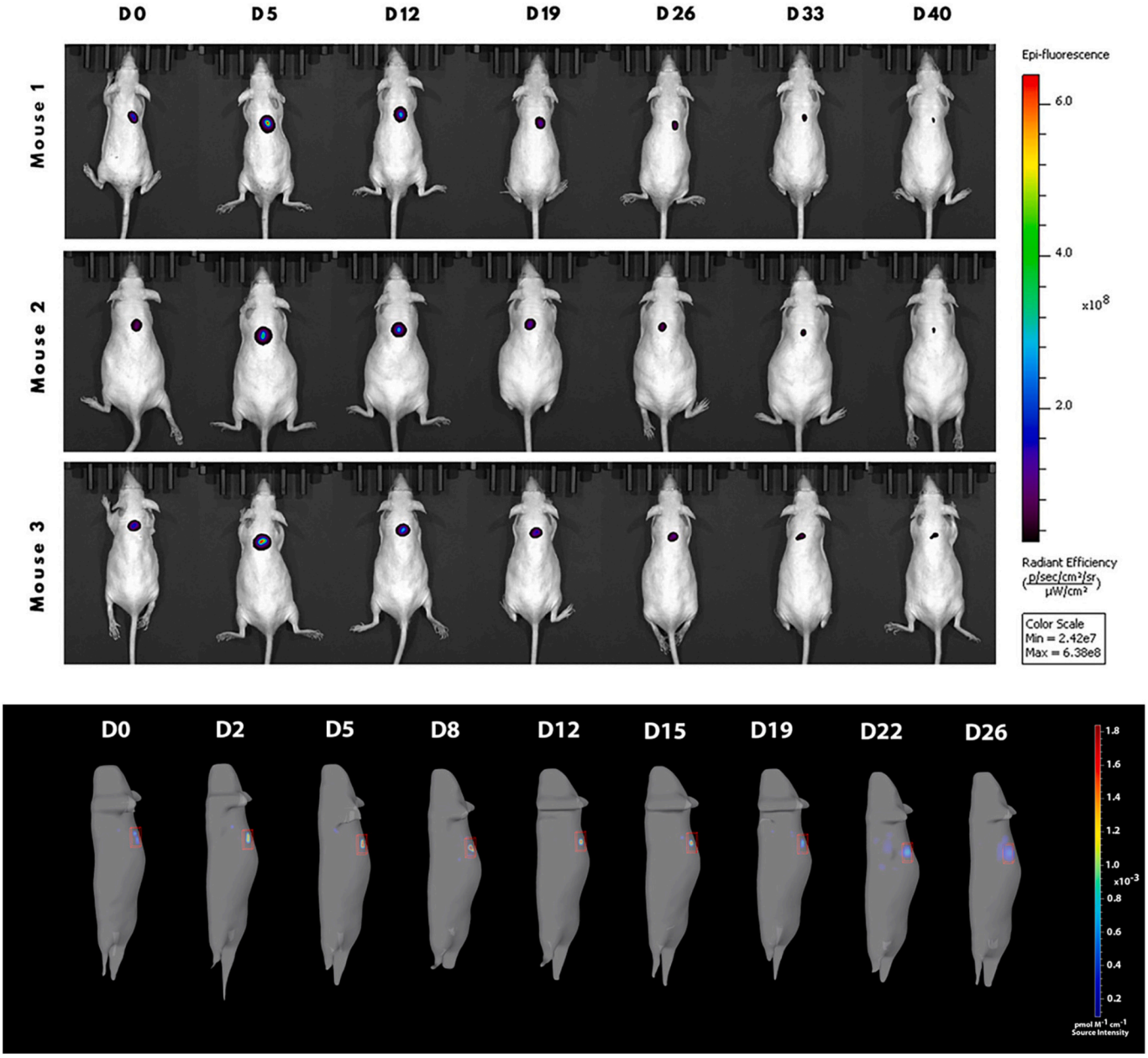

Fig. 11. Optical Images of DiR loaded starch implants: 2D imaging (Top), 3D reconstruction of the mouse 2 (Bottom).

3.8. *In vivo release 2D vs 3D*

Best 3D reconstructions are achieved with high signal intensity. It was expected that with the lower concentration of the dye (1.5 µg/g), the 3D measurement was only possible for a short period. We are aware about the risk of having nonlinear concertation / intensity relations for the higher concentration (50 µg/g) in the initial release period due to quenching effects, but nethertheless we did also use this concentration to prolong the overall measurement period *in vivo* in the 3D mode which is less sensitive compared to the 2D measurement. We also applied the lower DiR concentration of 1.5 µg/g which is in the linear region and avoids quenching problems. For the higher concentration of 50 µg/g we expected to see initially a period of increase in signal due to the quenching effect and then a decrease in signal intensity with the same behavior as an implant with 1.5 µg/g dye concentration. Fig. 11 shows the changes in fluorescent intensity assessed by 2D imaging and 3D reconstructions of the implant in mouse 2.

As can be seen in Fig. 11, the sensitivity of the device in epi-illumination (2D) is much higher than FLIT (3D). Because of this, the dye release can be assessed for a significantly longer period by 2D imaging in comparison to 3D reconstruction. Considering 2D images, the signal could be detected for 40 days. In contrast, 3D reconstruction of the implant was only possible for 33 days. Despite the limitation in sensitivity of the device, as can be seen in Fig. 12, the *in vivo* release curve obtained by 3D reconstructions matches the data obtained by 2D imaging until day 20. On day 25 an increase in signal intensity was observed in 3D probably due to artifacts which are formed in low concentrations of the dye close to the sensitivity limit of the device. Therefore applicable dye concentration range is much more limited in 3D mode data acquisition in comparison to 2D mode. This fact proves the need to use 2D measurements always as the established control method.

3.9. *Tolerability of the treatment, body weight and histology*

All treatments were well tolerated and no treatment-related adverse

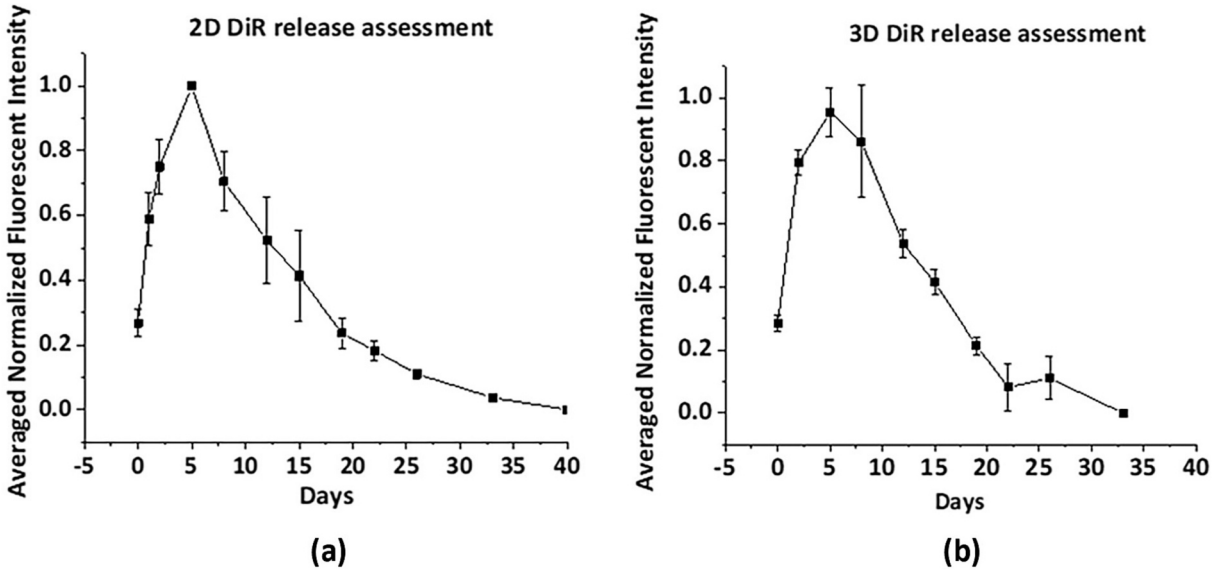

Fig. 12. Quantification of DiR signals detected *in vivo* (initial DiR concentration, 50 μg/g): (**a**) Quantification done by 2D images (epi-illumination). Error bars after day 20 are within the symbols; (**b**) Quantification done by 3D reconstructions (Mean ± SD, $n = 3$). A high DiR concentration was used to enable 3D measurements for prolonged times. The initial increase in signal intensity is due to the decrease of quenching effects.

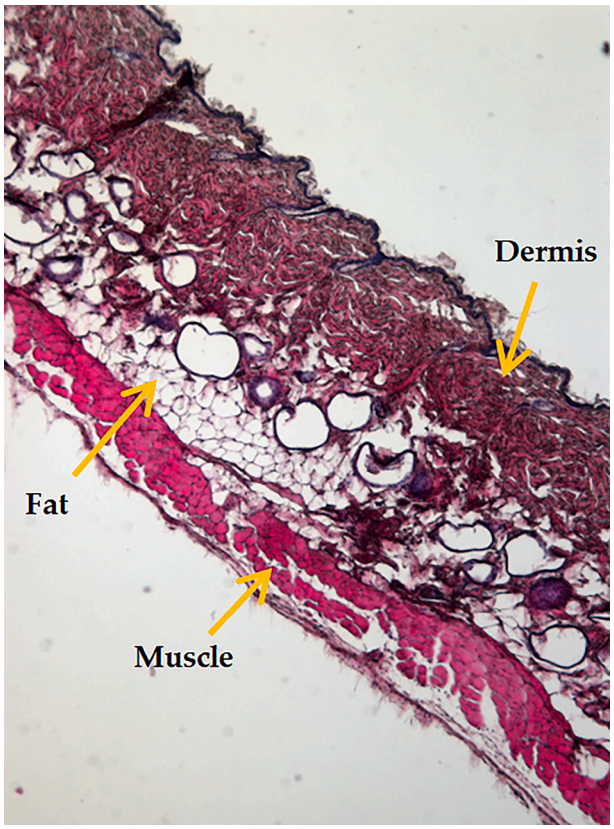

Fig. 13. The surrounding tissue of the injection site stained with hematoxylin–eosin (H&E).

effects were observed. The body weight of all mice involved in the study was either constant or increasing. Histological samples of the injection site were rated as normal (Fig. 13).

4. Conclusion

In this study, the *in vitro* and *in vivo* release from starch-based implants is investigated. The model compounds, namely ICG as a model of the hydrophilic drug and DiR as a model of a hydrophobic drug were loaded into the implants to assess the release kinetics by FI. The starch implants were injected SC in mice for further evaluation by FI. No inflammation or adverse effects were observed at the injection site. The ICG showed a fast release from the formulation both *in vitro* and *in vivo,* while DiR was released over 30 days. These results are in line with our previous study, where the EPR, as a non-invasive method, was utilized to assess the *in vitro* release kinetics from the formulation and water penetration into the implant using spin probes as model compounds. EPR data demonstrated the fast water penetration into the starch-based implant leading to the fast release of hydrophilic compound (Tempol) and sustained release of hydrophobic compound (Tempol Benzoate) *in vitro* [17]. In addition to the 2D FI, the 3D reconstruction of the implant was used to assess the release kinetics in 3D. The results of *in vivo* DiR release obtained by 3D reconstructed implant match the results obtained by 2D imaging. In this study, the 3D reconstruction was used for a very small implant with a regular shape. This can be expanded to the use of 3D reconstruction to assess the release kinetics in 3D mode from *in vivo* forming implants in future. After sacrificing the mice, the injection site was evaluated for the remaining part of the implant. The implant was completely degraded and no remaining part of the implant was detectable by unarmed eyes in any of the mice. In summary, the results prove the promising potential of the biodegradable biocompatible starch-based implant in forming a controlled release system for a hydrophobic drug.

Supplementary data to this article can be found online at https://doi.org/10.1016/j.jconrel.2023.05.006.

Funding

This research was funded by the European Social Fund (ESF) and the Federal State of Saxony-Anhalt.

Institutional review board statement

The study was conducted according to the guidelines of the

Declaration of Helsinki and approved by the Institutional Review Board of Saxony-Anhalt, Germany (42502–2-1500 MLU, date of approval: 18.07.2018).

CRediT authorship contribution statement

Golbarg Esfahani: Conceptualization, Methodology, Validation, Formal analysis, Investigation, Data curation, Writing – original draft. **Henrike Lucas:** Conceptualization, Methodology, Validation, Formal analysis, Investigation, Data curation, Writing – original draft. **Frank Syrowatka:** Methodology, Validation, Formal analysis, Investigation, Resources, Data curation. **Karsten Mäder:** Conceptualization, Methodology, Resources, Writing – review & editing, Supervision, Project administration, Funding acquisition.

Declaration of Competing Interest

The authors declare no conflict of interest.

Data availability

Data will be made available on request.

Acknowledgments

This study was supported by the IGS “Functional polymers” as a part of the AGRIPOLY program with funding from the European Social Fund (ESF). We would like to express our gratitude to Roquette (Lestrem, France) for providing us with the materials. We gratefully acknowledge the support of Dr. W. Knolle (Leibniz Institute of Surface Engineering) for the sterilization of the samples. Additionally, we would like to extend our appreciation to J. Kollan for all her help during the project and for teaching the H&E staining.

References

[1] C. Wischke, S.P. Schwendeman, Principles of encapsulating hydrophobic drugs in PLA/PLGA microparticles, Int. J. Pharm. 364 (2008), https://doi.org/10.1016/j.ijpharm.2008.04.042.
[2] Zoladex approved for prostate cancer, Drug. Ther. (NY) 20 (1990).
[3] D. Cuevas-Ramos, M. Fleseriu, Pasireotide: a novel treatment for patients with acromegaly, Drug. Des. Devel. Ther. 10 (2016), https://doi.org/10.2147/DDDT.S77999.
[4] A.G. Ding, S.P. Schwendeman, Acidic microclimate pH distribution in PLGA microspheres monitored by confocal laser scanning microscopy, Pharm. Res. (2008), https://doi.org/10.1007/s11095-008-9594-3.
[5] K. Mäder, B. Gallez, K.J. Liu, H.M. Swartz, Non-invasive in vivo characterization of release processes in biodegradable polymers by low-frequency electron paramagnetic resonance spectroscopy, Biomaterials. 17 (1996), https://doi.org/10.1016/0142-9612(96)89664-5.
[6] A. Schädlich, S. Kempe, K. Mäder, Non-invasive in vivo characterization of microclimate pH inside in situ forming PLGA implants using multispectral fluorescence imaging, J. Control. Release 179 (2014), https://doi.org/10.1016/j.jconrel.2014.01.024.
[7] M.A. Araújo, A.M. Cunha, M. Mota, Enzymatic degradation of starch-based thermoplastic compounds used in protheses: identification of the degradation products in solution, Biomaterials. 25 (2004), https://doi.org/10.1016/j.biomaterials.2003.09.093.
[8] M.A.V.T. Garcia, C.F. Garcia, A.A.G. Faraco, Pharmaceutical and biomedical applications of native and modified starch: a review, Starch/Staerke. 72 (2020), https://doi.org/10.1002/star.201900270.
[9] P.F. Builders, M.I. Arhewoh, Pharmaceutical applications of native starch in conventional drug delivery, Starch/Staerke. 68 (2016), https://doi.org/10.1002/star.201500337.
[10] R.C. Rowe, P.J. Sheskey, M.E. Quinn, Handbook of Pharmaceutical Excipients Sixth Edition, sixth edit, Rev. Des Nouv. Technol. l'Information., 2018.
[11] O.A. Odeku, Potentials of tropical starches as pharmaceutical excipients: a review, Starch/Staerke. 65 (2013), https://doi.org/10.1002/star.201200076.
[12] S. Jin, G. Yu, R. Hou, B. Shen, H. Jiang, Effect of hemodilution in vitro with hydroxyethyl starch on hemostasis, Med. Sci. Monit. 23 (2017), https://doi.org/10.12659/MSM.901588.
[13] A.J. Salgado, O.P. Coutinho, R.L. Reis, Novel starch-based scaffolds for bone tissue engineering: cytotoxicity, cell culture, and protein expression, Tissue Eng. (2004), https://doi.org/10.1089/107632704323061825.
[14] X. Zhang, Y. Liu, S. Gong, M. Li, S. Li, Y. Hemar, Probing the biotoxicity of starch nanoparticles in vivo and their mechanism to desensitize β-lactoglobulin, Food Hydrocoll. 135 (2023), 108166.
[15] H.D. Janowitz, D.A. Dreiling, The plasma amylase: source, regulation and diagnostic significance, Am. J. Med. 27 (1959) 924–935.
[16] S. Punia, Barley starch modifications: physical, chemical and enzymatic - a review, Int. J. Biol. Macromol. 144 (2020), https://doi.org/10.1016/j.ijbiomac.2019.12.088.
[17] G. Esfahani, O. Häusler, K. Mäder, Controlled release starch-lipid implant for the therapy of severe malaria, Int. J. Pharm. 622 (2022), https://doi.org/10.1016/j.ijpharm.2022.121879.
[18] J.A. Simón, E. Utomo, F. Pareja, M. Collantes, G. Quincoces, A. Otero, M. Ecay, J. Domínguez-Robles, E. Larrañeta, I. Peñuelas, Radiolabeled risperidone microSPECT/CT imaging for intranasal implant studies development, Pharmaceutics. 15 (2023) 843.
[19] D.A. Boas, D.H. Brooks, E.L. Miller, C.A. Dimarzio, M. Kilmer, R.J. Gaudette, Q. Zhang, Imaging the body with diffuse optical tomography, IEEE Signal Process. Mag. 18 (2001), https://doi.org/10.1109/79.962278.
[20] A.P. Gibson, J.C. Hebden, S.R. Arridge, Recent advances in diffuse optical imaging, Phys. Med. Biol. 50 (2005), https://doi.org/10.1088/0031-9155/50/4/R01.
[21] S. Zhu, R. Tian, A.L. Antaris, X. Chen, H. Dai, Near-infrared-II molecular dyes for Cancer imaging and surgery, Adv. Mater. 31 (2019), https://doi.org/10.1002/adma.201900321.
[22] FDA. Available online: https://www.accessdata.fda.gov/drugsatfda_docs/label/2006/011525s017lbl.pdf (accessed on 25.05.2022), (n.d.).
[23] J. Wang, F. Guo, M. Yu, L. Liu, F. Tan, R. Yan, N. Li, Rapamycin/DiR loaded lipid-polyaniline nanoparticles for dual-modal imaging guided enhanced photothermal and antiangiogenic combination therapy, J. Control. Release 237 (2016), https://doi.org/10.1016/j.jconrel.2016.07.005.
[24] H. Xin, X. Jiang, J. Gu, X. Sha, L. Chen, K. Law, Y. Chen, X. Wang, Y. Jiang, X. Fang, Angiopep-conjugated poly(ethylene glycol)-co-poly(ε-caprolactone) nanoparticles as dual-targeting drug delivery system for brain glioma, Biomaterials. 32 (2011), https://doi.org/10.1016/j.biomaterials.2011.02.044.
[25] J. Guillen, FELASA guidelines and recommendations, J. Am. Assoc. Lab. Anim. Sci. 51 (2012).
[26] H.M. Voipio, P. Baneux, I.A. Gomez De Segura, J. Hau, S. Wolfensohn, Guidelines for the veterinary care of laboratory animals: report of the FELASA/ECLAM/ESLAV joint working group on veterinary care, Lab. Anim. 42 (2008), https://doi.org/10.1258/la.2007.007027.
[27] M. Riehl, M. Harms, H. Lucas, T. Ebensen, C.A. Guzmán, K. Mäder, Dual dye in-vivo imaging of differentially charged PLGA carriers reveals antigen-depot effect, leading to improved immune responses in preclinical models, Eur. J. Pharm. Sci. (2018), https://doi.org/10.1016/j.ejps.2018.01.040.
[28] Perkin Elmer, Phantom Mouse, (n.d.). https://www.perkinelmer.com/product/xfm-2x-fluorescent-phantom-mouse-x-ray-133803 (accessed March 30, 2023).
[29] D.J. Thomas, W.A. Atwell, Eagan Press Handbook Series: Starches, Minnesota Eagan Press. Sch, St. Paul, 1999.
[30] H. Liu, L. Yu, Z. Tong, L. Chen, Retrogradation of waxy cornstarch studied by DSC, Starch/Staerke. 62 (2010), https://doi.org/10.1002/star.201000017.
[31] G. Choy, S. O'Connor, F.E. Diehn, N. Costouros, H.R. Alexander, P. Choyke, S. K. Libutti, Comparison of noninvasive fluorescent and bioluminescent small animal optical imaging, Biotechniques. 35 (2003), https://doi.org/10.2144/03355rr02.
[32] L. Liu, R.P. Mason, B. Gimi, Dynamic bioluminescence and fluorescence imaging of the effects of the antivascular agent Combretastatin-A4P (CA4P) on brain tumor xenografts, Cancer Lett. 356 (2015), https://doi.org/10.1016/j.canlet.2014.09.038.
[33] N. Zhao, C. Zhang, Y. Zhao, B. Bai, J. An, H. Zhang, J.B. Wu, C. Shi, Optical imaging of gastric cancer with near-infrared heptamethine carbocyanine fluorescence dyes, Oncotarget. 7 (2016), https://doi.org/10.18632/oncotarget.10031.
[34] I. Biancacci, Q. Sun, D. Möckel, F. Gremse, S. Rosenhain, F. Kiessling, M. Bartneck, Q. Hu, M. Thewissen, G. Storm, W.E. Hennink, Y. Shi, C.J.F. Rijcken, T. Lammers, A.M. Sofias, Optical imaging of the whole-body to cellular biodistribution of clinical-stage PEG-b-pHPMA-based core-crosslinked polymeric micelles, J. Control. Release 328 (2020), https://doi.org/10.1016/j.jconrel.2020.09.046.
[35] R. Choe, A. Corlu, K. Lee, T. Durduran, S.D. Konecky, M. Grosicka-Koptyra, S. R. Arridge, B.J. Czerniecki, D.L. Fraker, A. Demichele, B. Chance, M.A. Rosen, A. G. Yodh, Diffuse optical tomography of breast cancer during neoadjuvant chemotherapy: a case study with comparison to MRI, Med. Phys. 32 (2005), https://doi.org/10.1118/1.1869612.
[36] M. Schweiger, S.R. Arridge, Comparison of two- and three-dimensional reconstruction methods in optical tomography, Appl. Opt. 37 (1998), https://doi.org/10.1364/ao.37.007419.